Salts and cocrystals of substituted phenylacetic acids

By

REMI ROLLAND NGOMA TCHIBOUANGA

Thesis submitted in fulfilment of the requirements for the degree

Master of Applied Science: Chemistry

in the Faculty of Applied Sciences at the

CAPE PENINSULA UNIVERSITY OF TECHNOLOGY

Supervisor: Professor Ayesha Jacobs

Cape Town

December

2018

▪ DECLARATION

I, Remi Rolland Ngoma Tchibouanga, declare that the contents of this dissertation/thesis represent my own unaided work, and that the dissertation/thesis has not previously been submitted for academic examination towards any qualification. Furthermore, it represents my own opinions and not necessarily those of the Cape Peninsula University of Technology.

Signed **Date**

ABSTRACT

The prediction of the single crystal structure that will form due to the combination of two or more compounds to form a multicomponent crystal is one of the important areas of research in crystal engineering. Since these compounds display different properties when combined as a single crystal, knowledge of synthesis and design of the resulting compound is essential. The formation of a multicomponent crystal, such as a salt or a cocrystal generally depends on the complementarity of the functional groups present on both components. This means that basicity and acidity of the functional groups present on the selected compounds need to be considered.

This study investigated salts and cocrystals of 3-chloro-4-hydroxyphenylacetic acid (CHPAA) using the ΔpK_a rule. The calculated ΔpK_a values were recorded and correlated with the experimental analysis in predicting the outcome of the crystallisation experiments ie. salt or cocrystal formation. This was further confirmed by the analysis of the C-O bond lengths found in the crystal structures. Salts were obtained by combinations of CHPAA with several organic bases (co-formers) such as diethylamine, dibutylamine, 2-aminopyridine, 2-amino-4-methylpyridine, 2-amino-6-methylpyridine and 4-dimethylaminopyridine. The calculated ΔpK_a values were within the range of salt formation. Furthermore, the experimental analysis also showed that all resulting compounds were salts. Cocrystals were obtained by reactions of nicotinamide, isonicotinamide, phenazine and 4,4'-bipyridine with CHPAA. Again, the calculated ΔpK_a values predicted cocrystals as the new solid forms. Experimental analysis carried out also confirmed cocrystal formation. For all resulting compounds, the comparison of intermolecular interactions as well as supramolecular synthons were reported. All compounds were synthesised by slow evaporation techniques using various organic solvents and characterised by single crystal X-ray diffraction, powder X-ray diffraction, thermal analysis and Fourier transformer infrared spectroscopy.

From the structural analysis, it was found that all resulting structures displayed strong N-H•••O and O-H•••O intermolecular interactions including weak interactions of C-H•••Cl, C-H•••O and C-H•••π for a few of the structures. Furthermore, comparison of the crystal structures showed that no packing arrangement similarity existed between the compounds.

▪ ACKNOWLEDGEMENTS

I wish to thank:

- God for his infinite love
- My family, friends and colleagues for their support and encouragement
- My supervisor, Professor Ayesha Jacobs for her willingness to help, advice and support.
- The Cape Peninsula University of Technology, for increasing my knowledge and
- Any person who contributed to the accomplishment of this thesis directly or indirectly, may God bless you

- **DEDICATION**

I dedicate this thesis to my family and friends

TABLE OF CONTENTS

▪ LIST OF FIGURES

CHAPTER 1

CHAPTER 2

CHAPTER 3

CHAPTER 4

CHAPTER 5

CHAPTER 6

▪ LIST OF TABLES

CHAPTER 1

CHAPTER 2

CHAPTER 3

CHAPTER 4

CHAPTER 5

CHAPTER 6

▪ GLOSSARY

Terms/ Acronyms/ Abbreviations	Definition/ Explanation
CSD	Cambridge Structural Database
PXRD	Powder X-ray Diffraction
TGA	Thermogravimetric Analysis
DSC	Differential Scanning Calorimetry
a, b, c	Unit cell axes
α	Angle between b and c unit cell axes
β	Angle between a and c unit cell axes
γ	Angle between a and b unit cell axes
V	Unit cell volume
Z	Number of formula units per cell
T_{on}	Onset temperature
Dcal	Calculated density
Goof	Goodness of fit
DEA	Diethylamine
DIBUAM	Dibutylamine
2AMP	2-aminopyridine
2A4MP	2-amino-4-methylpyridine
2A6MP	2-amino-6-methylpyridine
DMAP	Dimethylaminopyridine
NAM	Nicotinamide
ISONAM	Isonicotinamide
BIPY	4,4'-Bipyridine
PHZN	Phenazine

- **ATOM COLOURS**

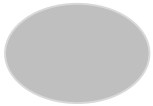
Carbon

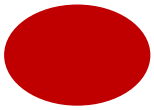
Oxygen


Nitrogen

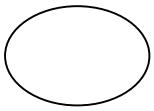
Hydrogen

Chlorine

CHAPTER ONE

INTRODUCTION

Chapter 1 : INTRODUCTION

1.1. Background

The crystallization process which involves two or more different components together in a single crystal is very challenging. The prediction of the crystal structures of new solid forms (known as multicomponent crystals)[1] is complex since these compounds are often affected by various factors, which include the lack of functional group recognition, stability, kinetic interactions and thermodynamics in the process of nucleation.[2] The formation of a new solid form, such as a salt or a cocrystal generally depends on the complementarity of the functional groups present on both components. Therefore, interpreting the mechanisms and kinetics of salt formation and cocrystallization, as well as the factors affecting cocrystal stability, gives greater control in synthesis and phase transformations.[3] Currently, crystal engineering is used as an important tool in supramolecular synthesis in the quest for supramolecular synthetic targets in the solid state. Intermolecular interactions such as hydrogen bonding and weaker van der Waals forces play an important role in the design of supramolecular synthons. The basicity and acidity of the functional groups present on the different components also have to be considered. A useful tool in predicting whether a salt or a cocrystal will form comes from inspection of the differences in the pK_a values of the acid and base.

1.2. Supramolecular chemistry

While molecular chemistry design and synthesis involve covalent bonding of atoms, in supramolecular chemistry, the association of two or more building blocks involve intermolecular interactions.[4] The design and synthesis of supramolecules are the main thrust of supramolecular chemistry. Jean-Marie Lehn thus defined it as ˝chemistry beyond the molecule˝, referring to how molecules of higher complexity can self-organise by holding together by means of intermolecular forces.[5] Moreover, Dunitz *et al.* noted that supramolecules are chemical entities held together by means of non-covalent interactions such as hydrogen bonds, halogen bonds and π-π interactions.[6] Supramolecular chemistry involves many disciplines eg. molecular self-assembly, molecular recognition and host-guest chemistry among others.[7]

The basis of intermolecular forces was first postulated in 1873 by Johannes Diderik van der Waals. However, the concept was proposed by the laureate Hermann Emil Fisher who highlighted later in 1890 that interactions involving enzymes to a substrate can be described as a˝lock and key”. In 1920, the work conducted by Latimer and Rodebush on the description of the hydrogen bond, extended broadly the concept of noncovalent interactions and also led to the expansion of protein structure analysis and other biological processes using these principles. Later in 1987, the Nobel Prize for chemistry, which was awarded to Donald J.Cram, Jean-Marie Lehn, and Charles J. Pedersen due to their work in this area, established the importance of supramolecular chemistry.[8] Figure 1.1 below illustrates the design of supramolecules.

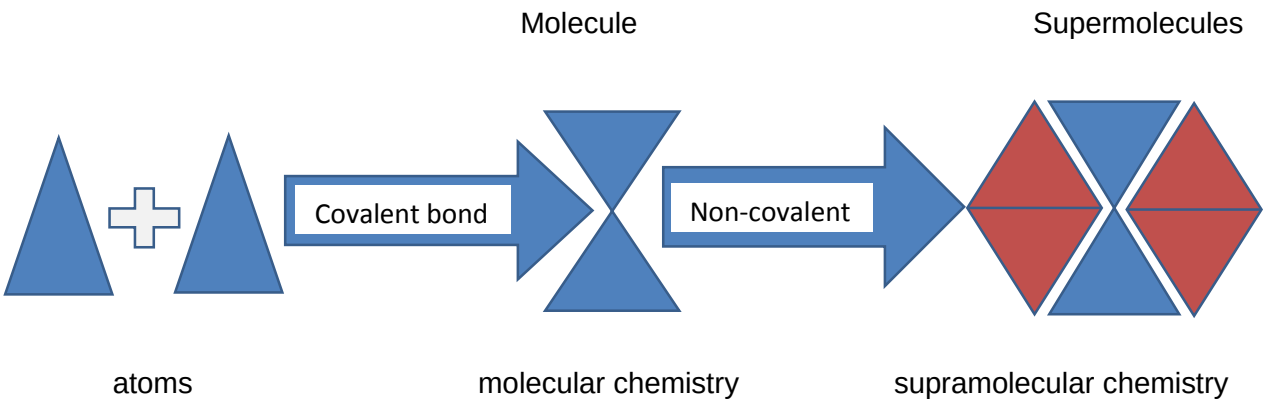

Figure 1. 1 : Illustration of the supramolecule's design.

Table 1. 1: History of supramolecular chemistry

Year	Author	Event
1810	Davy	Discovery of chlorine
1823	Faraday	Formula of chlorine hydrate
1841	Schafhäutl	Study of graphite intercalates
1849	Wöhler	β-quinol H_2S clathrate
1891	Vilier & Hebd	Cyclodextrin inclusion compounds
1893	Werner	Coordination chemistry
1894	Fischer	Lock and key concept
1906	Ehrlich	Introduction of the concept of a receptor
1937	Wolf	The term 'übermoleküle' is coined to describe organised entities arising from the association of coordinatively saturated species
1939	Pauling	Hydrogen bonds are included in the ground-breaking book "The Nature of the Chemical Bond"
1940	Bengen	Urea channel inclusion compounds
1945	Powell	X-ray crystal structures of β-quinol inclusion compounds; the term clathrate is introduced to describe compounds where one component is enclosed within the framework of another
1949	Brown & Farthing	Synthesis of [2,2] paracyclophane
1953	Watson & Crick	Structure of DNA
1956	Hodgkins	X-ray crystal structure of vitamin B12
1959	Cram	Attempted synthesis of cyclophane charge transfer complexes with (NC)2C=C(CN)2
1961	Curtis	First Schiff's base macrocycle from acetone and ethylene diamine
1964	Bush & Jäger	Schiff's base macrocyles
1967	Pedersen	Crown ethers
1968	Park & Simmons	Katapinand anion hosts
1969	Lehn	Synthesis of the first cryptands
1969	Atwood	Liquid clathrates from alkyl aluminium salts
1973	Cram	Spherand hosts produced to test the importance of pre-organisation
1978	Lehn	Introduction of the term 'supramolecular chemistry', defined as 'the chemistry of molecular assemblies and of the intermolecular bond'
1979	Gokel & Okahara	Development of the lariat ethers as a subclass of host compounds
1981	Vögtle & Weber	Podant hosts and development of nomenclature
1986	de Silva	Fluorescent sensing of alkali metal ions by crown ether derivatives
1987	Cram, Lehn & Pedersen	Award of the Nobel prize for chemistry to Donald J. Cram, Jean-Marie Lehn and Charles J. Pedersen for their work in supramolecular chemistry
1996	Atwood, Davies, MacNicol & Vögtle	Publication of "Comprehensive Supramolecular Chemistry" containing contributions from many key groups and summarising the development and state of the art
1996	Kroto, Smalley & Curl	Award of the Nobel prize for chemistry to Kroto, Smalley and Curl for their work on the chemistry of the fullerenes
2003	Agre & Roderick	Award of the Nobel prize for chemistry to Peter Agre and Roderick Mackinnon for their discovery of water channels and the characterisation of cation and anion channels, respectively.
2004	Stoddart	The first discrete Borromean-linked molecule, a landmark in topological synthesis.

1.2.1 Supramolecular synthons

The prediction of crystal structures from molecular structures in terms of understanding the conceptual design between the geometric and chemical model of the final crystal structures formation appears to be the central challenge of crystal engineering.[9] As Desiraju observed, most often crystal structures lack a direct correlation with the functional groups present in the respective molecular structures which therefore lead the structures to be dictated by both chemical and geometric models in a complex way.[10] Thus, being in this context and designing the correlation with the synthon from molecular chemistry, allowed the introduction of the supramolecular synthons concept. Desiraju thus defined supramolecular synthons as "structural units within molecules which can be formed and/or assembled by known or conceivable synthetic operations involving intermolecular interactions."[11] Zaworotko and co-workers later extended the concept into two distinct classes ie. supramolecular homosynthons and supramolecular heterosynthons.[12] A supramolecular homosynthon involves intermolecular interactions between identical self-complementary functional groups eg. carboxylic acid dimers and amide dimers; whereas, supramolecular heterosynthon is due to intermolecular interactions between two or more different functional groups such as carboxylic acid-amide and carboxylic acid-aromatic nitrogen. Almarsson and Zaworotko noted that heterosynthons that show recognition between different functionalities play a crucial role in cocrystal synthesis.[13] Similarly, the statistical study led by the Cambridge Crystallographic Data Centre (CCDC) confirmed that supramolecular heterosynthons are more reliable for the preparation of cocrystals than supramolecular homosynthons.[14] Figure 1.2 below illustrates the chemical structures of various supramolecular synthons.

In organic solids, the concept of the synthon is mostly based on the arrangement of molecules or ions which can be assembled predictably via specific nonbonding interactions and realize a robust geometry in the crystal.[15] Moreover, the observation made early in 2002 by Sarma and Desiraju, and later in 2008 by Thakur and Desiraju, confirmed that besides synthesis, the concept of supramolecular synthons can also be used with the crystal structure prediction (CSP) protocol.[16] CSP is a computational procedure that generates multiple crystal structures within reasonable energy and density ranges for a given molecule. After the realisation of the synthons concept, further study was done on weak synthons including halogen bonded synthons. However, halogen bonded synthons were not fully understood although noncovalent interactions with halogens were already identified years ago by Hassel.[17] Only in the late 1990s was a proper understanding of its supramolecular role and subsequent exploitation as a synthon in crystal engineering achieved.

Recently, several design strategies have been formulated by combining halogen bonds with hydrogen bonds in different ways and by using the graded strength of the halogen bonds that makes them an excellent tool for structural insulation.[18] Two types of halogen bonds were recognized by Sakurai et *al.*[19] and were subsequently named by Desiraju et *al.*[20] as type I and type II.

Type I contacts are formed by "head on" approach of two halogens making it more geometrical, whereas type II contacts, have a "side on approach of two" geometry that permits the interaction between an electropositive region on one halogen to the electronegative region on the other, thus qualifying as true halogen bonds which are more chemical in nature.[21]

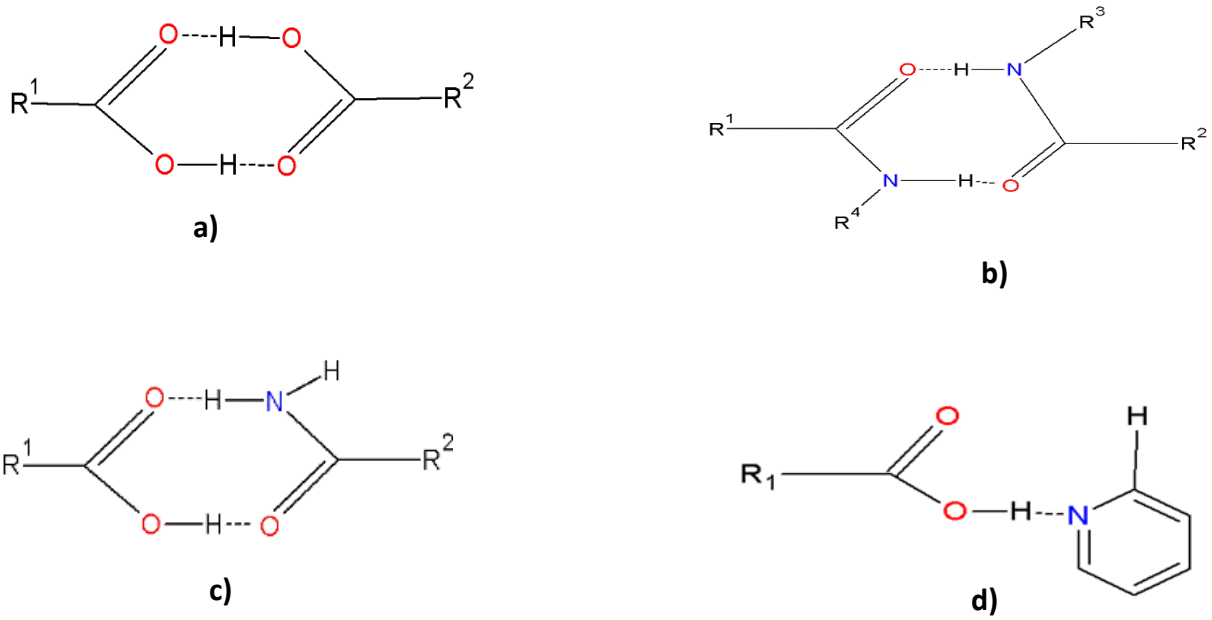

Figure 1. 2: Representation of supramolecular synthons: (a) carboxylic acid homosynthon, (b) amide homosynthon, (c) carboxylic acid-amide heterosynthon and (d) carboxylic acid-pyridine heterosynthon.

1.3 Crystalline structures and their properties

A material can be considered as crystalline if it has long range order and a regularly repeating unit. Crystalline solids result from self-arrangement of atoms, ions or molecules[22] and the concepts are well defined. [23,24] On the other hand a lack of long-range structural order throughout a solid results in an amorphous material.[22] Amorphous compounds can be defined as a class of solid lacking the defined regular internal structure.[25] Crystalline solids can be divided into four types namely: covalent network, ionic compounds, metallic compounds and molecular compounds.[26]

1.4 Types of crystalline solids

1.4.1 Ionic solids

Ionic solids can be described as compounds that are held together by means of electrostatic interactions. These solid forms are characterized by cationic and anionic species. Sodium chloride and caesium chloride are examples of ionic compounds. In ionic solids the arrangement of ions is made by the lattice sites occupation of anions and cations which subsequently result in the binding due to the electrostatic forces. The melting points of these solids are very high due to the strong electrostatic interactions between counterions and tend to be non- volatile at room temperature.[27]

1.4.2 Metallic solids

Metallic solid compounds can be easily characterized by their physical properties such as high thermal and electrical conductivities, malleability and ductility. The bonding model in this type of solid can be described using free electrons.[28] This replicates the solid as a close-packed array of atoms, with valence electrons completely delocalized over the extended structure. The strong interactions between neighbouring metal atoms in the solid within the compound gives rise to high melting points and boiling points which also result in very dense solid compounds with low volatility.[29]

1.4.3 Molecular solids

Molecular solids are compounds that are held together by means of weak intermolecular forces such as dipole-dipole, London dispersion, and hydrogen bonding.[30] These weak intermolecular forces characterize molecular solids with low melting points when compared to ionic or metallic bonding interactions. These can be observed in dry ice (solid CO_2), ice (solid H_2O), solid methane (CH_4), sugar ($C_6H_{12}O_6$) and polymers. The prediction of these structures is quite complex, especially when the molecules are large, but with the use of software, interaction energies can make practically consistent predictions. Such cases can be observed when dealing with hydrogen bonds which control the crystal structure, as in ice. These solids can be crystalline or amorphous, depending on the molecular packing in the bulk material.

1.4.4 Covalent network solids

The characterization of these solids is based on the strong arrangement of covalent bonds between atoms which generally results in a change in physical properties such as high melting point and bulk hardness.[31] These compounds are formed between non-metals by sharing electrons. Covalent solids are characteristically hard and often unreactive.[27] These can be observed in some of the compounds such as silicon, red phosphorus, boron nitride and more specifically diamond and graphite which are two allotropes of carbon. The bonding in these compounds is regularly extended network covalent when compared to molecular solids in which the bonding occurs by means of weak interactions to form molecular bonding. However, the presence of layers which are held together by van der Waals interactions may also be observed even though the discrete units of the extended solid are covalently bound.

1.4.5 Crystal structure

A crystal is characterized by the infinite lattice of duplicate units containing the smallest building block known as an asymmetric unit.[32] This asymmetric unit is duplicated to produce the contents of a unit cell by using the symmetry operator of the crystal such as rotation axes or mirror planes. The characterization of the crystal structures is of significant practical importance, since its implications today are widely useful in many areas such as geology,

materials, technologically advanced materials which include semiconductors and high-temperature superconductors, and biology.

One of the most important techniques for the determination of the structures of crystals is X-ray diffraction. These techniques provide detailed information about the location of all atoms in a molecule, even those as complicated as proteins. The first, and often very demanding, step in X-ray analysis of biological macromolecules is to form crystals in which the large molecules lie in ordered ranks.

1.4.6 Unit cells

A unit cell of the crystal is defined as the three-dimensional unit or parallelepiped that may be used to construct the entire crystal lattice by purely translational displacements.[33] There are seven crystal systems and fourteen crystal lattices known as Bravais lattices (Table 1.2). Primitive unit cells contain one lattice point as a result of parts of the lattice points present at each corner. A two-dimensional primitive unit cell is illustrated in Fig 1.3.

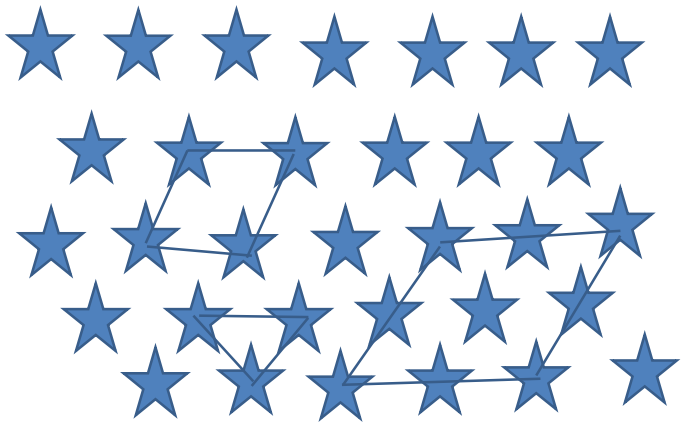

Figure 1. 3: Representation of some unit cell selections from a 2D array.

Table 1. 2: The fourteen Bravais lattices characteristics and parameters.[34]

Crystal systems	Numberof Bravais Lattices	Parameters	Possible unit cells
Hexagonal	1	a= b= c, α= β= 90° γ= 120°	Primitive
Triclinic	1	a≠ b≠ c, α≠ β≠ γ	Primitive
Trigonal	1	a= b = c, α = β=γ < 120°≠ 90°	Primitive
Tetragonal	2	a= b≠ c, α= β= γ= 90	Primitive,body-centred
Monoclinic	2	a≠ b≠ c, α=β=γ=90°	Primitive, base-centred
Cubic	3	a= b= c, α= β= γ= 90°	Primitive, body-centred, face-centred
Orthorhombic	4	a≠ b≠ c, α= β= γ= 90°	Primitive,body-centred, base-centred, face- centred

1.5 Intermolecular interactions

In contrast with intramolecular interactions which occur between the atoms within a molecule, intermolecular interactions occur between two or more molecules. These interactions occur in all types of molecules or ions. They range from the strong, long-distance electrical attraction and repulsion between ions to the relatively weak dispersion forces. Intermolecular interactions can be classified as (in order of decreasing strength of interactions): ion-ion, ion-dipole, dipole-dipole, hydrogen bonding, cation-π, π-π stacking and van der Waals.

1.5.1 Ion-ion interactions

Ion-ion interactions or ionic bonding are forces of attraction that arise between ions of opposite charges. Their bond strength is comparable to that of the covalent bond which ranges from 100 to 350 kJ mol^{-1}. In ion interactions, there is an attraction of two particles carrying opposite charges resulting in strong forces and a considerable amount of energy is required to break the bond between them. Figure 1.4 illustrates an example of this type of interaction.

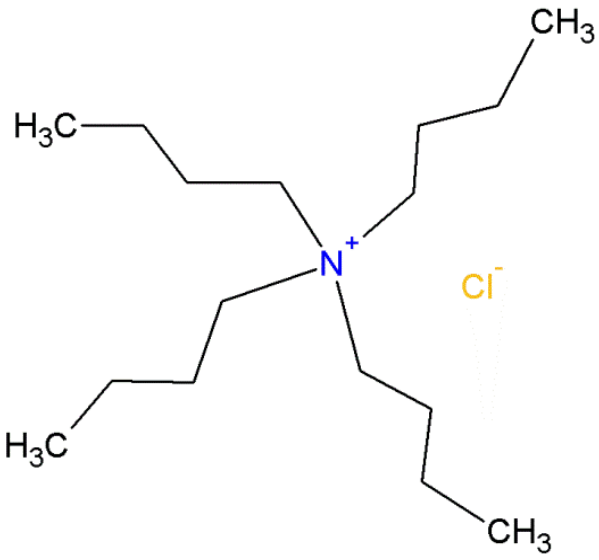

Figure 1. 4: Tetrabutylammonium chloride ion-ion interaction.

1.5.2 Ion-Dipole interactions

An ion dipole interaction is an attractive force that results from molecules that have a dipole. It usually occurs in both the solid state and in solution. The strength ranges from 50-200 kJ mol^{-1}.

Ion-dipole interactions are the result of the attractive forces between ions and polar molecules. These could also result in coordinative bonds such as the interactions seen in nonpolarizable metal cations and hard bases. Figure 1.5 below illustrates an example of an ion-dipole interaction.

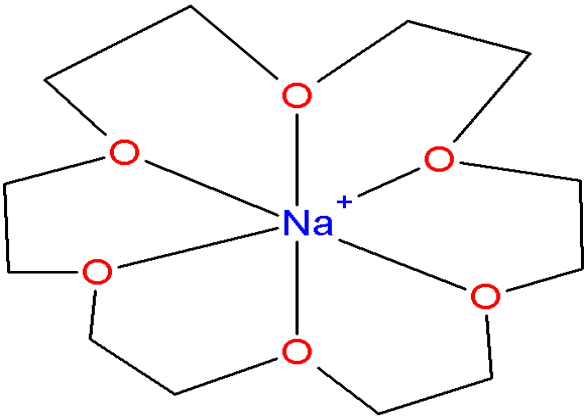

Figure 1. 5: Illustration of an ion-dipole interaction.

1.5.3 Dipole-Dipole interactions

Dipole-Dipole interactions are interactions that occur between two dipoles with partial charges. The strength ranges from 5-50 kJ mol^{-1}. This type of interaction occurs when two polar molecules carrying different partial dipoles (negative and positive poles) attract each other. These interactions can be observed in two different ways, namely: type I and type II resulting from two different types of interactions (adjacent or opposing).[35] Figure 1.6 represents both different types of interactions.

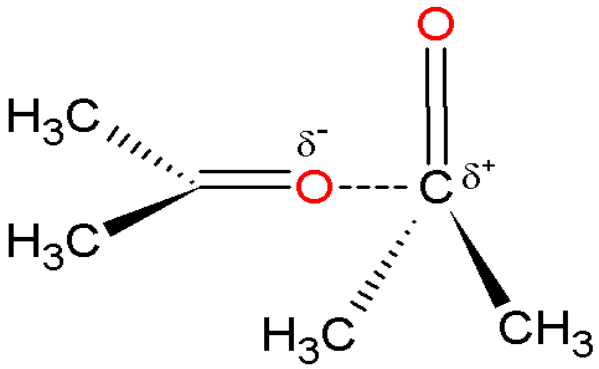

(a)

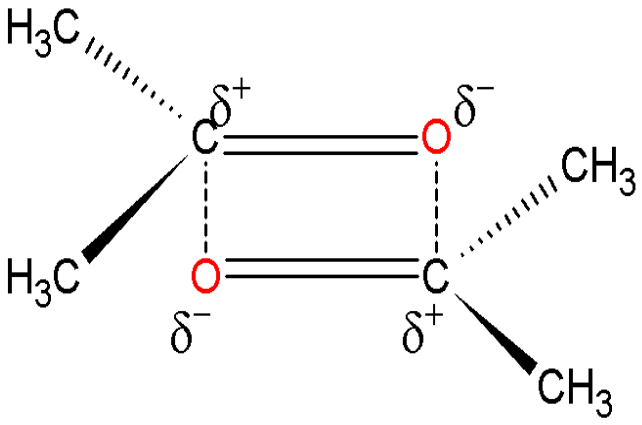

(b)

Figure 1. 6: Representation of type I (a) and II (b) dipole-dipole interactions.[36]

1.5.4 Cation-π interactions

Cation-π interactions occur between cations that have the ability to form complexes with olefinic (transition metal cations) and aromatic components.[35] It is a noncovalent intermolecular interaction between the face of an electron-rich π system such as benzene and an adjacent cation such as potassium (Figure 1.7). The interactions occur when the overall charge distribution is located in the centre or edges of aromatic hydrocarbons (benzene) creating the dipole leading to the electrostatic attraction on the face or outside of the benzene ring.[37]

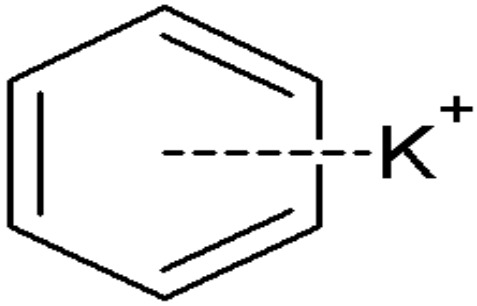

Figure 1. 7: Interaction of potassium with a benzene ring.[38]

1.5.5 π-π interactions

π-π interactions or π-π stacking results from the interactions of two aromatic rings that have different electron densities (relatively electron rich and electron poor).[35] Their energy strength range is 0-50 kJ mol^{-1}. They usually occur when one of the rings being relatively electron rich interacts with another ring which is relatively poor in electron density. Two main types of π-π interactions can be identified, namely: face to face and edge to face.

Face to face interactions arise when two aromatic rings interact by facing each other (Figure 1.8), whereas edge to face interactions (Figure 1.9) are observed when a weak hydrogen bond

is formed between the slightly poor electron density and the electron rich π-cloud of aromatic rings.[35]

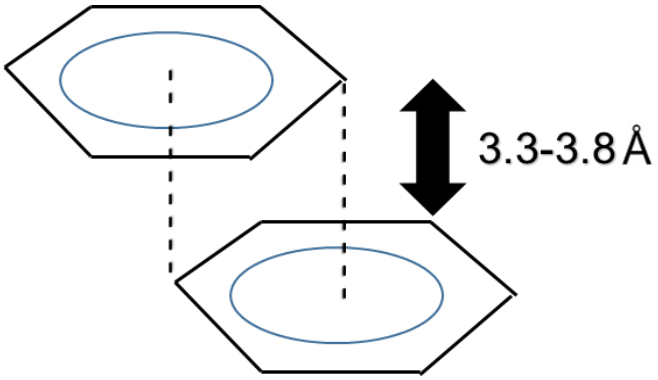

Figure 1. 8: Off-set face to face π-π stacking

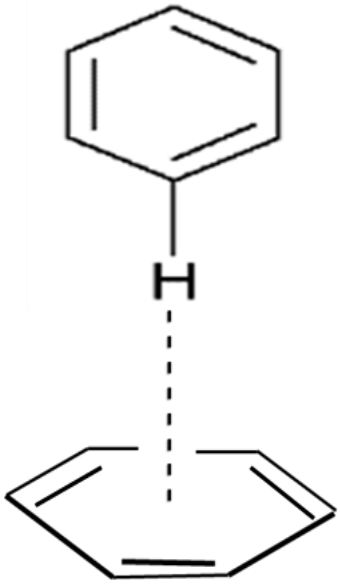

Figure 1. 9: Edge-to face π-π interaction.[39]

1.5.6 Van der Waals interactions

Van der Waals interactions or London forces are forces that arise between uncharged atoms or molecules. They are inversely proportional to the sixth power of the distance and sometimes to the seventh power of the distance depending on the characteristics of the interaction.[40] In chemistry, they are useful as they facilitate the inclusion of small molecules within the crystal lattice of specific compounds and are also responsible for the bonding found in solid states of rare gases, organic molecules and non-charged carbon layers.[35]

1.5.7 Hydrogen Bonding

Hydrogen bonding is the attractive force which occurs between the hydrogen attached to an electronegative atom of one molecule and an electronegative atom of another molecule. They can be considered as dipole-dipole interactions where the partially positive hydrogen atom is attached to a partially negative (O, N, Cl, F, I, F, etc,) atom.[35] In organic crystalline materials, hydrogen bonding is one of the most important interactions. Lehn thus described it as the ' *master key interaction* ' due to its strength (4-120 kJ mol^{-1}) and highly directional nature.[41] According to Desiraju, hydrogen bonding is the most consistent directional interaction, and therefore has a central role in crystal engineering.[42]

Based on the understanding of hydrogen bonding and its usefulness, Etter proposed three hydrogen bonding rules: (a) ` all acidic hydrogens available in a molecule will be used in hydrogen bonding in the crystal structure"; (b) ` all good proton acceptors will be used in hydrogen bonding when there are available hydrogen bond donors "; and (c) ` the best hydrogen bond donor and acceptor will preferentially form hydrogen bonds with one another".[43] Using these rules, hydrogen bond and synthon formation between the functionalities of different molecules can be predicted.[44,45]

Hydrogen bonding plays a vital role in biological systems.[46] Brown and co-workers described its important role in protein stabilization, muscles and other animal tissues.[47] It was also demonstrated that the hydrogen bonding strength depends mostly on the electron densities of the donors and acceptors.[48, 49] In addition to this, Li *et al* and Kolev *et al* observed that the larger the electron density in the proton acceptor and the lower the electron density in the proton donor, the greater the strength of the hydrogen-bonding interactions.[50,51] Desiraju *et al.* thus proposed a representative form of the hydrogen bond ie. D-H···A, where D represents

the donor group and A represents the acceptor group.[52] The distance notation between the donor and acceptor can be represented as $d_{D\cdots A}$ and $d_{H\cdots A}$ respectively and the angle between D-H⋯A atoms as θ. Furthermore, Jeffrey, observed that hydrogen bond properties can change relative to the groups of atoms nearby, and proposed three characteristic types of hydrogen bond; namely strong, moderate and weak interactions.[46] Similarly, Desiraju later extended the concept by describing different types of hydrogen bond properties (Table 1.3).[52] Early in 1990, Etter observed that there were several types of hydrogen bond interactions occurring amongst molecules, and proposed the graph set notation methodology.[53] This methodology does not consider the chemical nature of the compounds involved, but only the formation of certain hydrogen bonding patterns. Also, it allows the fragmentation of all hydrogen bonding so that they can easily be identified as chains (C), rings (R), finite complexes (D) and intermolecular interactions (S).[54] Using this methodology, the total number hydrogen bond acceptor (a) and donor (d) sites can be identified including the number of symmetry independent hydrogen bonds (n), and thus allow the graph-set designation $G_d^a\ (n)$.[46] Figure 1.10 illustrates representative types of hydrogen bonding between the donor (D) and the acceptor groups (A).

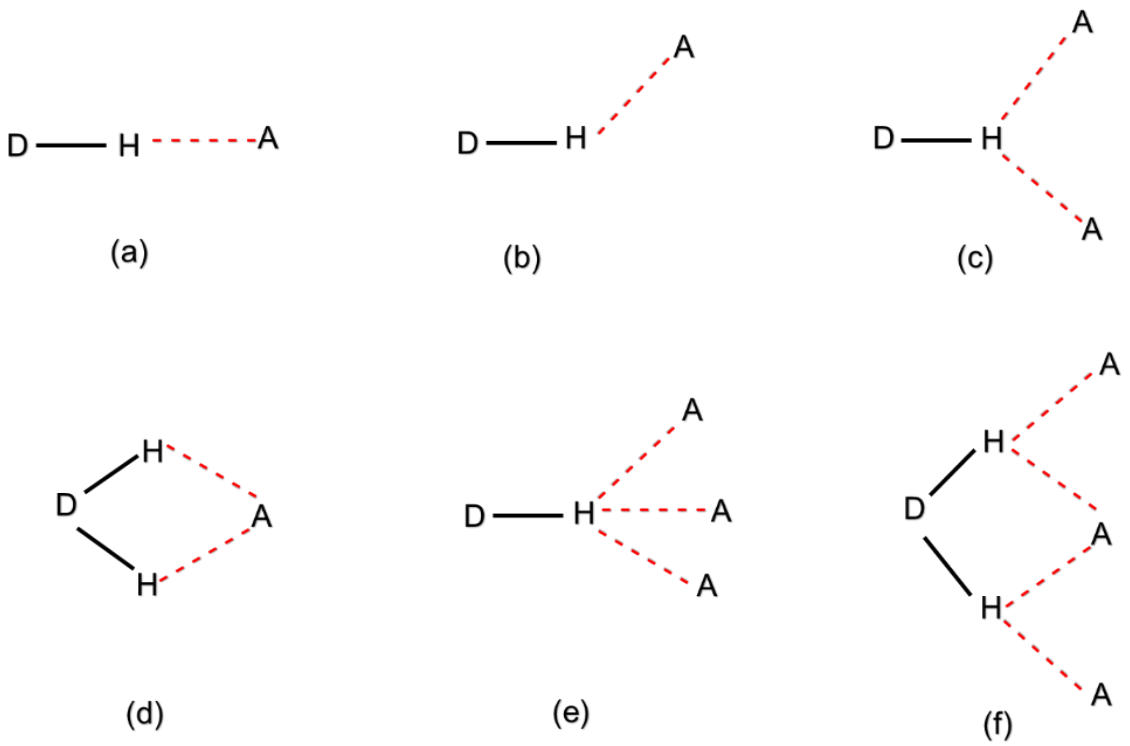

Figure 1. 10: Various types of hydrogen bonding between donor and acceptor groups: (a) linear, (b) bent, (c) donating bifurcated, (d) accepting bifurcated, (e) trifurcated and (f) three-centre bifurcated.[55]

Table 1. 3: Characteristic types of hydrogen bonds.[56,57]

Strength	Example	D···A ($d_{D\cdots A}$, Å)	H···A ($d_{H\cdots A}$,Å)	D-H···A (θ)
Very strong	$[F-H-F]^-$	2.2-2.25	1.2-1.5	175-180
Strong	O-H···O-H	2.6-3.0	1.6-2.2	145-180
	O-H···N-H	2.6-3.0	1.7-2.3	140-180
	N-H···O=C	2.8-3.0	1.8-2.3	150-180
	N-H···O-H	2.7-3.1	1.9-2.3	150-180
	N-H···N-H	2.8-3.1	2.0-2.5	150-180
Weak	C-H···O	3.0-4.0	2.0-3.0	110-180

1.6 Crystal engineering

Crystal engineering is a branch of supramolecular chemistry that concerns the crystalline solid state. The basis of crystal engineering was described early in 1961 by Von Hippel in detail under the term molecular engineering.[58] Later in 1971, Gerhard Schmidt used the principles in a crystalline cinnamic reaction with photodimerization.[59]

Today crystal engineering includes three distinct activities: 1) the study of intermolecular interactions; 2) the study of packing modes and 3) the study of crystal properties and their relationship with the crystal packing.[60] According to Desiraju, the main goal of crystal engineering is the construction of crystal structures from molecular structures.[61] Crystal engineering techniques cover many aspects of intermolecular interactions in the solid-state including crystal structure prediction, control and analysis[62] Desiraju, defined crystal engineering as" *the understanding of intermolecular interactions in the context of crystal packing, and the utilization of such understanding in the design of new solids, with desired physical and chemical properties*".[60] Several areas of intermolecular assemblies other than crystalline solids can be applied in crystal engineering. These areas include: protein ligand

recognition, supramolecular polymer design and drug delivery systems.[63] Based on this, crystal engineering has drawn together investigators from many disciplines including organic chemistry, inorganic chemistry, physical chemistry, X-ray crystallography, materials sciences and computational chemistry.[64]

1.7 Multicomponent Crystals

Multicomponent crystals can be considered as the mixture of two or more components in the crystal structure. Childs and co-workers defined it as the composition of two or more components (atoms, ions or molecules) held together by means of intermolecular interactions.[65] The first multicomponent crystal was described and made by Wöhler[66] in 1844 under the name quinhydrone (cocrystal of benzoquinone and hydroquinone). Subsequently several studies reported multicomponent crystals under different names (Table 1.4) including addition compounds,[67] organic molecular compounds,[68] complexes[69] and heteromolecular crystal.[70] Table 1.4 lists earlier reports on multicomponent crystals.

Table 1. 4: Earlier work on multicomponent crystals.

Year	Author	Event
1844	Wöhler	Quinhydrone
1937	Buck and co-worker	Addition compounds
1937	Anderson and co-worker	Organic molecular compounds
1960	Hall and co-worker	Complexes
2005	Pekker and co-workers	Heteromolecular crystal

Today, the definition and classification of multicomponent crystals has evolved. Several distinctive types of multicomponent crystal structures were finally classified which include solvates, hydrates, cocrystals and salts. This classification considers their nature in the mixture presented and their properties after being formed. For example, solvates are multicomponent crystals which result from a solid and a solvent. When the solvent present is water, the resultant crystal is called a hydrate. Cocrystals can be classified as a

multicomponent crystal resulting from two neutral compounds whereas salts are ionic compounds that result from the neutralization reaction of an acid and base. It must be noted that each of these compounds can display some other forms of crystal structures, called polymorphs, having different properties. Figure 1.11 illustrates the schematic representation of multicomponent crystals**.**

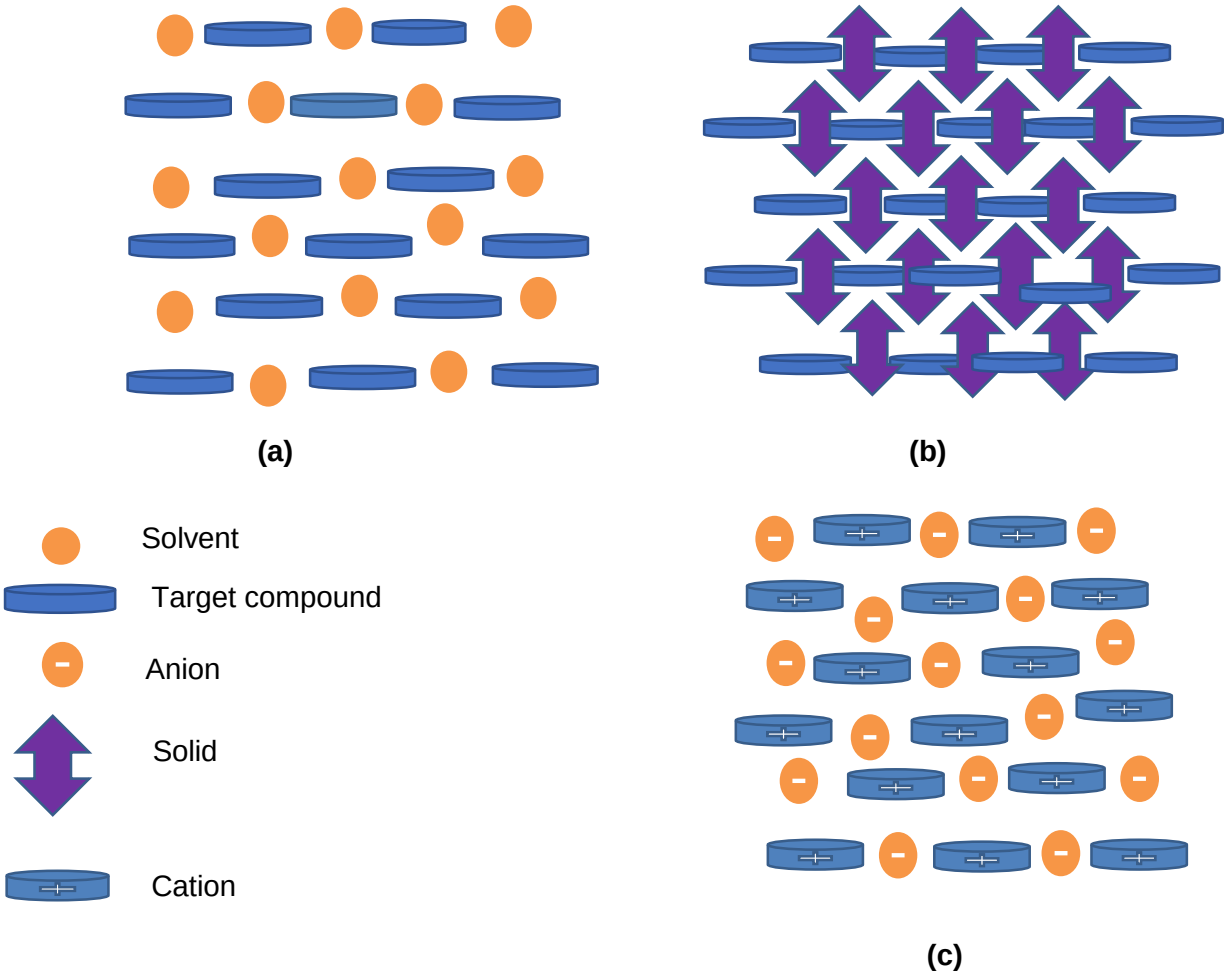

Figure 1. 121: Schematic representation of (a) molecular solvate/hydrate, (b) cocrystal and (c) salt.

1.8 Cocrystals

Although various approaches have been made to clarify the definition of a cocrystal, there is still debate surrounding it, but most agree with the general statement “a cocrystal is a crystalline solid containing multiple components”. According to the draft proposed by the United States Food and Drug Administration (FDA), `*cocrystals are solids that are crystalline single phase materials composed of two or more different molecular and/or ionic compounds having the molar ratio different from both solvates and salts*.”[71] Similarly, Shan *et al*. defined it as the crystalline structures resulting from the mixture of two or more components in a definite stoichiometric ratio where the arrangement in the crystal lattice is not based on ion pairing.[72] Furthermore, Almarsson *et al*. noted that a cocrystal is a multiple component crystal where all solid starting materials are under ambient conditions.[73]

The molecular recognition driven assembly process is important in the design and synthesis of cocrystals,[74] and its principal involvement in many areas of functional solid-state material.[73] Pharmaceutical cocrystals can be defined as molecular complexes, which contain an active pharmaceutical ingredient (API)[75,76] as a parent drug and a small neutral organic molecule called a co-former. The importance of pharmaceutical cocrystals lies in their ability to fine-tune physicochemical properties of APIs.[77] APIs can be represented in various crystalline forms, consequently each of those forms will display unique properties (morphology, hygrocospicity, thermal stability and solubility) which can affect the new solid form in terms of efficacy and delivery.[78]

Academic research and industrial application in the study of pharmaceutical cocrystals offers opportunities to access new solid forms and modify physical properties.[79] Cocrystal and salt formation have demonstrated the ability to improve physical properties including dissolution rate,[80] compressibility,[81] and physical stability.[82]

1.9 Salts

A salt can be defined as an ionic compound which results from the transfer of a proton between two compounds.[83,84] Salt formation is more attractive and effective to address the issue of poor aqueous solubility and enhance bioavailability. [85,86] Most medicines on the market are distributed in the form of salts containing the ionic API form which is the preferred solid state

product of the drug material.[87] In terms of solubility, Elder *et al*. accentuated several advantages of salts highlighting studies by Berge *et al*,[85] Gould,[88] and Serajuddin.[86] Salts can offer the following benefits: improvement of the APIs purity, isolation of the APIs, stability, and manufacturability and can strongly influence irritancy or toxicity of the dosage form. They also specified that, this can only be accomplished by influencing the solid-state properties of the APIs such as intrinsic dissolution rate, crystallinity, hygroscopicity, melting point, bulk physical properties and polymorphism or solvation. Similarly, Lara *et al,* and Almarsson *et al*, noted that salt preparation is one of the most attractive alternative crystalline solid forms due to low cost and practical procedures of preparation, high yield, producibility and purity.[89]

In this project, both salts and cocrystals were obtained and characterized. The prediction of outcome of the crystallisation experiments was made based on the pK_a rule.

1.10 Salts Vs Cocrystals

Salts and cocrystals are classified as multicomponent crystals that are formed by the mixture of two or more components in the crystal structure. The formation of a salt or a cocrystal can be predicted based on the ΔpK_a between the acid and the base. In general, a salt will form if $\Delta pK_a > 2$ or 3 with cocrystal formation predicted if $\Delta pK_a < 0$.[90, 91] Childs *et al.*[65] proposed a salt-cocrystal continuum highlighting that when ΔpK_a is between 0 and 3 prediction becomes difficult. These pK_a rules were further studied by Cruz-Cabeza[92] who proposed that for $-1 < \Delta pK_a < 4$ the probability of salt formation is directly related to the increase in the ΔpK_a values. For example, Mohamed *et al*.[93] studied the solid forms of pyridine and 4-dimethylpyridine with five different carboxylic acids. The pK_a values in aqueous solution were obtained from the literature. The acids formed salts and cocrystals with pyridine and the neutral $COOH\cdots N_{pyr}$ or ionic $COO^- \cdots H\text{-}N_{pyr}^+$ variants of hydrogen bonds were observed, whereas for 4-dimethylpiridine, only salts were found. These findings were consistent with the ΔpK_a rule. Furthermore, Stilinovic *et al*.[94] studied cocrystals and salts of gentisic acid ($pK_a = 2.82$) with twenty different pyridines (spanning a range of $-0.7 < \Delta pK_a < 4.7$) and obtained 22 complexes. Their pK_a values were determined experimentally in aqueous solution. The results showed that proton transfer did not occur for $\Delta pK_a < 2$, however proton transfer always occurred for $\Delta pK_a > 2.5$. The uncertainty range was found to be 0.5 of a unit and could be indicative of the larger range required to make accurate predictions from calculated (pK_a) instead of experimentally determined pK_a values.

In another study by Childs *et al*,[95] 2- aminopyridine complexes with a variety of carboxylic acids were investigated. It was observed that, in the range $0 < \Delta pK_a < 2$, eight cocrystals and

seven salts were formed. The intermediate range, where either a cocrystal or salt can form, is delineated by a transition range, and not fixed ΔpK_a values such as 0 and 3. The finding from this study was used to account not only for the poor correlation between pK_a values and proton transfer, but also for the unpredictability of the intermediate range and the molecular environment.

1.11 Objectives of the study

The objective of this study was to explore the methods (crystallisation, grinding and slurry experiments) of combining two components into a single solid form with well-defined stoichiometry by employing a substituted phenylacetic acid, 3-chloro-4-hydroxyphenylacetic acid, with organic bases. In this study the differences in pKa values was used to predict the formation of salts or cocrystals and determine whether this agrees with the experimental findings. Furthermore, the study also investigated intermolecular interactions of all new solid forms including their correlating properties (eg thermal stability) with their structures. All solid forms were characterised using well-known techniques including:

- Thermal analysis (thermogravimetry (TG), and differential scanning calorimetry (DSC)).
- Powder X-ray diffraction and single crystal X-ray diffraction.
- Fourier transform infrared spectroscopy (FTIR)

References

[1] Stahly, G. P. 2007. *Cryst Growth Des, 7, 1007-1026.*

[2] Desiraju, G. R. Crystal engineering. From molecules to materials. *J. Mol Struct.* (2003). 54-56.

[3] Nehm, S. J., Rodriguez-S, B., Rodriguez-H, N. 2006. *Cryst Growth Des*, 6, 592-600.

[4] Vögtle, F. 1991. Supramolecular chemistry. *John Wiley & sons, Ldt: Chichester.*

[5] Lehn, J.-M. 2002. Supramolecular chemistry and self-assembly special features: Toward complex matter: Supramolecular chemistry and self-organization. *Proc. Nat. Acad. Sci. USA,* 99, 4763-4768.

[6] Dunitz, J. D. 2007. Thoughts on crystals as Supramolecules. *John Wiley & Sons, Ltd*, 1-30.

[7] Gennady, V., Oshovsky, D., Reinhoudt, N., Willem, V. 2007. Supramolecular Chemistry in Water. *Angew. Chem. Int Ed.* 46, 14, 2366-2393.

[8] Harold, M., Schmeck, J. R. 1987. Chemistry and Physics Nobel Hail Discoveries on Life Superconductors; Three Share Prize for Synthesis of Vital Enzymes. *N.Y Times* October 15.

[9] Mukherjee, A. 2015. *Cryst Growth Des*, 15, 3076-3085.

[10] Desiraju, G. R. 2010. *J. Chem. Sci*, 122, 5, 667-675.

[11] Desiraju, G. R. 1995*. Angew. Chem. Int. Ed, 34, 21, 2311-2327.*

[12] Walsh, R. D. B.; Bradner, M. W., Fleischman, S., Morales, L. A., Moulton, B., Rodriguez-Hornedo, N., Zaworotko, M. J. 2003. *Chem Commun*. 186-187.

[13] Almarsson, O., Zaworotko, M. J. 2004. *Chem. Commun.* 17, 1889-1896.

[14] (a) Leiserowitz, L. 1976. *Acta Cryst*, B32, 775-802. (b) Allen, F. H., Raithby, P. R., Shields, G. P. & Taylor, R. 1998. *Chem. Commun*, 9, 1043-1044. (C). Allen, F. H.; Motherwell, W. D. S.; Raithby, P. R., Shields, G. P. & Taylor, R. 1999. *New. J. Chem*, 23, 25-34.

[15] Peresypkina, E., Virovets, A., Scheer, M. 2016. *Cryst Growth Des*, 16, 2335-2341.

[16] (a) Sarma, J. A. R. P., Desiraju, G. R. 2002. *Cryst Growth Des*, 2, 2, 93-100. (b) Thakur, T. S; Desiraju, G. R. 2008. *Cryst. Growth Des,* 8, 11,: 4031-4044.

[17] Hassel, O. 1970. *Sci,* 170, 3957, 497-502.

[18] Mukherjee, A., Tothadi, S., Desiraju, G. R. 2014. *Acc. Chem. Res*. 47, 8, 2514-2524.

[19] Sakurai, T., Sundaralingam, M., Jeffrey, G. A. 1963*. Acta Crystallogr*, 16, 5, 354.

[20] Desiraju, G. R., Parthasarathy, R. J. 1989*. J. Am. Chem. Soc*. 111, 23, 8725-8726.

[21] Metrangolo, P., Resnati, G. 2014*. IUCrJ*. 1 (1): 5-7.

[22] Zallen, R. 1983. The principe of amorphous solids. *John Wiley and Sons. New York.*

[23] Bassett, L. G., Bunce, S. C., Carter, A. E., Clarck, H. M. & Hollinger, H. B. 1966. Principles of chemistry. New Jersey: Prentice-Hall: 147-177.

[24] Snyder, M. K. 1966. Chemistry: structure and reactions. United states of America: *Holt, Rinehart and Winston.*

[25] Bauer, R. C., J. P. & Marks, P. S. 2007. A conceptual introduction to chemistry. McGraw-Hiller *Higher Education*: 362-399.

[26] Drago, R. S. 1974. Principles of chemistry with practical perspectives, Boston. Allyn & Bacon.

[27] Clugston, M. J., Flemming, R. & Vogt, D. 2002. Chemistry: An introduction for Southern African Students. *Oxford: Oxford University Press*.

[28] Schroers, J., Johnson, W. L. 2000. *J. Appl. Phys. 88,1, 44-48.*

[29] Miller, G. H. 1972. Principles of college chemistry. San Fransisco: *Canfield Press*

[30] Dera, P., Lavina, B., Borkowski, L. A., Prakapenka, V. B., Sutton, S. R., River, M. L., Downs, R. T., Boctor, N. Z., Prewitt, C. T. 2008*. Geophys. Res. Lett, 35, L10301*.

[31] Petrucci, R. H. & Harwood, W. S. 1997. General chemistry: principles and modern applications. 7th *ed. New Jersey:* Prentice Hall.

[32] Fahlman, B. 2011. Material chemistry. Hardcover, XI, p 29.

[33] Glusker, J. P & Trueblood K. N. 1972. Crystal Structure Analysis*, Acta Cryst, 28, 680*.

[34] Butler, I. S. & Harrod, J. F. 1989*. Inorganic chemistry: principles and applications*.

Redwood City, Calif: Benjamin-Cummings Pub Co.

[35] Steed, J. W. & Atwood, J. L. 2009. Supramolecular Chemistry. *John Wiley & Sons, Ltd*: 27-36.

[36] Steed, J. W., Turner, D. R. & Wallace, K. 2007. *Core concepts in supramolecular chemistry and nanochemistry*. Chichester: John Wiley.

[37] Lindoy, L. F., Atkinson, I. M. 2000. Self-assembly in Supramolecular Systems. *RSC of Chem*.

[38] Dougherty, D. A. 2007. Cation-π interactions involving aromatic amino acids. *J. Nutr*, 137(6):1504S–1508S.

[39] Schneider, H. J. 2004. Van der Waals Forces. *Encyclo SupramolChem*, 2:1550-1555. New York, Taylor and Francis.

[40] Itzykson, C. & Zuber, J. B. 1980. Quantum Field Theory*. McGraw-Hill, New York.*

[41] Lehn, J.-M. 1995. Supramolecular Chemistry. *1 ed.; VCH: Weinheim*.

[42] Desiraju, G. R. 1989. The design of organic solids, Crystal Engineering, *Amsterdam: Elsevier.*

[43] (a). Etter, M. C. 1982. *J. Am. Chem. Soc*, 104, 1095-1096., (b). Etter, M. C. 1990. *Acc. Chem. Res,* 23, 120., (c). Etter, M. C. 1991. *J. Phys. Chem*, 95, 4601.

[44] Leiserowitz, L., Schmidt, G. M. J. 1969. *J. Chem. Soc. A*, 16, 2372.

[45] Etter, M.C. 1985. *Isreal. J. Chem*, 25, 312-319.

[46] Jeffrey, G. A. 1997. An Introduction to Hydrogen Bonding, *New York, Oxford University Press*, chapter 2.

[47] Brown, T. L., LeMay, H. E., Bursten, B. E., Burdge, J. R. 2003. *Chemistry, The Central Sc, 9th ed, Prentice Hall,* chapter 11.

[48] Parthasarathi, R., Subramanian, V & Sathyamurthy, N. 2006. *J. Phys. Chem. A*. 110, 3349-3351.

[49] Mohajeri, A & Nobandegani, F. F. 2008. *J. Phys. Chem. A*. 112, 281-295.

[50] Li, Q. Z., An, M. L., Luan, F., Li, W. Z., Gong, B. A & Cheng, J. B. 2008. *J. Phys. Chem. A*. 112, 3985-3990.

[51] Kolev, S. K., Pektov, P. St., Rangelov, M. A & Vayssilov, G. N. 2011. *J. Phys. Chem. A.* 115, 14054-14068.

[52] Desiraju, G. R. 2011. Pharmaceutical salts and co-crystals: retrospect and prospects.

[53] Etter, M. C. 1990. *Accts. Chem. Res*., 23, 120.

[54] Bernst, J., Davis, R. E., Shimoni, L., Chang, N. L. 1995. *Angew. Chem, Int. Engl*., 34, 1555.

[55] Desiraju, G. R. & Steiner, T. 1999. The Weak Hydrogen Bond in Structural Chemistry and Biology, Oxford University Press, Oxford.

[56] Jeffrey, G. A. 1997. An Introduction to Hydrogen Bonding. *New York, Oxford University Press*, Chapter 2.

[57] Moore, M. & Stezowski, J. J. 1995 *Cryst Rev*. *CRRVEN*., 4:211-282.

[58] Hippel, V. AR. 1962. Molecular designing of materials. *Sc,* 138(3537), 91-108.

[59] Schmidt, G. M. J. 1971. Photodimerization in the solid state, *Pure App. Chem.* 27, 647

[60] Desiraju, G. R. 1989. The design of organic solids, Crystal engineering. *Elsevier: Amsterdam.*

[61] Desiraju, G. R. 2005. Chemistry-The middle kingdom *Curr. Sci.* 88, 374-380.

[62] Steed, J. W & Atwood, J. L 2002. Supramolecular Chemistry, *John Wiley and Sons. Ldt, Chichester. Vol*, 15, 236.

[63] Desiraju, G. R. 2010. *J. Chem. Sci, Vol*. 122. 667-675

[64] Sharma, C. V. K. 2002. *Cryst Growth Des*. 2, 465-474.

[65] Childs, S. L., Stahly, G. P., Park, A. 2007. *Mol Pharm. Vol* 4, 3, 323-338.

[66] Wöhler, F. 1844. Untersuchungen über das chinon. Annalen., 51: 153.

[67] Buck, J. S. & Ide, W. S. 1937. *J. Am. Chem. Soc*. 53: 2784-2787.

[68] Anderson, J. S. 1937. Structure of organic molecular compounds. *Nature*. 140: 583-584.

[69] Hall, B. & Devlin, J. P. 1967. *J. Phys. Chem,* 71: 465-466

[70] Pekker, S., Kováts, É., Oszlányi, G., Bényei, G., Klupp, G., Bortel, G., Jalsovszky, I., Jakab, E., Borondics, F., Kamarás, K., Bokor, M., Kriza, G., Tompa, K., Faigel, G. 2005. Rotor-stator molecular crystals of fullurenes and cubane. *Nature Mat*, 4: 764-767.

[71] Aitipamula, S., Banerjee, R., Bansal, A. K., Biradha, K., Cheney, M. L., Choudhury, A. R., Desiraju, G. R., Dikundwar, A. G., Dubey, R., Duggirala, N., Ghogale, P. P., Gosh, S., Goswami, K. P., Goud, N. R., Jetti, R. R. K., Karpinski, P., Kaushik, P., Kumar, D., Kumar, V., Moulton, B., Mukherjee, A., Mukherjee, G., Myerson, A. S., Puri, V., Ramanan, A., Rajamannar, T., Reddy, C. M., Rodriguez-Hernedo, N., Rogers, R. D., Row, T. N. G., Sanphui, P., Shan, N., Shete, G., Singh, A., Sun, C. C., Swirft, J. A., Thaimattam, R., Thakur, T. S., Thaper, R. K., Thomas, S. P., Tothadi, S., Vangala, V. R., Variankaval, N.,Vishweshar, P., Weyna, D. R & Zoworotko, M. J. 2012. *Cryst Growth Des*, 2147-2152.

[72] Shan, N., Zoworotko, M. J. 2008. The role of cocrystal in the pharmaceutical science, *Drug Disc. Today*, 13, 440-446.

[73] Almarsson, ö., Zoworotko, M. J. 2004. *Chem. Commun*., 1889-1896.

[74] Aakeröy, C. B., Desper, J., Urbina, J. F. 2005. *Chem. Comm*, 2820.

[75] Qiao, N., Li, M., Schlindwein, W., Malek, N., Davies, A., Trappitt, G. 2011*. Int. J. Pharm, 419,1-11.*

[76] Nate, S. & Ann, N. 2009**.** *Crystal Growth & Design,* 9, 6, 2950-2967.

[77] (a) Brittain, H. G. 2013. *J. Pharm. Sci*, 102, 311-317; (b) Babu, N. J. & Nangia, A. 2011. *Cryst Growth Des*, 11, 2662-2679.

[78] (a) Aakeröy, C. B., Fasulo, M. E & Desper, J. 2007. *Mol. Pharm*, 4, 317-322; (b) Almarsson, ö. & Zoworotko, M. J. 2004. *Chem. Commun,* 1889-1896; (c) Vishweshwar, P., McMahon, J., Bis, J. A. & Zoworotko, M. J. 2006. *J. Pharm. Sci*, 95, 499-516.

[79] Wood, P. A., Feeder, N., Furlow, M., Galek, P. T. A., Groom, C. R & Pidcock, E. 2014. *CrystEngComm*,16, 5839-5848.

[80] Zegarac, M., Leksic, E., Sket, P., Plavec, J., Bogdanovic, M. D., Bučar, D-K., Dumic, M. & Mestrovic, E. 2012. *CrystEngComm.*, 16, 32-35.

[81] Karki, S., Friščić, T., Fábián, L., Laity, P. R., Day, G. M. & Jones, W. 2009. Adv. Mater., 21, 3905-3909.

[82] Trask, A. V., Motherwll, W. D. S & Jones, W. 2006*. J. Pharm,* 320, 114-123.

[83] Jampilek, J. & Dohnal, J. 2012. Investigation of carbohydrates and their derivatives as crystallization modifiers. In Chang, C.F. (ed). *Carbohydrates - comprehensive studies on glycobiology and glycotechnology*

[84] Sekhon, B. S. 2009. *ARS Pharm*: 50, 3, 99-117

[85] Berge, S. M., Bighley, L. D., Monkhouse, D. C. 1997. *Pharm. Sci*, 66, 1-19.

[86] Serajuddin, A. T. M. 2007. *Adv. Drug Del. Rev*. 59, 603-616

[87] Stahl, P. H. & Wermuth, C. G. 2008. Handbook of pharmaceutical salts. Properties, selection and use. Weinheim*: John Wiley & Sons.*

[88] Elder, D. P., Holm, R., Diego, H. L. 2013. *J. Pharm*. 453, 88-100.

[89] Lara-Ochoa, F. & Espinosa-Pérez. 2013. *Cryst Growth Des*, 7, 1213.

[90] Bhogala, B. R., Basavoju, S., Nangia, A. 2005. *CrystEngComm*, 7, 551-562.

[91] Almarsson, ö. & Zaworotko. 2004. *Chem. Commun*, 1889.

[92] Cruz-Cabeza, A. J. 2012. *CrystEngComm*, 4: 6362-6365.

[93] Mohamed, S., Tocher, D. A., Vickers, M., Karamertzanis, P. G and Price, S. L. 2009. *Cryst Growth Desc*, 9, 2881-2889.

[94] Stilinovic, V & Kaitner, B. 2012. *Cryst Growth Des*, 12, 5763-5772.

[95] Childs S. L., Stahly G. P & Pak, A. 2007. *Mol. Pharm*, 4, 323-338

CHAPTER TWO

EXPERIMENTAL METHODS AND MATERIALS

Chapter 2 : EXPERIMENTAL METHODS AND MATERIALS

2.1 Introduction

Phenylacetic acid is an auxin (a type of plant hormone), found mostly in fruits.[1] The compound is an oxidation product of phenethylamine when acted on by the enzyme monoamine oxidase, found in humans and many organisms. It is used in perfumes, in the production of penicillin G, and in the treatment of hyperammonemia.[2] 3-chloro-4-hydroxyphenylacetic acid is a synthetic compound used to disrupt auxin influx.[3]

The crystal structure of phenylacetic acid (PAA)[4,5] has been reported in the Cambridge Structural Database[6](version 5.39, November 2017), however that of 3-chloro-4-hydroxyphenylacetic acid (CHPAA) has not been reported (version 5.39, February 2018).

The current research began with several attempted crystallizations of the target compound CHPAA using various organic solvents. Solvents were selected based on their ability to dissolve CHPAA. In the cases where CHPAA was found to be insoluble in a certain solvent a co-solvent was chosen to achieve dissolution.

2.2 Co-formers

Co-former can be described as a small neutral organic compound that is combined with a parent drug called an API to form a cocrystal.[7,8] Several groups of compounds were selected as co-formers based on their ability to hydrogen bond with the target compound. Altogether, ten co-formers were selected in this study to form new solid forms with CHPAA. The co-formers were distinctly classified based on their structural forms such as those which are linear vs those which contain aromatic rings. The linear derivatives included diethylamine (DEA) and dibutylamine (DIBUAM). The aromatic compounds included the aminopyridines (AMP) ie. 2-aminopyridine (2AMP), 2-amino-4-methylpyridine (2A4MP), 2-amino-6methylpyridine (2A6MP), 4-dimethylaminopyridine (4DMAP), nicotinamide (NAM), isonicotinamide (ISONAM), phenazine (PHZN) and 4,4'-bipyridine (BIPY). Figure 2.1 below represents the chemical structures of the target compound (CHPAA) and the co-formers used in this study.

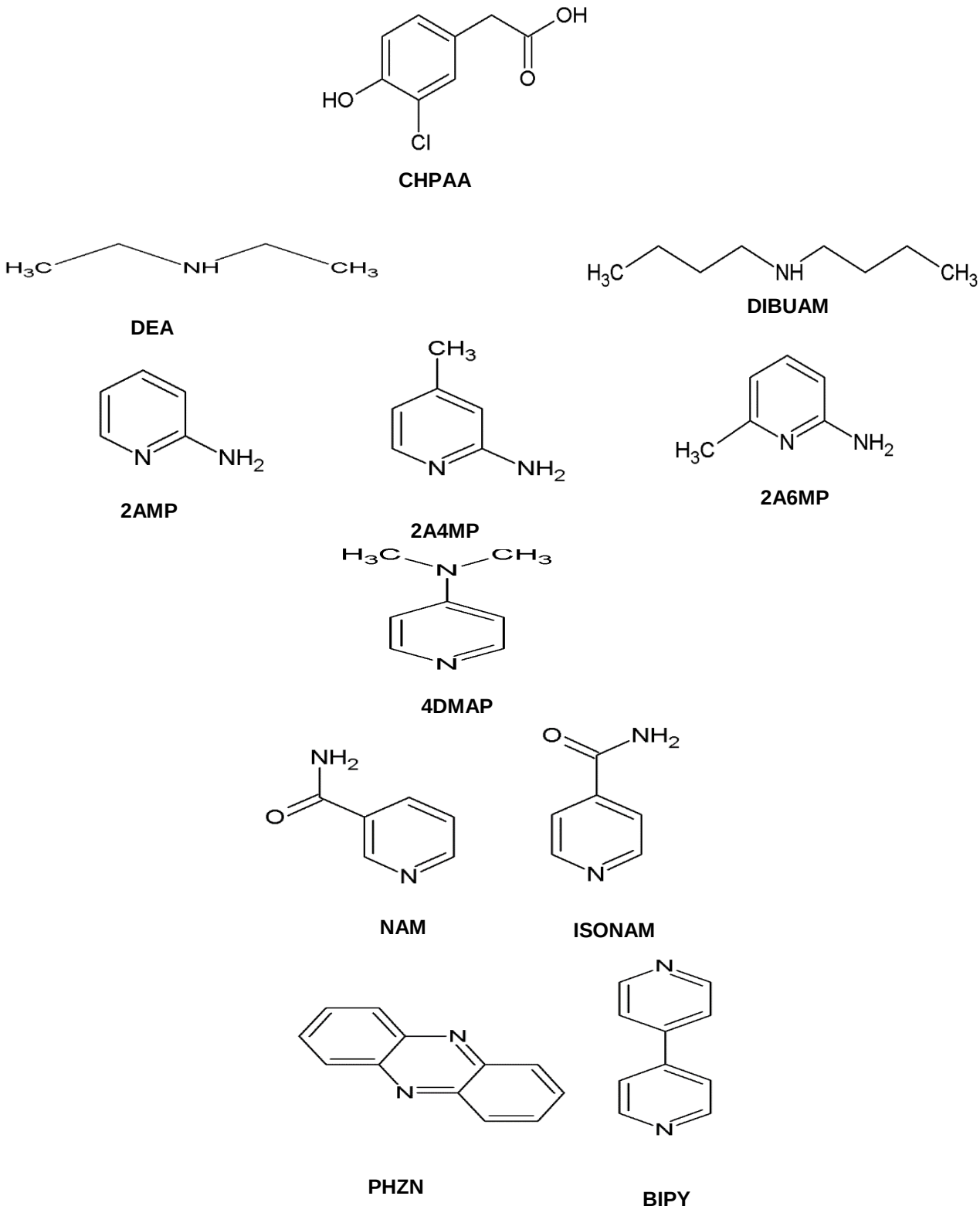

Figure 2. 1: Chemical structures of compounds used in study.

Table 2.1 lists the physical properties of the co-formers used. The software Chemicalize by ChemAxon was used to calculate the pK_a values.[9]

Table 2.1: Physical properties and pK_a of the guest compounds used in this study.

Compound	Condensed formula	Formula weight (g mol^{-1})	Melting point (°C)	pK_a
2-aminopyridine	$C_5H_6N_2$	94.117	59-60	6.84
2-amino-4-methylpyridine	$C_6H_8N_2$	108.14	96-99	7.62
2-amino-6-methylpyridine	$C_6H_8N_2$	108.14	40-44	7.60
4-Dimethylaminopyridine	$C_7H_{10}N_2$	122.12	108-110	9.7
Nicotinamide	$C_6H_6N_2O$	122.1	1 28	3.63
Isonicotinamide	$C_6H_6N_2O$	122.1	155-157	3.45
Phenazine	$C_{12}H_8N_2$	180.21	172-176	1.23
4,4'-Bipyridine	$C_{10}H_8N_2$	56.18	114	4.44/5.25
Diethylamine	$C_4H_{11}N$	73.16	/	11.09
Di-*N*-butylamine	$C_8H_{19}N$	129.28	/	11.31

2.3 Materials used

2.3.1 3-Chloro-4-hydroxyphenylacetic acid (CHPAA)

No crystal structures containing CHPAA have been reported in the Cambridge Structural Database (version 5.39, 2017). CHPAA contains a carboxylic acid functional group (Figure 2.2) which is one of the most commonly used in crystal engineering[10-11] because of its ability to form hydrogen bonds with several functional groups such as amides, amines, alcohol and many others.[12] Furthermore, CHPAA contains a hydroxyl group which can also form hydrogen bonds with suitable co-formers, as well as a chlorine atom in the *meta* position, which has the ability to form halogen bonds. Table 2.2 below lists the physical properties of CHPAA.

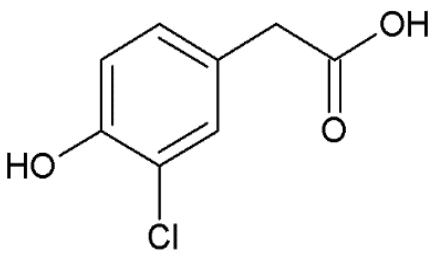

Figure 2. 2: Structural representation of 3-chloro-4-hydroxyphenylacetic acid.

Table 2. 2: Physical properties and pK_a value of CHPAA.

Compound	Condensed formula	Formula weight (g mol^{-1})	Melting point (°C)	pKa
3-Chloro-4-hydroxyphenylacetic acid	$C_8H_7ClO_3$	186.6	108-110	3.46

2.3.2 Solvents

Various solvents were used in this study and the selection was made based on their ability to dissolve the solid mixtures. Ethanol was found to be the most efficient choice of solvent either on its own or together with a co-solvent. All solvents were purchased from Sigma Aldrich and no further purification was performed. Table 2.3 lists various solvents used in this study.

Table 2. 3: Physical properties and pK_a values of solvents used.

Solvent	Acronyms	Condensed formula	Formula weight (g mol^{-1})	Boiling point (°C)	pK_a
Methanol	MeOH	CH_3OH	32.02	64.7	15.5
Ethanol	ETOH	C_2H_5OH	46.068	78.37	15.9
Chloroform	CHF	$CHCl_3$	119.38	61.2	15.5
Ether	PET	C_6H_{14}	86.18	42-62	/
Ethylacetate	ETOAC	$C_4H_8O_2$	88.11	83.47	25
1,2-Dichloroethane	DCE	$C_2H_4Cl_2$	98.96	83.47	/
Dichloromethane	DCM	CH_2Cl_2	84.93	39.6	/

2.4 Techniques

Several techniques were used in this study which include the following:

- Crystallisation
- Thermal analysis (differential scanning calorimetry and thermogravimetric analysis)
- Single crystal X-ray diffraction
- Powder X-ray diffraction
- Cocrystals and salts preparation methods
- Fourier transform infrared spectroscopy

2.4.1 Crystal Growth

The process of crystal formation from a solution is called crystallisation. Crystallisation is the process whereby molecules rearrange themselves to form a new crystalline lattice. [13,14] The main processes of crystallisation are nucleation and crystal growth. Nucleation is the step whereby solute molecules start to gather into clusters. These molecular aggregates must be stable otherwise they will redissolve. In crystal growth, nucleation and growth occur simultaneously with supersaturation. Supersaturation is the driving force of the crystallization process. A large number of techniques are available for the crystallisation of small organic molecules such as diffusion methods, slow cooling, slow evaporation and other techniques.[15] In this study, the slow evaporation technique was used in all crystallisations.

The new solid form (salt/cocrystal) was obtained by dissolving the target compound and co-former in a 1:1 molar ratio in different organic solvents, followed by gentle heating on the hot plate and stirring until the solution turned clear. At times, co-solvents were used when incomplete dissolution of the mixture was observed. The co-solvent was selected based on their ability to completely dissolve the solid mixture. The solvent was left to evaporate slowly at ambient temperature and crystals were observed after a few weeks or months.

2.4.2 Thermal Analysis

Thermal analysis refers to a category of analytical chemistry techniques whereby physical and chemical changes of a sample are monitored as the sample temperature is either increased or decreased. [16- 17] Thermal analysis techniques which include both thermogravimetry (TG) and differential scanning calorimetry (DSC) were used to determine the thermal decomposition of the resulting compounds. Both TG and DSC were performed on a Perkin-Elmer Pyris 6 system under nitrogen purge gas with a flow rate of 20 $mLmin^{-1}$. Samples of 2-5 mg were removed from the mother liquor, dried with filter paper then crushed to a fine powder and placed in an open pan for TG analysis and vented pan for DSC analysis. Table 2.4 provides different parameters of the thermal analysis instruments used in this study.

2.4.3 Differential Scanning Calorimetry (DSC)

Differential scanning calorimetry is a technique used to measure the difference in the energy between a sample and an inert reference as a function of time and temperature. In this technique, the energy released or absorbed by the sample when heated or cooled is observed as endothermic or exothermic peaks. The endothermic peaks are plotted upwards ($\Delta H>0$) and the exothermic peaks are plotted downwards ($\Delta H<0$). Thus, results of DSC analysis provide information on melting point, reaction energy and temperature as well as crystalline temperature.[18] The DSC instrument requires an empty standard aluminium pan as a reference, and a second pan for holding the sample. These are positioned in the furnace. Heat flow is measured by comparing the difference in temperature throughout both the test sample and the reference.

In this study, the technique was conducted to estimate the onset temperatures and the enthalpy changes during the loss of a volatile component from the solid. This enthalpy change could be due to desolvation, phase transformation, melting and other thermal events. The temperature of both pans is increased at a constant rate. [19]

2.4.4 Thermogravimetric Analysis (TGA)

Thermogravimetric analysis is the technique used to measure the change in mass of a material as a function of increased temperature.[16,18] A TGA instrument contains a thermobalance which is an analytical microbalance, furnace, temperature programmer, and sample holder, an enclosure for establishing the required atmosphere, and a recorder to display the data. The temperature range for the furnace is from room temperature to 1000°C, with a heating rate up to 100°Cmin^{-1}. A curve resulting from the TGA analysis is referred to as a mass loss curve. Generally, the TGA results yield a graph displaying mass loss versus temperature/time due to various events such as dehydration, decomposition or oxidation of a certain compound.[20]The crystals were removed from the mother liquor and placed on filter paper, crushed to a fine powder and placed in open ceramic pans for TG analysis. Thus, the data retrieved from the TGA results are the temperature at which a change in mass occurs, the temperature at which a solvent is released from a crystal lattice and also information on the kinetics of desolvation of the compound undergoing analysis. Several events such as decomposition stages and

fractional weight loss can be evaluated by this technique. Table 2.4 below illustrates the thermal analysis parameters.

Table 2. 4: Thermal analysis parameters.

	DSC and TGA
Model	Perkin-Elmer DSC 6 System
Purge gas	Nitrogen gas @ 20 $mLmin^{-1}$
Temperature programme	303-573 K @ 10 $Kmin^{-1}$

2.4.5 Single Crystal X-Ray Diffraction

Single crystal X-ray diffraction is one of the most definitive methods for elucidating the crystal structures of compounds. [21- 22]

X-rays are electromagnetic radiation with a very short wavelength ($\lambda = 10^{-10}$ m = 1 Å).[23] X-ray diffraction is a non-destructive analytical technique used to determine crystal structures and atomic spacing. Unit cell dimensions, bond length, bond angles and details of site-ordering of crystalline materials can be obtained with the technique.

X-ray diffraction studies of crystalline materials have four major steps: crystallization, data collection, structure solution and refinement. Diffraction data for all compounds were collected on a Bruker APEX II diffractometer with a graphite-monochromated MoK_{α} = 0.71073 Å at 173 K using an Oxford Crystream 700.[24]

SHELXS-97[25] was the computer programme used to solve structures and the graphical user interface was X-seed.[26] The space group was determined by using the collected intensities and pre-determined cell parameters as inputs to the programme XPREP.[27] SHELXL-97 was used for the refinement of the structures and uses full-matrix least-squares against F^2 for unique reflections.

$$\sum \boldsymbol{w}\,(\boldsymbol{F_0^2} - \boldsymbol{kF_C^2})^2$$

The agreement between the observed structure factors (F_o) and the calculated structure factors (F_c) were monitored by assessing the residual index R. The indirect measurement of the accuracy of the structure is the residual R which must be low in value if the model is satisfactory.

The residual index R_1 is the agreement between the observed and calculated structure factors based on F $(Eq\ 1)$ while the residual index *w*R is the agreement based on F^2 $(\mathrm{Eq.}\,2)$.

$$\mathrm{R}_1 = \frac{\sum ||\boldsymbol{F_0}| - |\boldsymbol{F_c}||}{\sum |\boldsymbol{F_o}|} \qquad (Eq.1)$$

$$w\mathrm{R} = \left[\frac{\sum \boldsymbol{w}(\boldsymbol{F_o^2} - \boldsymbol{F_c^2})^2}{\sum \boldsymbol{w}(\boldsymbol{F_o^2})^2}\right]^{\boldsymbol{1/2}} \qquad (Eq.2)$$

Where *w* is the weight allocated to the structure factor during the refinement.

$$w = \frac{\boldsymbol{1}}{\boldsymbol{\sigma^2(F_o^2) + (aP)^2 + bP}} \qquad (Eq.3)$$

where $$\mathbf{P} = \frac{\boldsymbol{\max(0, F_o^2) + 2F_c^2}}{\boldsymbol{3}} \qquad (Eq.4)$$

while a and b were also refined for each structure.

The Goodness of Fit (S) was obtained for all the structures and is dependent on F^2 $(see\ Eq.5)$

$$\mathbf{S} = \left[\frac{\boldsymbol{W}(|\boldsymbol{F_O}|^2 - |\boldsymbol{F_c}|^2)^2}{(\boldsymbol{N} - \boldsymbol{n_p})}\right]^{\boldsymbol{1/2}} \qquad (Eq.5)$$

where N is the number of reflections and n_p is the total number of parameters refined.

X-ray powder patterns were calculated using LAZY PULVERIX[28] and compared to experimental powder patterns for crystallization. All crystal packing diagrams were generated with POV-RAY.[29] The program LAYER[30] was utilized to test systematic absences and space group symmetry.

2.4.6 Computing Packages

LazyPulverix[28]: calculates the theoretical powder X-Ray diffraction pattern from single crystal data.

PovRay[29]: renders graphics for structures.

PovLabel[31]: X-Seed component used to edit the atomic labels of PovRay.

Xprep[27] : processing of Bruker diffraction data. SHELX input files can be set up and the space group determined.

Platon[32]: used to calculate the structure molecular parameters.

ConQuest[33]: the primary program for searching and retrieving information from the Cambridge Structural Database.

Mercury[34] : Software which allows for the investigation and analysis of crystal structures. It can be used to generate packing diagrams, define and display Miller planes and take a slice through a crystal in any direction. Also, it calculates voids based either on contact surface or solvent accessible surface and intermolecular potentials.

2.4.7 Powder X-Ray Diffraction (PXRD)

Powder X-ray diffraction is an analytical method used for the identification of crystalline phases and it also provides information regarding unit cell dimensions.[22,35] PXRD can generate a fingerprint pattern for a particular crystalline structure thus making its use in qualitative analysis of importance.[18] It is a technique where X-rays are used for structural characterization of materials. The phenomenon is based on interference between X-ray radiation and the crystalline material.

The diffraction is described by Bragg's law:

$$\mathbf{n}\lambda = 2d\sin\theta$$

θ: glancing angle between the X-ray beam and the plane of the crystal under irradiation.

d: distance between atomic layers in a crystal.

λ : the wavelength of the incident X-ray beam

n: the integer

Diffraction occurs only when the Bragg's law is satisfied.

This technique was used to identify new phases and compounds as each compound shows a unique pattern due to its structural features. Samples were powdered manually by grinding both the target compound and the co-former in 1:1 molar ratio with solvent drops for a few minutes and the resulting powder was placed in a sample holder in the path of the X-ray beam. A D2 PHASER Bruker diffractometer with Cu-Kα radiation (1.54184 Å) was the instrument used in this study. The voltage tube and current were at 30 kV and 10 mA max, respectively with scintillation counter, 1-dim LYNXEYE detector. The scanning process of each sample was between 4-50˚ 2θ.

The experimental powder patterns were compared to that of the starting material and to the calculated patterns (generated from the known structures) using LAZYPULVERIX.[28]

2.5 Alternative methods of preparation of salts and cocrystals

The slow evaporation technique was generally used for the preparation of the salts and cocrystal. However, this method was found to be challenging in terms of solvent selection as well as utilising more solvent than other greener methods such as grinding and solvent drop grinding. The solids obtained from these alternative methods were compared to those obtained from the slow evaporation technique.

2.5.1 Preparation of salt/cocrystal by grinding

Solid state grinding is where the materials are mixed and crushed in a mortar and pestle. In solvent drop grinding, the sample together with a few drops of solvent is added to a mortar. The mixture was then ground for a specified time and the resultant powder was analysed using PXRD. The PXRD pattern was compared to the calculated PXRD pattern obtained from LAZYPULVERIX.[28]

2.5.2 Preparation of salt/cocrystal by slurry

A slurry is obtained from the suspension of solid particles in a liquid or solvent. Dilute mixtures of the compounds were heated until dissolution occurred. The hot plate was then switched off and the mixture was stirred until a slurry was formed. The powder obtained was analysed using PXRD and the resultant patterns were compared to the calculated one obtained from LAZYPULVERIX.[28]

References

[1] Wightman & Lighty, D. L. 1922. *Physiologia Planturam. Plant Sc.* 55,1, 17-24.

[2] Adams, R., Thal, A. F. 1922. *Org. Synth*, 2, 63.

[3] Lankova, M., Smith, R. S., Pesek, B., Kubes, M., Zazimalova, E., Petrasek, J., Hoyerovâ, K. 2010. *J. Exp B,* 6113, 3589-3598.

[4] Patterson, A. L.1927. *Philos. Mag,* 3, 1252.

[5] Hodgson, D. J., Asplund, R. O. 1991. *Acta Cryst*. 47, 1986-1987.

[6] Groom, C. R., Bruno, I. J., Lightfoot, M. P., Ward, S. C. 2016. The Cambridge Structural Database, *Acta Cryst*. B72, 171-179.

[7] Trash, V. A. 2007. *Mol. Pharm*, 4, 301.

[8] Stahly, G. P. 2006. Cryst Growth Des, 6, 925

[9] Chemicalize was used for the prediction of pK_a values https://chemicalize.com/ developed by *ChemAxon (*http://www.chemaxon.com)", *August* 2018.

[10] Fábián, L., Hamill, N., Eccles, K. S., Moynihan, H., & Maguire, A. R. 2011. *J. Am. Chem. Soc*, 11: 3522-3528.

[11] Bacchi, A., Cantoni, G., Crocco, D., Granelli, M., Pagano, P. & Pelagatti, P. 2014. *CrystEngComm,* 16, 6, 1001-1009.

[12] Zhang, Y., Evans, J., Rowe, W., Dinehart, K., Quinn, B. & Connelly, P. 2012. *CrystEngComm*, 14,2422-2427.

[13] Atwood, J. L. & Steed, J. W. 2004. Encyclopaedia of Supramolecular Chemistry. *New York, CRC Press.*

[14] SamorÂ, P. & Cacialli, F. 2014. Functional supramolecular architectures: for organic electronics and nanotechnology, *Weinheim: Wiley-VCH.*

[15] Laudise, R. A. 1970. The Growth of Single Crystal. Solid State Physical Electronic Series *Inc, New Jersey.*

[16] Wunderlich, B. 1990. Thermal analysis. Boston: *Academic Press.*

[17] Brown, M. E. & Gallagher, P. K. 2008. Handbook of thermal analysis and calorimetry: recent advances, techniques and applications. Ohio: *Elsevier Science.*

[18] Steed, J. W. 2013. *Sciences,* 34, 185-193.

[19] Caira, M. R. & Nassimbeni, L. R. 1996. Phase transformations in inclusion compounds, kinetics and thermodynamics of enclathration. In Comprehensive Supramolecular Chemistry, Vol. 6, Chapter 5.

[20] Haines, P. J. Thermal Methods of Analysis. Blackie *Academic & Professional, London*. 1995.

[21] Clegg, W., Blake, A. J., Gould, R. O. & Main, P. 2001. Crystal structure analysis: principles and practice. Chester: International Union of Crystallography; *Oxford University Press*.

[22] Karki, S., Fábián, L., Friščić, T. & Jones, W. 2007. *Org Lett*. 9, 3133-3136.

[23] Rissanen, K. 2014. X-Ray Crystallography. Encyclopedia of Supramolecular Chemistry, 2: 1586-1591.

[24] Bruker 2005. APEX2. Version 1.0-27. *Bruker AXS Inc, Madison, Wisconsin, USA.*

[25] Sheldrick, G. M. & Schneider, T. R. 1997. SHELXL: High resolution refinement. *Macromol. Cryst,* 277, 319-343.

[26] Barbour, L. J. 2003. X-Seed: Graphical interface for SHELX program. *J. Supramol. Chem, 1,* 189-191.

[27] XPREP, Data Preparation and Reciprocal Space Exploration, Version 5.1/NT© 1997, Bruker Analytical X-ray Systems.

[28] Yvon, K., Jeitschko, W. & Parthe, E. J. 1997. LAZY PULVERIX, a computer program, for calculating X-ray and neutron diffraction powder patterns. *J. Appl. Cryst,* 10: 73-74.

[29] Pov-Ray for Windows, Version 3. le Watcom. win32. The persistence of vision development team, © 1991-1999.

[30] Barbour, L. J. 1999. LAYER. *J. Appl. Cryst*, 32: 351.

[31] Barbour, L. J. 2001. X-Seed – A software Tool for Supramolecular Crystallography, *J. Supramol. Chem,* 1: 189-191.

[32] Spek, A. L. 2009. *Acta Cryst, D65, 148-155.*

[33] Allen, F. H. 2002. *Acta Cryst*, B, 58-380.

[34] Wolff, S. K., Grimwood, D. J., McKinnon, J. J., Jayatilaka, D. & Spackman, M. A. 2007. *Crystal Explorer* 2.1. University of Western Australia, Perth.

[35] Peterson, M. L., Stanto, M. K., Kelly, R. C., Staples, R. & Cheng, A. 2011. *CrystEngComm,* 13, 4, 1170-1180.

CHAPTER THREE

SALTS OF 3-CHLORO-4-HYDROXYPHENYLACETIC ACID WITH LINEAR AMINE DERIVATIVES

Chapter 3 : SALTS OF 3-CHLORO-4-HYDROXYPHENYLACETIC ACID WITH LINEAR AMINE DERIVATIVES

Salts are crystalline ionic compounds that result from the proton transfer occurring between an acid and a base. In this chapter, two linear amine derivatives, diethylamine (DEA) and di-*N*-butylamine (DIBUAM) were chosen as co-formers to form new solid forms with 3-chloro-4-hydroxyphenylacetic acid (CHPAA). Both co-formers were selected based on their pK_a values which showed the strong expectation of salt formation when combined with CHPAA. The pK_a differences between each co-former and the acid were calculated and found to be as follows: ΔpK_a (DEA-CHPAA) = 10.58 - 3.46 = 7.12 and ΔpK_a (DIBUAM-CHPAA) = 10.75- 3.46 = 7.29. These results validate the ΔpKa rule,[1] since proton transfer is expected to occur for ΔpK_a greater than 2-3. This was confirmed by the crystal structure solutions and analysis. The C-O distance of the acid was also analysed to confirm the formation of salts. Further studies were done to determine the properties and thermal correlations of the new solid forms.

.

3.1 Salts of 3-chloro-4-hydroxyphenylacetic acid (CHPAA) with Diethylamine (DEA) and Dibutylamine (DIBUAM)

3.1.1 Introduction

A salt is an ionic compound resulting from the transfer of the proton between two compounds such as an acid and a base. During the chemical reaction involving an acid and a base, the probability of having a charge distribution is strong. Thus, if the charge distribution occurs from acid to base, the process is called proton transfer and the resulting compound is then a salt. In this study, groups of compounds were selected based on their abilities to form hydrogen bonds with the acid. Both linear and aromatic bases were selected as co-formers in the study. The linear bases, which are part of the discussions in this chapter, are diethylamine (DEA) and dibutylamine (DIBUAM). The multicomponent compounds of CHPAA with aromatic bases are discussed in chapter 4. 3-chloro-4-hydroxyphenylacetic acid was selected as a target molecule to form new solid forms with different co-formers (bases). The pK_a rule was used to predict whether the final compound should be a cocrystal or a salt.[2] The experimental results were compared to the crystal structures obtained from single crystal X-ray diffraction. The new solid crystal forms were characterized using well-established techniques including thermal analysis (thermogravimetry and differential scanning calorimetry), powder X-ray diffraction and Fourier transform infrared spectroscopy. Different methods of preparation of the new solid forms were also explored including neat grinding, solvent drop grinding and slurry experiments.

Both salts were prepared in a similar way by introducing together in a vial 30 mg of 3-chloro-4-hydroxyphenylacetic acid with 3 ml of the respective amine followed by addition of a few drops of ethanol. The solutions were slightly heated by stirring at 30 °C for a few minutes using the hot plate. The vials were sealed and kept at room temperature (25°C). After 1-3 weeks, the crystals were obtained and analysed using several experiments which confirmed the presence of new solid forms. Figure 3.1 below illustrates the molecular structure diagram of compounds involved in this chapter.

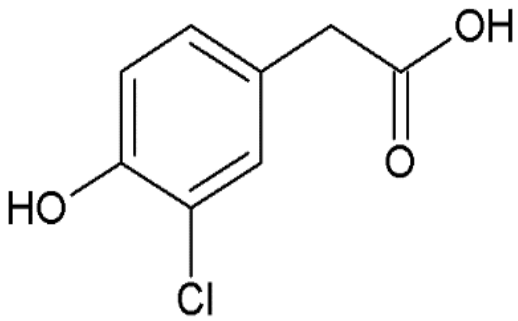

CHPAA

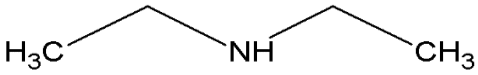

DEA

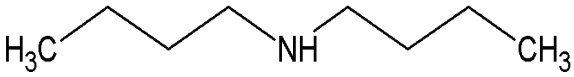

DIBUAM

Figure 3. 1: Chemical structures of CHPAA and the linear amines.

3.2 Structural analysis

Both salts formed block-like crystals, with a dark yellow colour observed for the dibutylaminium-3-chloro-4-hydroxyphenylacetate salt $(CHPAA^{-})(DIBUAM^{+})$, while the diethylaminium-3-chloro-4-hydroxyphenylacetate salt $(CHPAA^{2-})(2DEA^{+})$ formed yellow-green crystals. Both structures were solved using direct methods with SHELXS-97.[3] The model was refined by full-matrix least squares on F^2 using SHELXL-97. Table 3.1 below illustrates crystal data parameters.

Table 3. 1: Crystal data and data collection parameters

Compound	$(CHPAA^{2-})(2DEA^{+})$	$(CHPAA^{-})(DIBUAM^{+})$
Host:guest ratio	1:1	1:1
Molecular formula	$C_{16}H_{29}ClN_2O_3$	$C_{16}H_{26}ClNO_3$
Formula weight [g mol^{-1}]	332.86	315.83
Crystal system	Triclinic	Monoclinic
Space group	*P*$\bar{1}$	C2/*c*
Z	2	8
D_{cal} [g cm^{-3}]	1.212	1.225
a [Å]	8.0728(16)	22.063(4)
b [Å]	8.9900(18)	13.192(3)
c [Å]	13.506(3)	14.638(3)
α [°]	87.09	90.00
β [°]	81.25	126.49(3)
γ [°]	70.27(3)	90.00
Volume [Å^3]	911.9(3)	3425.4(12)
μ(Mo-Kα) [mm^{-1}]	0.223	0.232
T[K]	173(2)	173(2)
F(000)	360	1360
No. of reflections collected	26693	34213
No. of unique reflections	4525	4106
No. of reflections with I>2σ(I)	3594	377
Index ranges	h±10; k:±11; -17<l<18	h±29; k:±17 ; l:±19
GooF	1.029	1.028
Final R indices [I>2σ]	R_1=0.0364; wR_2=0.0972	R_1=0.0352; wR_2 =0.1281
R indices [all data]	R_1=0.0494; wR_2=0.0896	R_1=0.0460; wR_2=0.1146
Largest diff peak and hole [eÅ^{-3}]	0.280; -0.246	0.248; -0.270
$2\theta_{max}$ [°]	56.6	55.92

3.2.1 Salt of diethylaminium-3-chloro-4-hydroxyphenylacetate

The salt of $(CHPAA^{2-})(2DEA^{+})$ crystallized in the triclinic space group ($P\bar{1}$) and its asymmetric unit contains one $CHPAA^{2-}$ anion and two DEA^{+} cations (Figure 3.2). The unit cell consists of two $CHPAA^{2-}$ anions and four DEA^{+} cations (Z = 2). For the $CHPAA^{2-}$ anion the C-O bond length difference (Δd_{C-O}) was found to be 0.0033 Å. Proton transfer occurred from the carboxylic acid to the nitrogen of one of the DEA bases (Figure 3.2); therefore, the compound is a salt. Furthermore, the hydroxyl hydrogen of the CHPAA molecule was transferred to the nitrogen of the second DEA base. It should be noted that for all numbering schemes, the hydrogen atoms were omitted except for those involved in major hydrogen bonding. This was applied throughout the thesis where applicable. Figure 3.3 below illustrates the hydrogen bond numbering scheme.

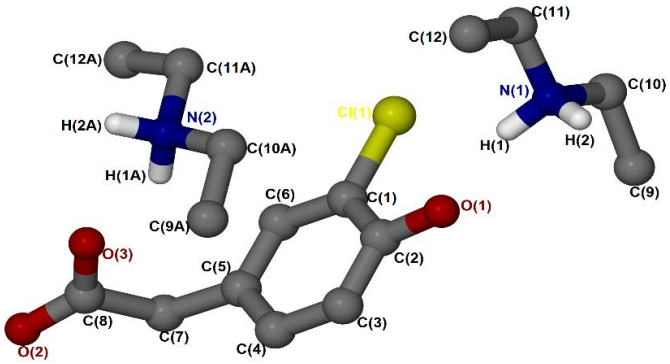

Figure 3. 2: Asymmetric unit of $(CHPAA^{2-})(2DEA^{+})$.

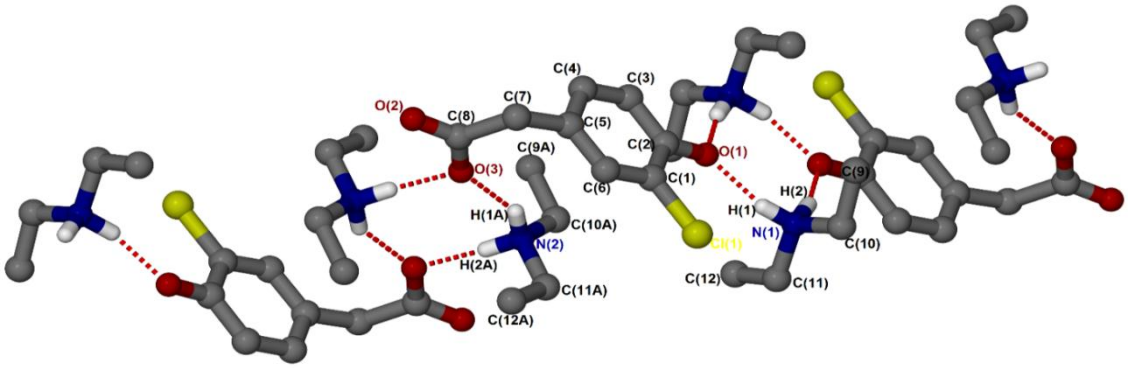

Figure 3. 3: Hydrogen bond numbering scheme of ($CHPAA^{2-}$)($2DEA^{+}$).

Based on the structural analysis (Figure 3.3), it was observed that $(CHPAA^{2-})(2DEA^{+})$ presents two major intermolecular interactions of N-H•••O. These interactions include N1-H1•••O1 and N2-H1A•••O3 generating two $R_4^2(8)$ rings[4]. Furthermore, the structure also displays C3-H3•••O3 and C11-H11•••Cl1 weak interactions. The hydrogen bond parameters are summarised below in table 3.2. The C3-O3 distance also correlates with those discussed by Desiraju *et al*.[5] Figures 3.4 and 3.5 below illustrate the packing diagram and voids of $(CHPAA^{2-})(2DEA^{+})$ along [100].

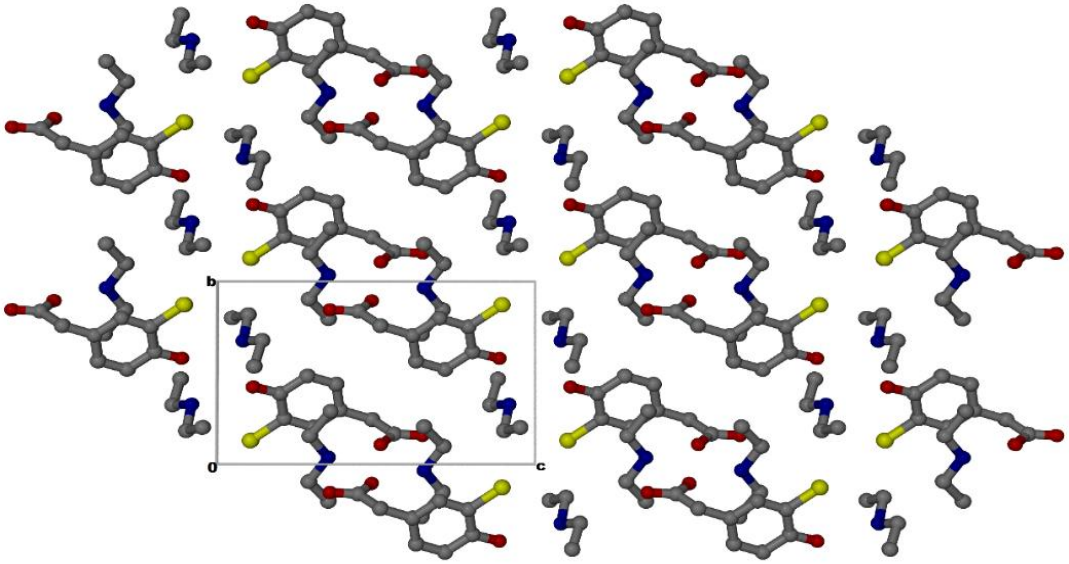

Figure 3. 4: Packing diagram of ($CHPAA^{2-}$)($2DEA^{+}$) along [100].

CHPAA molecules are aligned in an up and down fashion with respect to the chlorine, whereas the cations (DEA^{+}) alternate in the opposite direction. The cations were deleted from the structure to show the channels occupied by the solvent (Figure 3.5) and this was applied throughout the thesis where applicable.

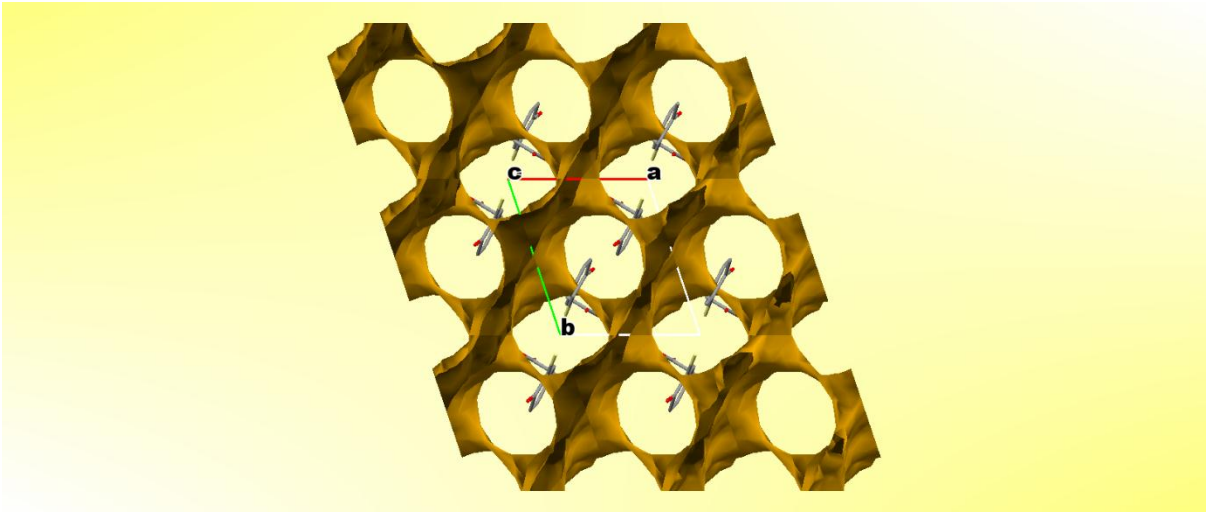

Figure 3. 5: Channels in which the DEA^{+} cations of ($CHPAA^{2-}$)($2DEA^{+}$) are situated, as viewed along [001].

3.2.2 Salt of dibutylaminium-3-chloro-4-hydroxyphenylacetate

The crystal structure of the salt $(CHPAA^{-})(DIBUAM^{+})$, was successfully solved in the monoclinic space group (*C2/c*) and its asymmetric unit displayed one $CHPAA^{-}$ anion and one $DIBUAM^{+}$ cation (Figure 3.6). The unit cell consists of eight $CHPAA^{-}$ anions and eight $DIBUAM^{+}$ cations (Z= 8). The C-O difference (Δd_{C-O}) was found to be 0.02 Å indicating salt formation with proton transfer occurring from the carboxylic acid group to the nitrogen. Figure 3.7 below illustrates the hydrogen bond numbering scheme.

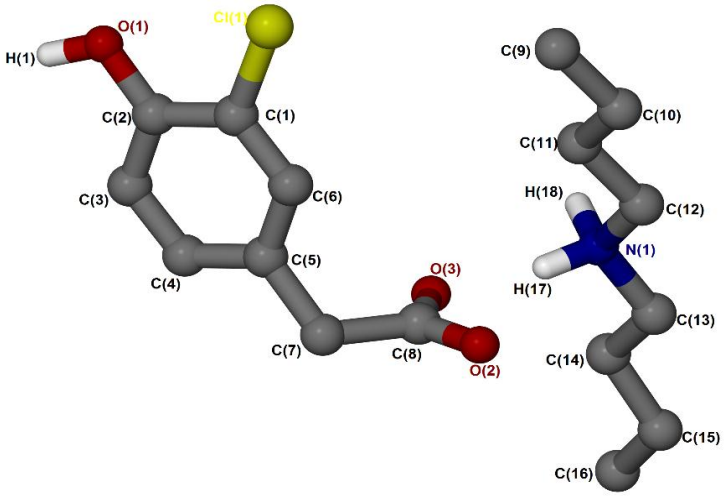

Figure 3. 6: Asymmetric unit of ($CHPAA^{-}$)($DIBUAM^{+}$).

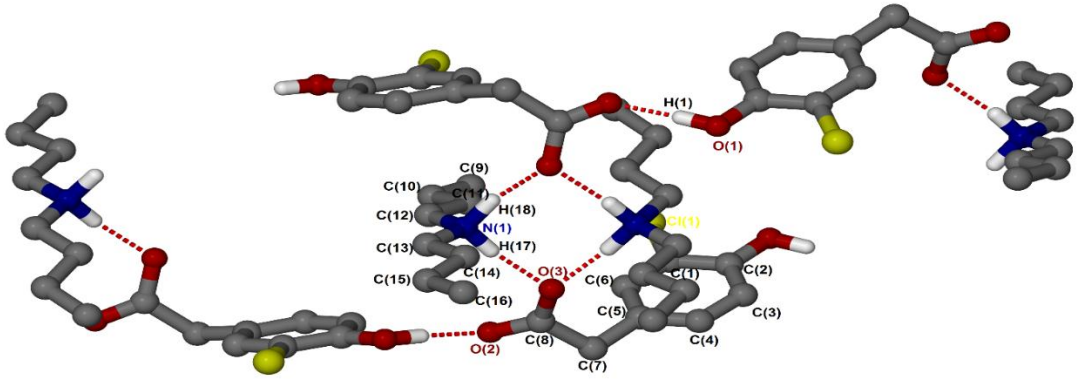

Figure 3. 7: Hydrogen bond numbering scheme of ($CHPAA^-$)($DIBUAM^+$).

In the case of $(CHPAA^-)(DIBUAM^+)$, both N-H groups are involved in hydrogen bonding to a carboxylate forming $R_4^2(8)$ rings, with the hydroxyl group also forming O-H•••O hydrogen bonds to neighbouring carboxylate oxygens (Figure 3.7). Furthermore, N-H•••O (amine-acid) and O-H•••O (acid-acid) interactions form the extended network system by generating a chain with a graph set notation of $C_1^1(9)$. The structure also displays a weak interaction namely C10-H10A•••Cl (Table 3.2). Figures 3.8 and 3.9 below illustrate the packing diagram and void space in which the cations are situated in $(CHPAA^-)(DIBUAM^+)$. Figures 3.8 and 3.9 show that the acid (CHPAA) is oriented to form chains allowing the cation ($DIBUAM^+$) to accommodate in channels.

Crystal structures in both cases show that the molecules in the solid-state are packed in a manner that does not facilitate aromatic π-stacking interactions between the carboxylic acids. Thus, no π- π stacking interactions were observed in both cases.

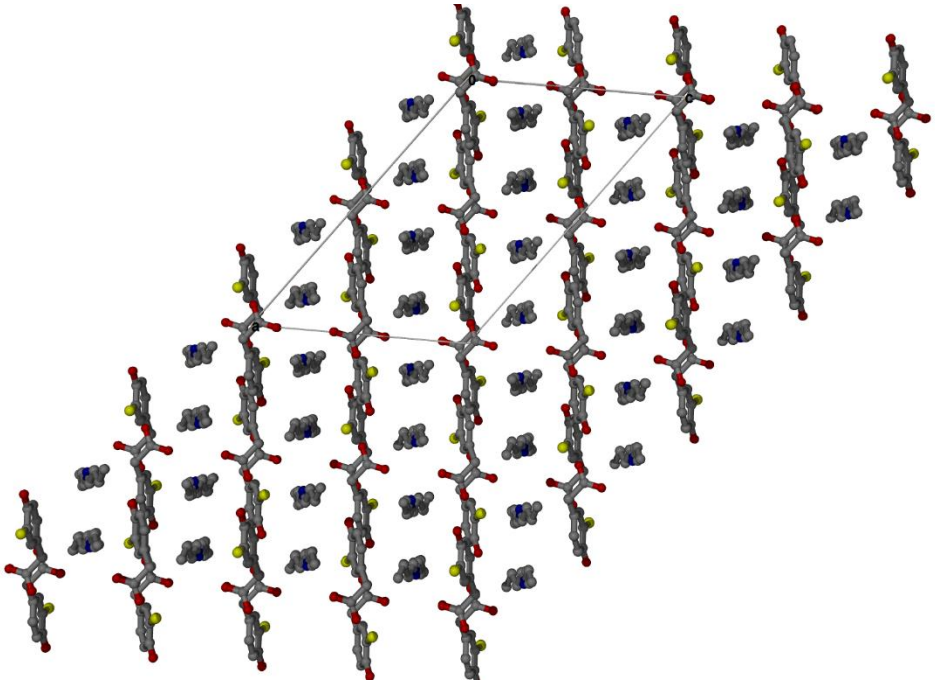

Figure 3. 8: Packing diagram of ($CHPAA^-$)($DIBUAM^+$) along [010].

.

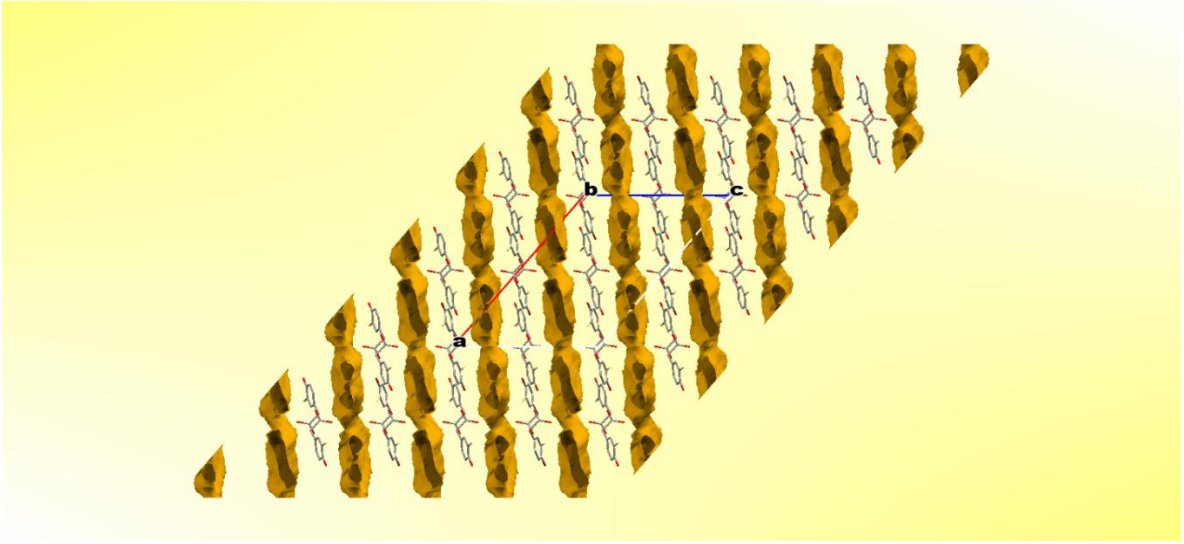

Figure 3. 9: Packing voids of ($CHPAA^-$)($DIBUAM^+$) along [010].

Table 3. 2: Geometric data of hydrogen bonding in salts formed by of CHPAA.

D-H•••A	d(D-H) Å	d(H•••A) Å	d(D•••A) Å	D-H•••A (^{0})	Symmetry operator
$(\boldsymbol{CHPAA^{2-}})(\boldsymbol{2DEA^{+}})$					
N1-H1⋯O1	0.91	1.85	2.717(2)	159	-
N2-H1A⋯O3	0.90	1.95	2.756(2)	148	-
N1-H2⋯O1	0.92	1.74	2.653(2)	169	-x+1, -y+1, -z
N2-H2A⋯O3	0.89	1.80	2.685(2)	176	-x+1, -y, -z+1
C3-H3•••O2	0.95	2.73	3.613(2)	155	1-x, 1-y, 1-z
C11-H11•••Cl1	0.99	2.98	3.821(2)	143	2-x, -y, -z
$(\boldsymbol{CHPAA^{-}})(\boldsymbol{DIBUAM^{+}})$					
N1-H17⋯O3	0.91	1.85	2.753(1)	171	-
N1-H18⋯O3	1.01	1.75	2.740(2)	166	-x, y, ½-z
O1-H1⋯O2	0.91	1.70	2.606(2)	174	½+x, -y-½, ½+z
C10-H10A•••Cl	0.99	3.09	2.766(2)	126	-x, y, ½+z

3.3 Torsion angles of CHPAA$^-$

The substituted phenylacetic acid (CHPAA) was found to adopt two major conformations when interacting with DEA and DIBUAM, which can be described by two torsion angles (Figure 3.10). For the diethylaminium salt, the torsion angles of the CHPAA anion involving the ring and the twisting of the acetic acid group are τ_1(C6-C5-C7-C8) = 96.7^0 and τ_2(O2-C8-C7-C5) =161.8 ^{0} . In the case of the dibutylaminium salt, the torsion angles are τ_1(C6-C5-C7-C8) = 58.2^0 and τ_2 (O2-C8-C7-C5) = 125.6 ^{0} . Based on the obtained values, it was concluded that, 3-chloro-4-hydroxyphenylacetate has more freedom of rotation when combined with DEA than with DIBUAM. It should be noted that the negative and positive signs observed with the angle measurement were not considered during the analysis. The CHPAA$^-$ anions in both structures were overlayed (Fig 3.11) using Mercury (version 3.5, 2017). Table 3.3 illustrate torsion angles of CHPAA$^-$.

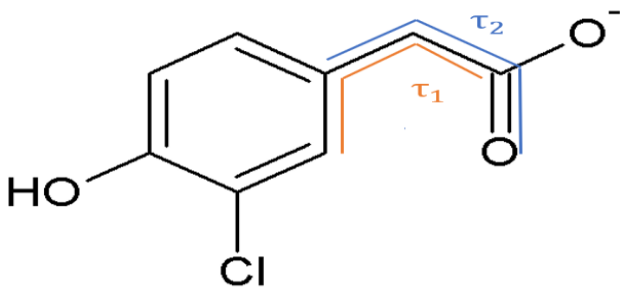

Figure 3. 10: Torsion angles of CHPAA$^-$.

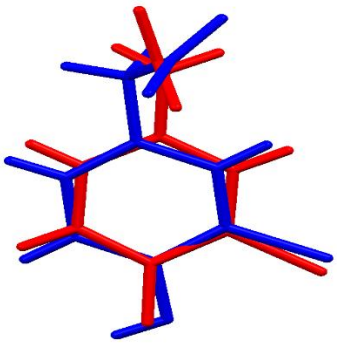

Figure 3. 11: Overlay of CHPAA^{-} from (CHPAA^{2-})(2DEA^{+}) red and (CHPAA^{-})(DIBUAM^{+}) blue.

Table 3. 3: Torsion angles of (CHPAA^{2-})(2DEA^{+}) and (CHPAA^{-})(DIBUAM^{+}).

	$(CHPAA^{2-})(2DEA^{+})$	$(CHPAA^{-})(DIBUAM^{+})$
Torsion angles/°		
τ_1(C6-C5-C7-C8)	96.7	58.2
τ_2(O2-C8-C7-C5)	161.8	125.6

3.4 Thermal analysis of (CHPAA^{2-})(2DEA^{+}) and (CHPAA^{-})(DIBUAM^{+})

The TGA for both salts is given in Figure 3.12. Two mass loss steps were observed for $(CHPAA^{2-})(2DEA^{+})$. The first mass loss of 10.5% (Figure 3.12a) was observed at around 315 K and the second mass loss at 396 K overlaps with the decomposition of the CHPAA. The first mass loss of 10.5% is due to the loss of half molecule of the DEA which correlated with its low boiling point. The DSC curve of $(CHPAA^{2-})(2DEA^{+})$ below shows two endotherm peaks. The first peak at 316 K corresponds to the partial loss of DEA and the second peak at 391 K is due to the melt of CHPAA and the loss of the remaining DEA.

In the case of $(CHPAA^{-})(DIBUAM^{+})$, a continuous mass loss was observed at approximately 400 K, due to the loss of DIBUAM and the melt of the CHPAA. The higher temperature at which DIBUAM was released also correlated to its higher boiling point compared to DEA. Table 3.4 below illustrates the thermal analysis data for both salts.

Table 3. 4: Thermal analysis data of $(CHPAA^{2-})(2DEA^{+})$ and $(CHPAA^{-})(DIBUAM^{+})$

Salts	$(CHPAA^{2-})(2DEA^{+})$	$(CHPAA^{-})(DIBUAM^{+})$
Host: Guest ratio	1:2	1:1
TG theo.% mass loss	44.4	41
Exp. % mass loss	10.5 (initial step)	-
DSC endotherm for loss of solvent (T_{on}/K)	316	-
DSC endotherm for the melt of CHPAA (T_{on}/K)	391	392 (including loss of remaining DIBUAM)
Solvent normal bp (K)[6,7]	329	433

The DSC curve of $(CHPAA^{-})(DIBUAM^{+})$ below shows only one endotherm peak, which is due to the release of the solvent at the same time as the melting of the acid occurs. This peak also appeared at the same temperature range as the decomposition mass loss observed in the TGA.

The diethylaminium salt has a higher (1:2) stoichiometric relationship with 3-chloro-4-hydroxyphenylacetic acid than the salt of dibutylamine (1:1) and this can be correlated to the molecular sizes. The short chain of *N*-ethylamine is approximately half the size of the *N*-dibutylamine chain and two DEA molecules will occupy approximately the same free spaces in the crystal as one DIBUAM molecule.

In summary the thermal stability trend for the salts can be related to the physicochemical properties of the amines. These include: boiling points, pK_a values and chain lengths. The boiling point is also related to the chain length, the longer the chain, the higher the boiling point and therefore the more stable the compound. DIBUAM has the longer chain, higher boiling point (433 K) and has a slightly higher pK_a value (pK_a=10.75) than the DEA (pK_a= 10.58). The thermal stability trend is: $(CHPAA^{-})(DIBUAM^{+}) > (CHPAA^{2-})(2DEA^{+})$.

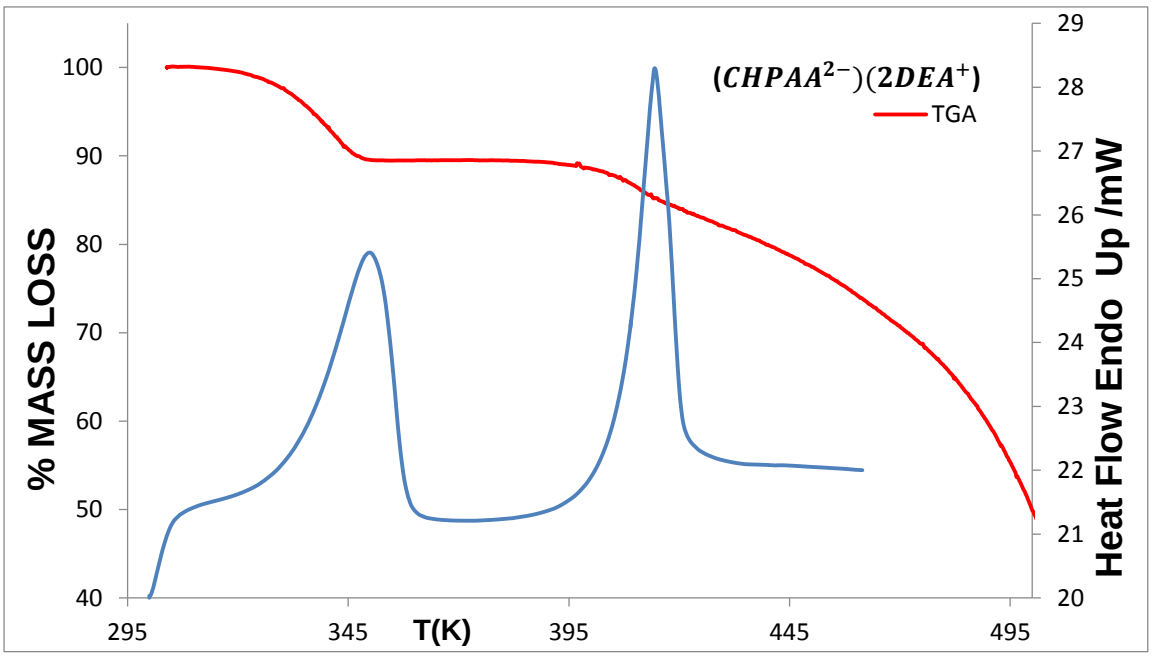

(a)

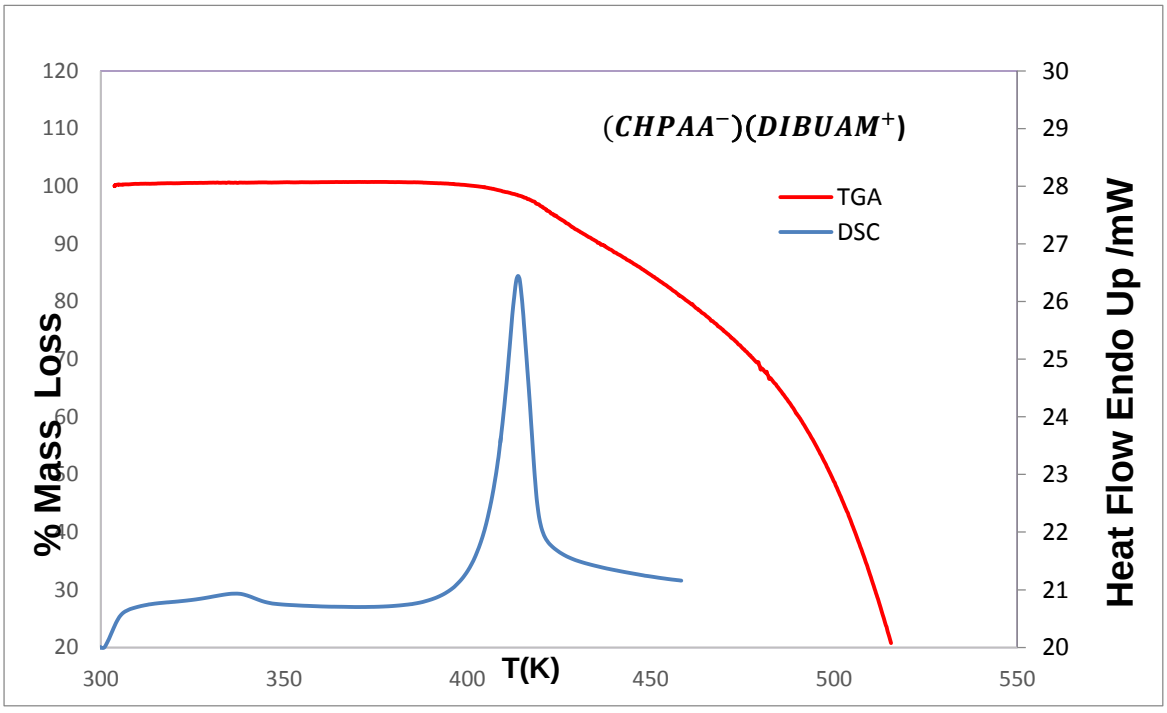

(b)

Figure 3. 12: TGA and DSC curves of a: ($CHPAA^{2-}$)($2DEA^{+}$) and b: ($CHPAA^{-}$)($DIBUAM^{+}$).

3.5 Grinding and slurry experiments of ($CHPAA^{2-}$)($2DEA^{+}$) and ($CHPAA^{-}$) ($DIBUAM^{+}$)

PXRD analyses of the powders obtained from the grinding and slurry experiments were performed to show that both salts obtained by the slow evaporation technique can also be prepared using other techniques. The calculated PXRD patterns obtained from LAZYPULVERIX[8] were compared to the PXRD of the single crystal and the starting material as well as those obtained from the various preparation methods. The results are shown in Figures 3.13 and 3.14. Pure 3-chloro-4-hydroxyphenylacetic acid and di-*N*-butylamine were mixed in a 1:1 ratio and ground for 15 minutes followed by the addition of a few drops of ethanol. The PXRD pattern of the ground product is shown in green. The slurry experiment was done by dissolving about 30 mg of 3-chloro-4-hydroxyphenylacetic acid in excess of di-*N*-butylamine followed by the addition of a few drops of ethanol to dissolve the solute completely. The resulting powder was filtered and left to dry at ambient temperature. The slurry PXRD pattern was collected (yellow) after a few minutes. It was observed that the calculated PXRD pattern (red) was similar to the slurry PXRD pattern (yellow). The PXRD pattern of the ground product (green) was slightly similar to the calculated PXRD pattern but still contained peaks present in the starting material (blue), indicating that the reaction was incomplete. Similarly, 3-chloro-4-hydroxyphenylacetic acid and diethylamine were mixed in a 1:1 ratio and ground for 15 minutes followed by the addition of a few ethanol drops. After 30 minutes, the PXRD pattern of the ground product (green) was obtained. The slurry experiment was done in the same way as the first one. It was observed that the PXRD pattern of the ground product was similar to the slurry pattern (yellow) but different to the calculated (red) and starting material (blue) patterns, indicating that these reactions was also incomplete.

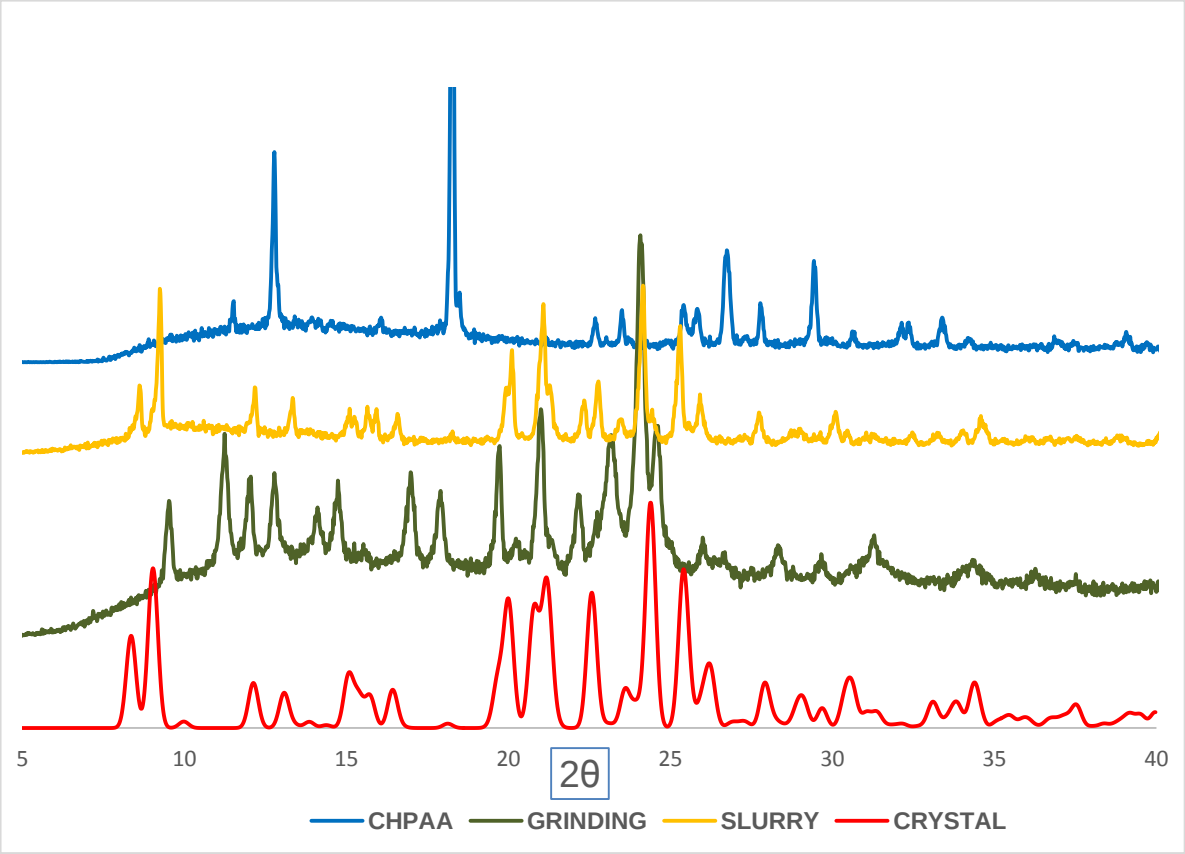

Figure 3. 13: PXRD patterns of ($CHPAA^-$)($DIBUAM^+$).

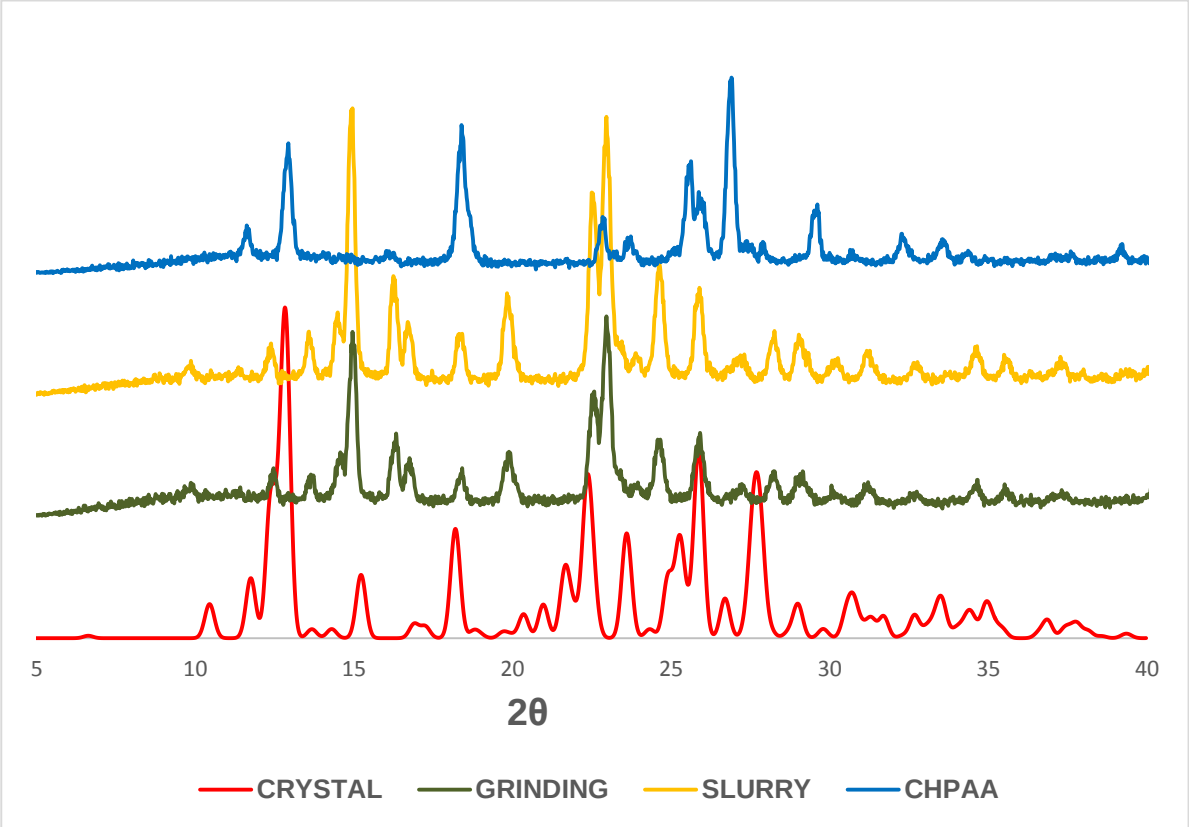

Figure 3. 14: PXRD patterns of ($CHPAA^{2-}$)($2DEA^{+}$).

3.6 FTIR spectroscopy

FTIR spectroscopy was done to characterise the new solids formed. Different functional groups have different vibrational modes that correspond to absorption of radiation at characteristic wavelengths. Both salts produced bond absorptions at different locations and intensities in the IR spectra. Recognizing the functional groups in each starting material helps in interpreting and confirming the results of the new solids synthesised. Spectra were obtained from the universal attenuated total reflectance (UTAR) infrared spectrometer Perkin Elmer spectrum two.[9] Sample spectra were measured over the range of 4000-400 cm $^{-1}$. The IR spectra of $(CHPAA^{2-})(2DEA^{+})$ and $(CHPAA^{-})(DIBUAM^{+})$ are shown in Figures 3.15 and 3.16**,** and both salts exhibited different spectra when compared to the starting material (CHPAA). This change in spectra indicated the formation of new solids. In this part of the study we were only interested in two major bands involving new solid forms. These bands are OH and COO^{-} or COO, characterising the nature of the new solid forms. It should be noted that our discussion is based on the proton transfer process. This allows us to indicate the nature of the new solid forms whether it is a salt or a neutral cocrystal and this was applied throughout the thesis where applicable. If proton transfer occurred, the free OH band absorption at 3440 cm^{-1} (a) should not be expected in the spectrum of new solid forms (b) and thus, the nature of the resulting compound should be a salt. The COO^{-} band should also be present confirming the formation of an anion. However, if proton transfer did not occur, we expected the free OH band to reappear in each spectrum (red) of the new solid forms and the COO band as a confirmation of neutral molecules. This indicated that the free OH group was not involved in the proton transfer process and therefore, the nature of the new compound should be a cocrystal. Both IR spectra displayed free OH bands at 3440 cm-^{1}(a) and the bands are absent in both new solid spectra (b and c). This indicated that OH was involved in the proton transfer process and thus, the resulting compounds are salts. This was also further confirmed by the formation of COO^{-} band at 1641cm^{-1} (b and c). The band at 2920 cm^{-1} (a) assigned to the carboxylic acid, also reappeared in both new solid forms spectra but shifted. This can be explained by the intermolecular interactions between the amine and the carbonyl group. The C-O band appeared at about 1387cm^{-1} (b and c).

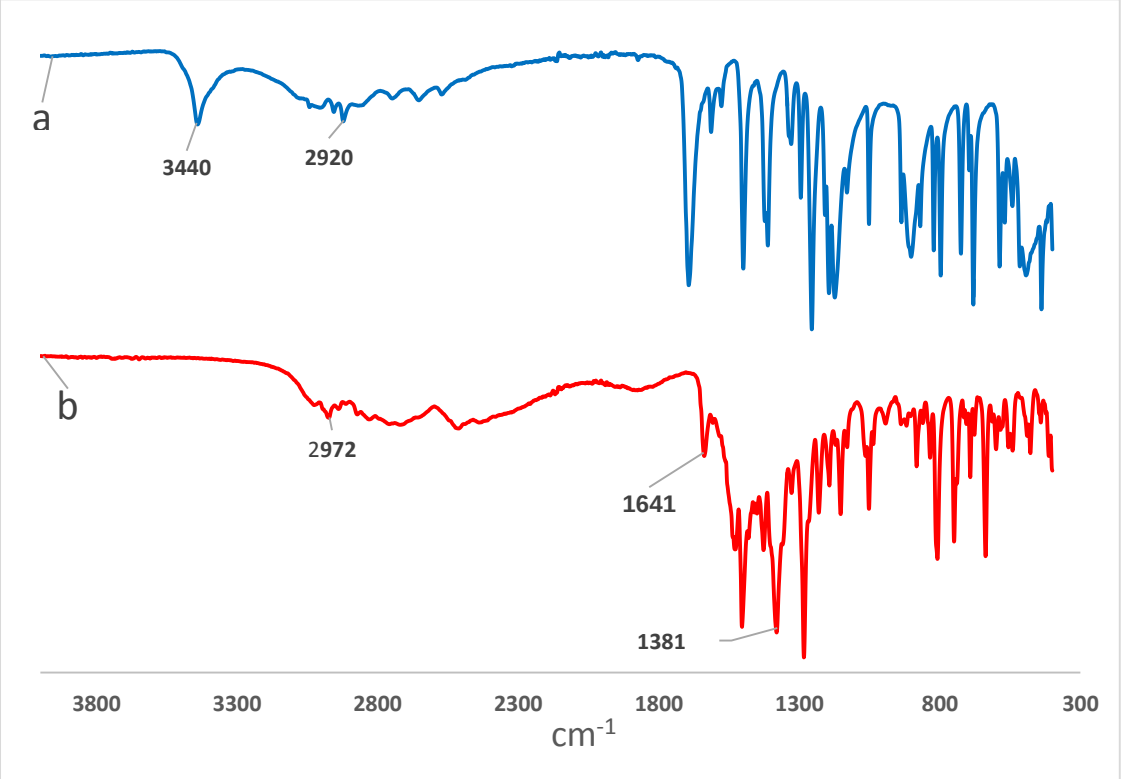

Figure 3. 15: FTIR spectroscopy of a :(CHPAA) and b: ($(CHPAA^{2-})(2DEA^{+})$).

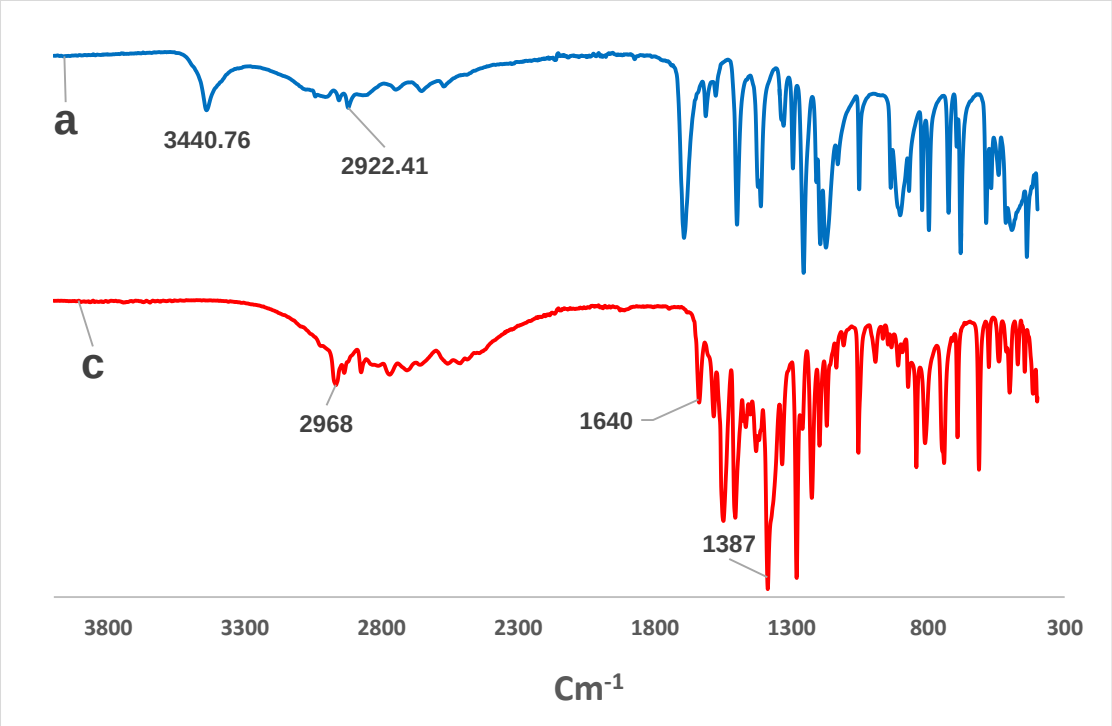

Figure 3. 16: FTIR spectroscopy of a: (CHPAA) and c: ($CHPAA^-$)($DIBUAM^+$).

3.7 Conclusion

In conclusion, two multicomponent salts of CHPAA with DEA and DIBUAM were successfully synthesised using the pK_a rule. The expected results were consistent with the experimental analysis results. Both salts were synthesized by slow evaporation techniques and structures were characterized using various instrumental techniques including FTIR, PXRD, DSC, TGA and single crystal X-ray diffraction. The FTIR of both structures were consistent with the formation of salts, and the DSC and TGA showed that the salt of $(CHPAA^{2-})(2DEA^{+})$ was unstable when compared to that of $(CHPAA^{-})(DIBUAM^{+})$. This was confirmed by the thermal stability trend found as follows: $(CHPAA^{-})(DIBUAM^{+}) > (CHPAA^{2-})(2DEA^{+})$. The reproduction of both salts through slurry and grinding experiments occurred only partially.

References

[1] Stahl, P. H. & Wermuth, C. G. 2008. Handbook of pharmaceutical salts. Properties, selection, and use. Weinheim: *John Wiley & sons*.

[2] Stahl, P. H. & Wermuth, C. G. 2008. Handbook of pharmaceutical salts. Properties, selection, and use. Weinheim: *John Wiley & sons*.

[3] Sheldrick, G. M. SHELXS-97. 1997. Program for crystal structure resolution, University of GÖttingen, GÖttingen, Germany.

[4] Etter, M. C., MacDonald J. C., Bernstein, J. 1900. *Acta Cryst*, Sect. B*: Struct. Sci*, 46, 256-262.

[5] Desiraju, G. R., Vittal, J. J & Ramanan, A. 2011. *Crystal engineering: a textbook. Hackensack: World Scientific: IISc Press.*

[6] O'Neil, M. J. 2013. The *Merck Index-An Encyclopaedia of chemicals, Drugs, and Biologicals. Cambridge, UK: RSC, 564.*

[7] Budavaris, S. 1996. The Merck Index-Ancyclopedia of chemicals, drugs, and Biologicals. Whitehouse Station, NJ: *Merck and co.,* Inc, 514.

[8] Yvon, K., Jeitschko, W. & Parthe, E. J. 1997. LAZY PULVERIX, a computer program, for calculating X-ray and neutron diffraction powder patterns*. J. Appl. Crystallography*, 10: 73-74.

[9] www. *Perkinelme*r.com.

CHAPTER FOUR

SALTS OF 3-CHLOROPHENYLACETIC ACID WITH AROMATIC AMINE DERIVATIVES

Chapter 4 : SALTS OF 3-CHLORO-4-HYDROXYPHENYLACETIC ACID WITH AROMATIC AMINE DERIVATIVES

The overall aim of this chapter was to design and develop new multicomponent crystals with specific new properties, by cocrystallisation of aromatic amine derivatives with 3-chloro-4-hydroxyphenylacetic acid. Several aromatic amine derivatives were selected as co-formers based on the well-known ability of the amine and carboxylic acid functional groups to interact and form hydrogen bonds. The crystallization outcome of the new solid forms was predicted based on the pK_a values. These values were recorded and were found to be as follows: 3.38; 4.16; 4.14; and 6.15 for $(CHPAA^-)(2AMP^+)$, $(CHPAA^-)(2A4MP^+)$, $(CHPAA^-)(2A6MP^+)$ and $(CHPAA^-)(DMAP^+)$ respectively. From the calculated values and including the experimental analysis, it was then concluded that all new solid forms were salts. Furthermore, the (Δd_{c-0}) differences were also measured to confirm the salt formation. All salt compounds were synthesized by the slow evaporation technique using various organic solvents. The characterization of compounds was carried out using several instrumentation techniques including DSC, FTIR, PXRD and Single crystal X-ray diffraction.

4.1 Salts of 3-chloro-4-hydroxyphenylacetic acid with aminopyridine derivatives

4.1.1 Introduction

Aminopyridine derivatives are pyridine compounds substituted with an amine group at various positions of the pyridine ring. The hydrogen bonding capabilities of aromatic amines with hydroxyl and carboxylic acid groups are widely reported, and it is often the most studied in the solid state. It has been reported that the carboxylic acid group is one of the most commonly used in crystal engineering.[1,2] This functional group has the ability to interact and hydrogen bond with several other functional groups such as amines, amides, alcohol and many others.[3] In this study, a series of 2-aminopyridine derivatives and 4-dimethylaminopyridine were selected to react with CHPAA.

The ΔpK_a values of all compounds mentioned above, fall within the range described by Cruz-Cabeza for the probability of salt formation.[4] This was further confirmed by the calculations of the (Δd_{c-0}) distances in each case. These values were as follows: 0.046 Å; 0.007 Å; 0.034 Å and 0.001 Å for $(CHPAA^-)(2AMP^+)$, $(CHPAA^-)(2A4MP^+)$, $(CHPAA^-)(2A6MP^+)$ and $(CHPAA^-)(DMAP^+)$ respectively. The recorded values are also within the range described by Desiraju for the expectation of salts.[5]

All salt compounds were prepared in the same way by introducing together in a vial a 1:1 ratio of each starting material. The resulting mixtures were dissolved respectively in various organic solvents. Solutions were slightly heated by stirring at 30^0 C for a few minutes using the hot plate. In cases where insolubility of the mixtures was observed, co-solvents were added to dissolve the mixtures completely. After clear solutions were obtained, the vials were sealed and kept at room temperature to crystallize by slow evaporation. After 1-2 weeks, crystals were obtained and analysed using several experiments which confirmed the presence of the new solid forms as salts. For all structures, the carboxylic acid proton was transferred to the pyridine nitrogen of the base indicating salt formation.

All crystal structures formed intermolecular interactions of N-H•••O and O-H•••O as well as weak interactions of C-H•••O including C-H•••Cl for some of the structures. It should be noted that the chlorine-hydrogen contacts obtained with all structures were long, ranging from 2.93 to 3.22 Å (Table 4.20) with angles also ranging from 100 to 137 ^{0} . These values fall within the range described by Hathwar *et al*.[6]

The structure of the salts of 2-aminopyridine derivatives exhibited different space groups viz. monoclinic ($P2_1/c$) and triclinic ($P\bar{1}$) whereas the crystal structure of the salt of 4-dimethylaminopyridine was solved in the orthorhombic space group (*Pbca*).

The N-H•••O heterosynthon is present in all the salt structures generating similar graph set notations of $R_2^2(8)$ and $R_4^2(8)$ motifs except with 4-dimethylaminopyridine. These type of motif interactions were also observed by Etter *et al*,[7,8] and were described by Vishweshwar *et al*,[9] as rigid two-point recognition supramolecular heterosynthons. Futhermore, all compounds exhibited different packing diagrams. This difference in packing was most probably due to the presence of the methyl groups substituted at various positions of the pyridine ring. The diagram below (Figure 4.1) illustrates the chemical structures compounds used.

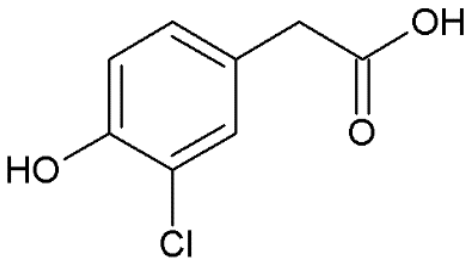

CHPAA

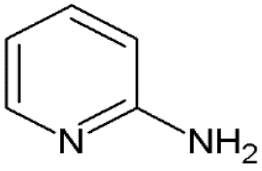

2AMP

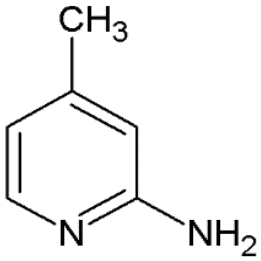

2A4MP

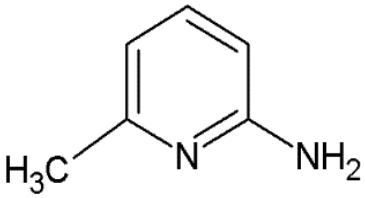

2A6MP

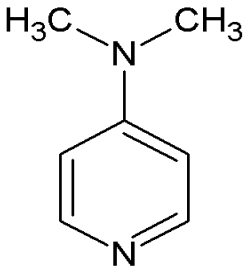

DMAP

Figure 4. 1: Chemical structures of CHPAA and aminopyridine derivatives.

4.2 Structural analysis

Most of the salts formed block-like crystals of various colours. A dark yellow colour was observed for 2-aminopyridinium-3-chloro-4-hydroxyphenylacetate ($CHPAA^-$)($2AMP^+$); a yellow-green for both 4-dimethylpyridinium-3-chloro-4-hydroxyphenylacetate ($CHPAA^-$)($DMAP^+$) and 2-amino-4-methylpyridinium-3-chloro-4-hydroxyphenylacetate ($CHPAA^-$)($2A4MP^+$) and a colorless crystal for 2-amino-6-methylpyridinium-3-chloro-4-hydroxylphenylacetate ($2CHPAA^-$)($2A6MP^+$) All structures were solved using direct methods with SHELXS-97.[10] The model was refined by full matrix least squares on F^2 with SHELXL-97. The crystal data is summarised in Table 4.1 below.

Table 4. 1: Crystal data and data collection parameters of salts.

Compound	$(CHPAA^-)(2AMP^+)$	$(CHPAA^-)(DMAP^+)$	$(CHPAA^-)(2A4MP^+)$	$(2CHPAA^-)(2A6MP^+)$
Host:guest ratio	1:1	1:1	1:1	2:2
Molecular formula	$C_{13}H_{13}ClN_2O_3$	$C_{15}H_{17}ClN_2O_3$	$C_{14}H_{15}ClN_2O_3$	$C_{28}H_{30}Cl_2N_4O_6$
Formula weight [g mol^{-1}]	280.70	308.76	294.74	589.48
Crystal system	Triclinic	Orthorhombic	Monoclinic	Triclinic
Space group	$P\bar{1}$	$Pbca$	$P2_1/c$	$P\bar{1}$
Z	2	8	4	2
D_{cal} [g cm^{-3}]	1.424	1.398	1 .375	1.4358
a [Å]	8.9470(18)	10.042(2)	8.94 (18)	8.0965
b [Å]	9.0283(18)	14.734(3)	12.556(3)	8.7236
c [Å]	9.0599(18)	19.827(4)	12.940(3)	20.743
α [°]	78.52(3)	90.00	90.00	87.611
β [°]	76.89(3)	90.00	101.52(3)	88.178
γ [°]	67.78(3)	90.00	90.00	68.667
Volume [A^3]	654.6(2)	2933.5(10)	1423.7(5)	1363.30(5)
M(Mo-K_α)[mm^{-1}]	0.297	0.272	0.277	0.29
T[K]	173(2)	173(2)	173(2)	173(2)
F(000)	292	1296	616	616
No.of reflections collected	10460	61114	25351	23066
No. of unique reflections	3130	3364	3542	6794
No. of reflection with I>2σ(I)	2703	2302	2807	4959
Index ranges	h:±11;k±11;l±11	h:±13;k:±19;l:25	h:±11;k:±16;l:17	h:±10; k=±11;8 ; l:±27
GooF	1.041	1.143	1.066	1.638
Final R indices [I>2σ]	R_1=0.0412; wR_2= 0.1140	R_1=0.0670; wR_2= 0.2695	R_1= 0.0416; wR_2= 0.1468	R_1 = 0.0754; wR_2= 0.2547
R indices [all data]	R_1=0.0472; wR_2= 0.1087	R_1=0.1251; wR_2= 0.1772	R_1 = 0.0545; wR_2= 0.1326	R_1 = 0.1016; wR_2= 0.2457
Largest diff peak and hole [$eÅ^{-3}$]	0.502; -0.489	0.925;-1.348	0.423; -0.406	0.727; -0.608
$2\theta_{max}$[°]	56	55	57	57

4.2.1 Salt of 2-aminopyridinium-3-chloro-4-hydroxyphenylacetate

$(CHPAA^{-})(2AMP^{+})$ crystallises in the triclinic space group $P\bar{1}$ and its asymmetric unit contains one $CHPAA^{-}$ anion and one $(2AMP^{+})$ cation (Figure 4.2). The carboxylic acid proton from $CHPAA^{-}$ was transferred to one of the nitrogens (N1) of $2AMP^{+}$ confirming salt formation. The unit cell consists of two $CHPAA^{-}$ anions and two $(2AMP^{+})$ cations (Z=2). The C-O difference (Δd_{C-O}) was found to be 0.046 Å. Figure 4.3 below illustrates the hydrogen bond numbering scheme for $(CHPAA^{-})(2AMP^{+})$.

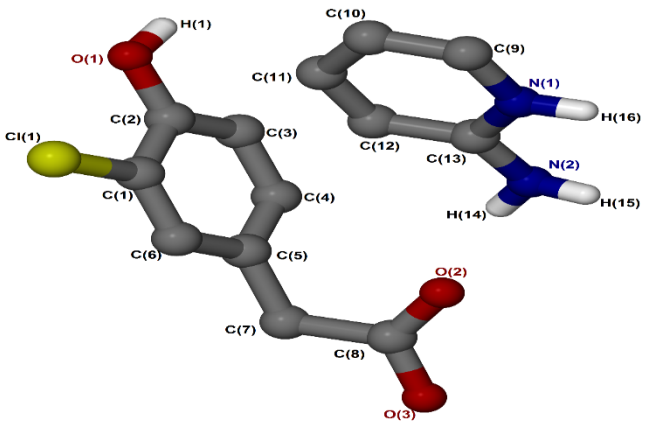

Figure 4. 2: Asymmetric unit of ($CHPAA^{-}$)($2AMP^{+}$).

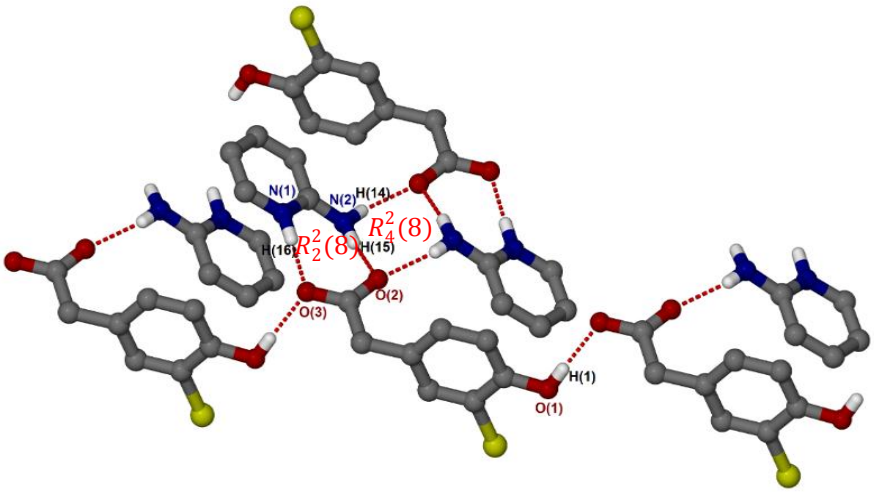

Figure 4. 3: Hydrogen bond numbering scheme of ($CHPAA^-$)($2AMP^+$).

The 1:1 salt of $(CHPAA^-)(2AMP^+)$ shows that the crystal structure is dominated by supramolecular heterosynthons. The hydrogen bonding consists of N-H•••O hydrogen bonds, as well as O-H•••O linkages between the hydroxyl group and neighbouring carboxylate oxygens (Figure 4.3). The primary amines and the carboxylate oxygens form $R_4^2(8)$ motifs with the hydrogen bonding extended to include the pyridinium nitrogen to form $R_2^2(8)$ motifs. The hydrogen atoms of the primary amine moiety H15 and H14 (Figure 4.4) were described by Bis *et al*,[11] as *syn* oriented (H15) and *anti* oriented (H14). The hydrogen bond metrics are summarised in Table 4.2. The structure also contains weak additional C12-H12•••π and C10-H10•••Cl interactions. This C-H•••π interaction also contributes to the conformation of the acid ring being orthogonal to the heterosynthons, since the aromatic ring of the acid is approximately perpendicular to the hydrogen bonding synthons. Figure 4.5 below illustrates the packing diagram of $(CHPAA^-)(2AMP^+)$ down [010].

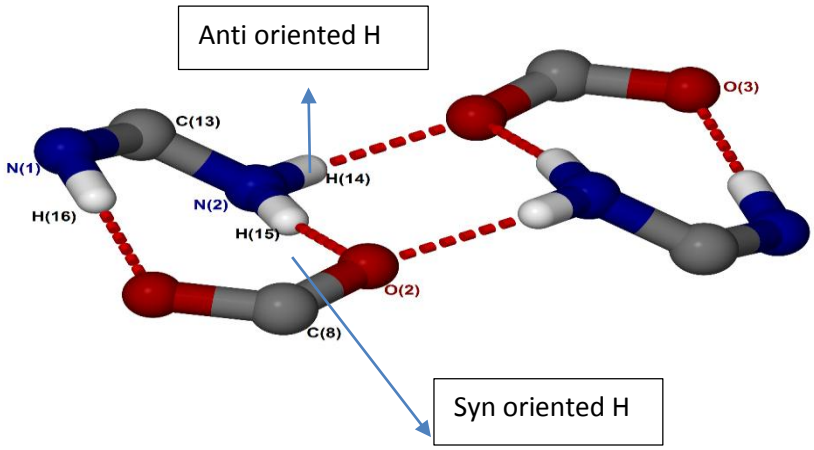

Figure 4. 4: Heterosynthon motif of ($CHPAA^-$)($2AMP^+$).

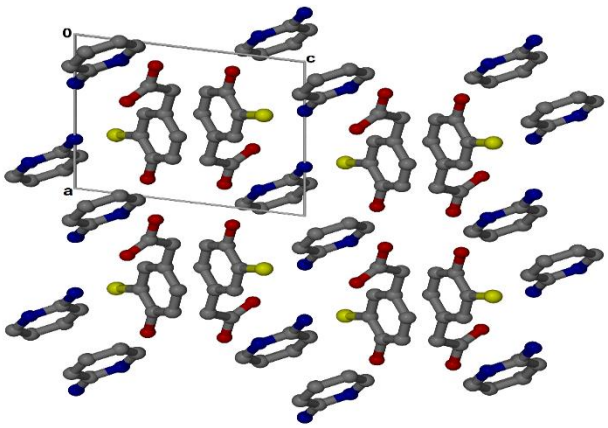

Figure 4. 5: Packing diagram of ($CHPAA^-$)($2AMP^+$) along [010].

The cations and anions are arranged in alternate columns with the packing stabilised by $\pi - \pi$ stacking with a centroid… centroid distance of 3.639 Å.

4.2.2 Salt of 2-amino-4-methylpyridinium- 3-chloro-4-hydroxyphenylacetate

$(CHPAA^{-})(2A4MP^{+})$ crystallises in the monoclinic space group *P2₁/c* and its asymmetric unit contains one $CHPAA^{-}$ anion and one $(2A4MP^{+})$ cation (Figure 4.6). The unit cell consists of four $CHPAA^{-}$ anions and four $(2A4MP^{+})$ cations. The C-O difference (Δd_{C-O}) was found to be 0.007 Å which is consistent with salt formation. Figure 4.7 below illustrates the hydrogen bond numbering scheme.

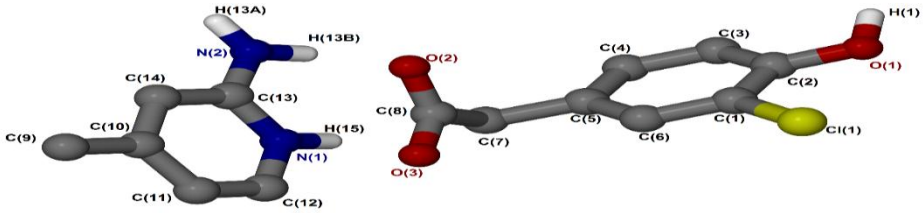

Figure 4. 6: Asymmetric unit of ($CHPAA^{-}$)($2A4MP^{+}$).

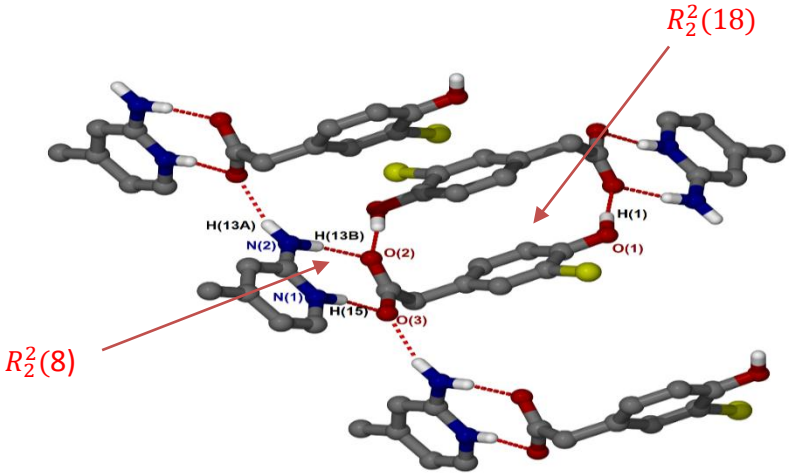

Figure 4. 7: Hydrogen bond numbering scheme of ($CHPAA^-$)($2A4MP^+$).

The 1:1 salt of $(CHPAA^-)(2A4MP^+)$, shows that the carboxylate and aminopyridinium interactions also form the $R_2^2(8)$ supramolecular heterosynthon. However in this structure the acid anions dimerize to form the $R_2^2(18)$ homosynthon involving the hydroxyl group and a carboxylate oxygen (O-H•••O interaction) (Figure 4.7). Furthermore, the hydrogen *anti* oriented (H13A) on the primary amine forms an additional hydrogen bond, allowing the structure to generate an extended network system described as chains with $C_2^2(8)$ and $C_2^2(6)$ motifs via N-H•••O interactions. The chlorine atom also interacts with one of the carbons of the cation forming of C3-H3•••Cl interaction. This generated the closest contact of 3.5072(16) Å for d(C3•••Cl) with the angle of 100 ^{0} for C3-H3•••Cl (see hydrogen bond table 4.2).The packing diagram is shown in Figure 4.8.

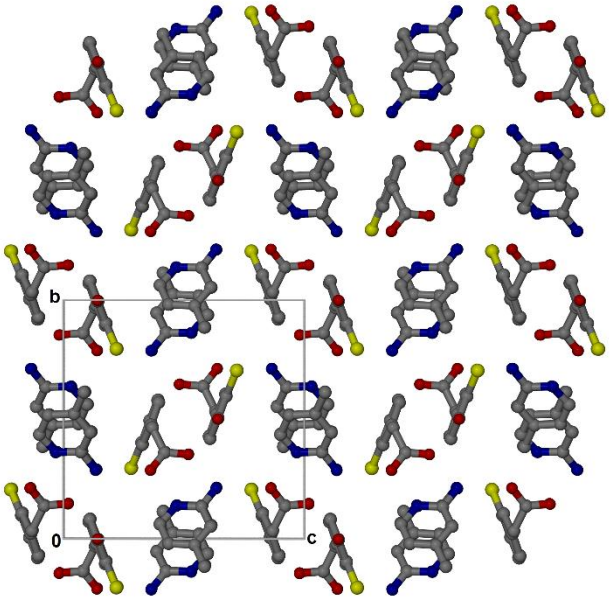

Figure 4. 8: Packing diagram of ($CHPAA^-$)($2A4MP^+$) along [100].

Columns of cations and anions are arranged in an alternating fashion along [100]. The packing is further stabilised by π-π stacking including acid-acid (3.229 Å) and cation-cation (4.185Å) .

4.2.3 Salt of 2-amino-6-methylpyridinium-3-chloro-4hydroxyphenylacetate

$(2CHPAA^-)(2A6MP^+)$ crystallises in the triclinic space group $P\bar{1}$ and its asymmetric unit contains two $(CHPAA^-)$ anions and two $(2A6MP^+)$ cations (Figure 4.9). The unit cell consists of four $CHPAA^-$ anions and four $(2A6MP^+)$ cations (Z = 2). The C-O difference (Δd_{C-O}) was found to be 0.034 Å. Figure 4.10 below illustrates the hydrogen bond numbering scheme.

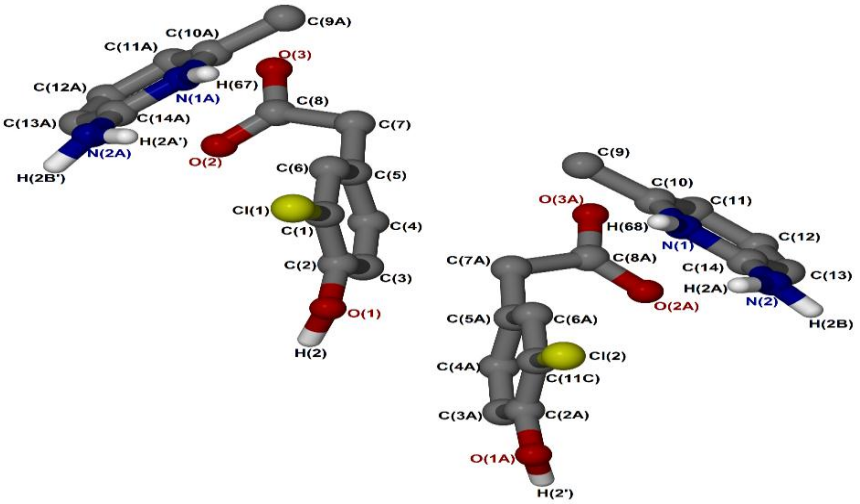

Figure 4. 9: Asymmetric unit of (2CHPAA^{-})(2A6MP^{+}).

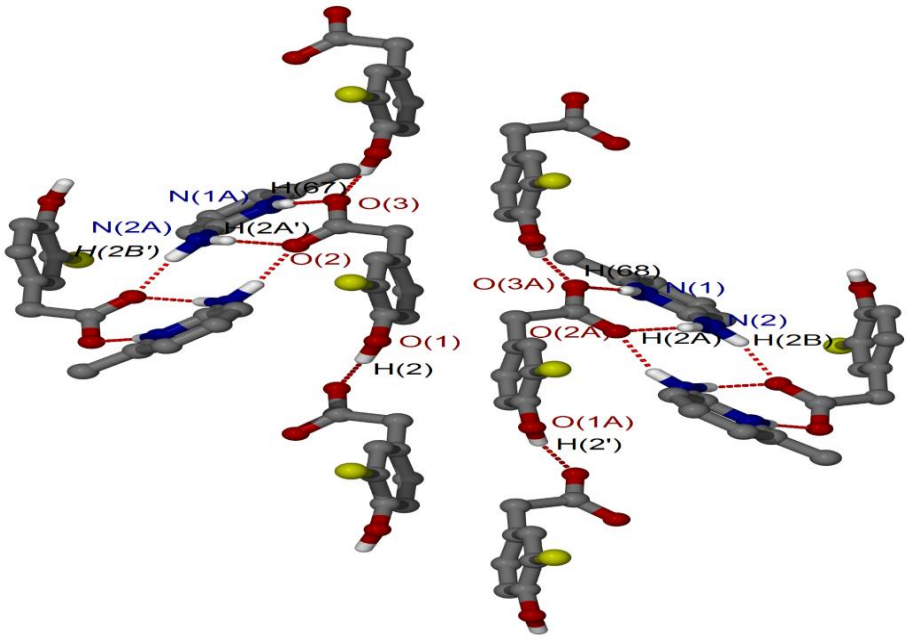

Figure 4. 10: Hydrogen bond numbering scheme of (CHPAA^{-})(2A6MP^{+}).

In the 2:2 salt of $(2CHPAA^{-})(2A6MP^{+})$, the anions $(CHPAA^{-})$ interact with 2-amino-6-methylpyridinium cations $(2A6MP^{+})$ via supramolecular heterosynthons consisting of $R_2^2(8)\ and\ R_4^2(8)$ rings. These types of motifs were also observed by Aakeroy *et al*.[12] and Robert *et al*,[13] using aminopyridine and the carboxylic acid. The hydroxyl group is also involved in O-H•••O interactions which extends the hydrogen bond network along the *a* axis. The salt also exhibits C9A-H9A'•••Cl weak intermolecular interaction. The packing diagram (Figure 4.11) shows columns of cations located between two columns of anions generating 2D channels along the b axis.

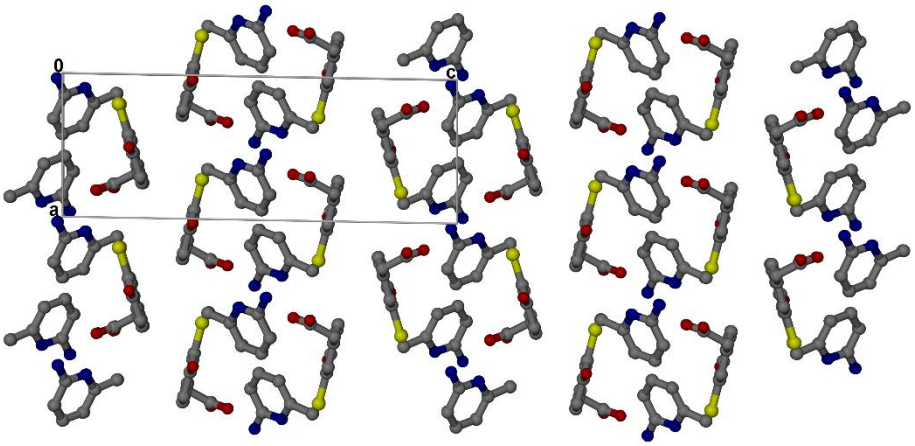

Figure 4. 11: Packing diagram of (CHPAA^{-})(2A6MP^{+}) along [010].

4.2.4 Salt of 4-dimethylaminopyridinium-3-chloro-4-hydroxyphenylacetate

The salt of 4-dimethylaminopyridinium-3-chloro-4-hydroxyphenylacetate $(CHPAA^{-})(DMAP^{+})$ crystallises in the orthorhombic space group *Pbca* and its asymmetric unit contains one $CHPAA^{-}$ anion and one $DMAP^{+}$ cation (Figure 4.12). The unit cell consists of eight $CHPAA^{-}$ anions and eight $(DMAP^{+})$ cations (Z = 8). The C-O difference (Δ_{C-O}) was found to be 0.001 Å. Figure 4.13 illustrates the hydrogen bond numbering scheme.

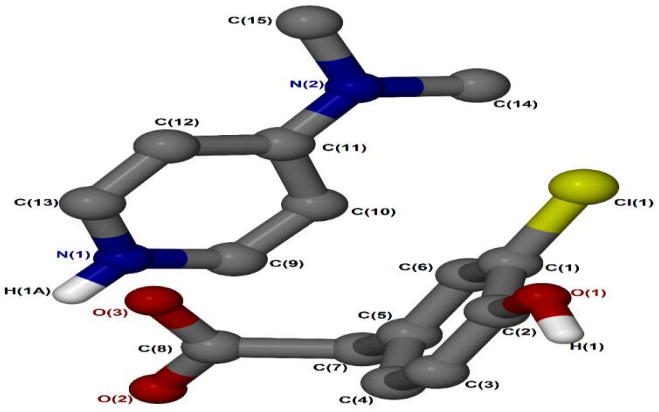

Figure 4. 12: Asymmetric unit of ($CHPAA^{-}$)($DMAP^{+}$).

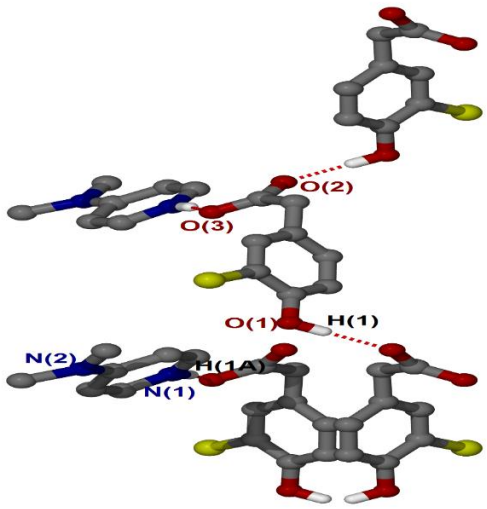

Figure 4. 13: Hydrogen bond numbering scheme of ($CHPAA^-$)($DMAP^+$).

The 1:1 salt of $(CHPAA^-)(DMAP^+)$ forms intermolecular interactions via N-H•••O. The neighbouring hydroxyl group also interacts with the free O2 of the other carboxylate forming extended channels with a $C_1^1(9)$ motif via O-H•••O interactions. The proton (H16) was transferred from the acid to one of the nitrogens (N1) of the cation. Therefore, the resulting compound is a salt. As expected there are no hydrogen bonded ring motifs due to the absence of the NH_2 group, as was seen in the previous structures. The structure also contains C4-H4•••Cl weak intermolecular interaction as obserbed in previous structures. Figure 4.14 illustrates the packing mode of $(CHPAA^-)(DMAP^+)$ along the c axis.

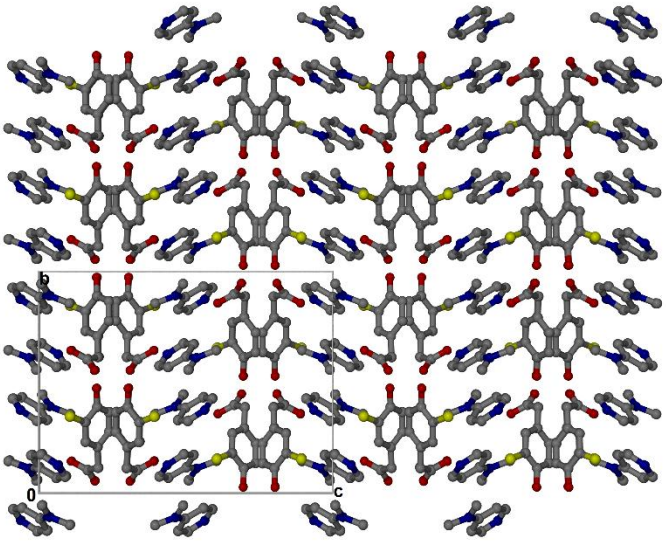

Figure 4. 14: Packing diagram of ($CHPAA^-$)($DMAP^+$) along [001].

The resulting salt compound packs in columns where carboxylates are aligned in the same direction and the cations oriented in the opposite direction. The packing alternates along the *c* axis forming wave-like sheets.

Table 4. 2: Geometric data of the hydrogen bonding in salts formed by CHPAA.

D-H•••A	d(D-H) Å	d(H•••A) Å	d(D•••A)Å	D-H•••A (^{0})	Symmetry operator
$(\boldsymbol{CHPAA^-})(\boldsymbol{2AMP^+})$					
N2-H14···O2	0.81	2.08	2.870(2)	163	-
N2-H15···O2	0.84	2.02	2.850(19)	167	-x+1, -y+2, -z+2
N1-H16···O3	0.90	1.82	2.720(17)	179	-x+1, -y+2, -z+2
O1-H1•••O3	0.80	1.85	2.650(16)	170	x-1, y, z
C10-H10•••Cl1	0.95	3.06	3.780(17)	134	-x, 1-y, 2-z
$(\boldsymbol{CHPAA^-})(\boldsymbol{2A4MP^+})$					
N1-H15···O3	0.91	1.91	2.717(18)	169	-
N1A-H13B···O2	1.92	1.94	2.857(18)	173	-
N2-H13A···O3	0.88	2.02	2.887(18)	165	x, -y+3/2, z-1/2
O1-H1•••O2	0.91	1.70	2.613(18)	173	-x+1, -y+2, -z
C3-H3•••Cl	0.95	3.22	3.507(16)	100	1-x, ½+y, ½-z
$(\boldsymbol{CHPAA^-})(\boldsymbol{2A6MP^+})$					
N1-H68···O3A	0.89	1.93	2.822(4)	170	x-1, y, z
N1A-H13B···O3	0.92	1.89	2.809(4)	171	x-1, y, z
N2-H2A···O2A	0.95	1.86	2.784(4)	161	x-1, y, z
N2A-H2A'···O2	0.94	1.87	2.798(4)	164	x-1, y, z
N2A-H2B'···O2	0.95	1.91	2.863(4)	169	-x+1, -y+1, -z
N2-H2B···O2A	0.91	1.97	2.858(4)	162	-x+2, -y+1, -z+1
O1A-H2'···O3A	0.81	1.88	2.679(4)	163	x, y-1, z
O1-H2···O3	0.98	1.68	2.677(4)	176	x, y-1, z
C9A-H9A'···Cl	0.98	3.15	3.823(4)	127	x, 1+y, z
$(\boldsymbol{CHPAA^-})(\boldsymbol{DMAP^+})$					
N1-H16···O3	0.88	1.80	2.663(4)	168	-x+3/2, y-1/2, z
O1-H1···O3	0.84	1.73	2.568(3)	172	-x+1, y-½, -z+3/2
C4-H4···Cl	0.95	2.93	3.593(3)	128	½+x, y, 3/2-z

4.3 Torsion angles of $CHPAA^-$

The target compound, 3-chloro-4-hydroxyphenylacetic acid (CHPAA) adopted various conformations when combined with selected aminopyridines and dimethylaminopyridine. These conformations, involving the twisting of the acetic acid group relative to the aromatic ring, are described as torsion angles. In each salt, two major conformations were observed involving the ring and the twisting of the acetic acid group (Figure 4.15). For 2-aminopyridinium-3-chloro-4-hydroxyphenylacetate salt (I), the torsion angles of the $CHPAA^-$ anion are τ_1(C6-C5-C7-C8)= 102.94^0 and τ_2(O2-C8-C7-C5)= 1.42^0 ; 4-dimethylaminopyridinium-3-chloro-4-hydroxyphenylacetate salt (II), τ_1(C6-C5-C7-C8)= 106.19 ^{0} and τ_2(O2-C8-C7-C5) =140.9 ^{0} ; 2-amino-4-methylpyridinium-3-chloro-4-hydroxyphenylacetate salt (III), τ_1(C6-C5-C7-C8)= 47.89 ^{0} and τ_2(O2-C8-C7-C5)= 74.80 ^{0} and 2-amino-6-methylpyridinium-3-chloro-4-hydroxyphenylacetate salt (IV), °τ_1(C6-C5-C7-C8)= 95.75 ^{0} and τ_2(O2-C8-C7-C5)= 7.43 ^{0} . CHPAA molecules from two different structures were overlayed to determine any conformational similarity. Figure 4.16 illustrates this in the following order: I and II; I and III; I and IV; II and III; II and IV; III and IV, and thereafter all structures from I to IV were combined in Figure 4.16. This was done in Mercury (version 3.5, 2017). Table 4.3 below summarises torsion angles obtained.

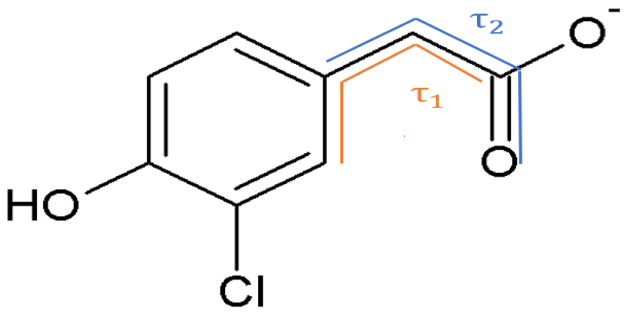

Figure 4. 15: Torsion angles of $CHPAA^-$

Table 4. 3: Torsion angle summary of salts formed by CHPAA and aminopyridine derivatives

No	Torsion angles	τ_1:C6-C5-C7-C8	τ_2: O2-C8-C7-C5
I	$(\boldsymbol{CHPAA^-})(\boldsymbol{2AMP^+})$	102.94	1.44
II	$(\boldsymbol{CHPAA^-})(\boldsymbol{2A4MP^+})$	47.89	74.80
III	$(\boldsymbol{CHPAA^-})(\boldsymbol{2A6MP^+})$	95.70	7.43
IV	$(\boldsymbol{CHPAA^-})(\boldsymbol{DMAP^+})$	106.19	140.91

Based on the overlaying, it was found that the $CHPAA^-$ anion has a similar conformation in I and III (Fig 4.16 b)

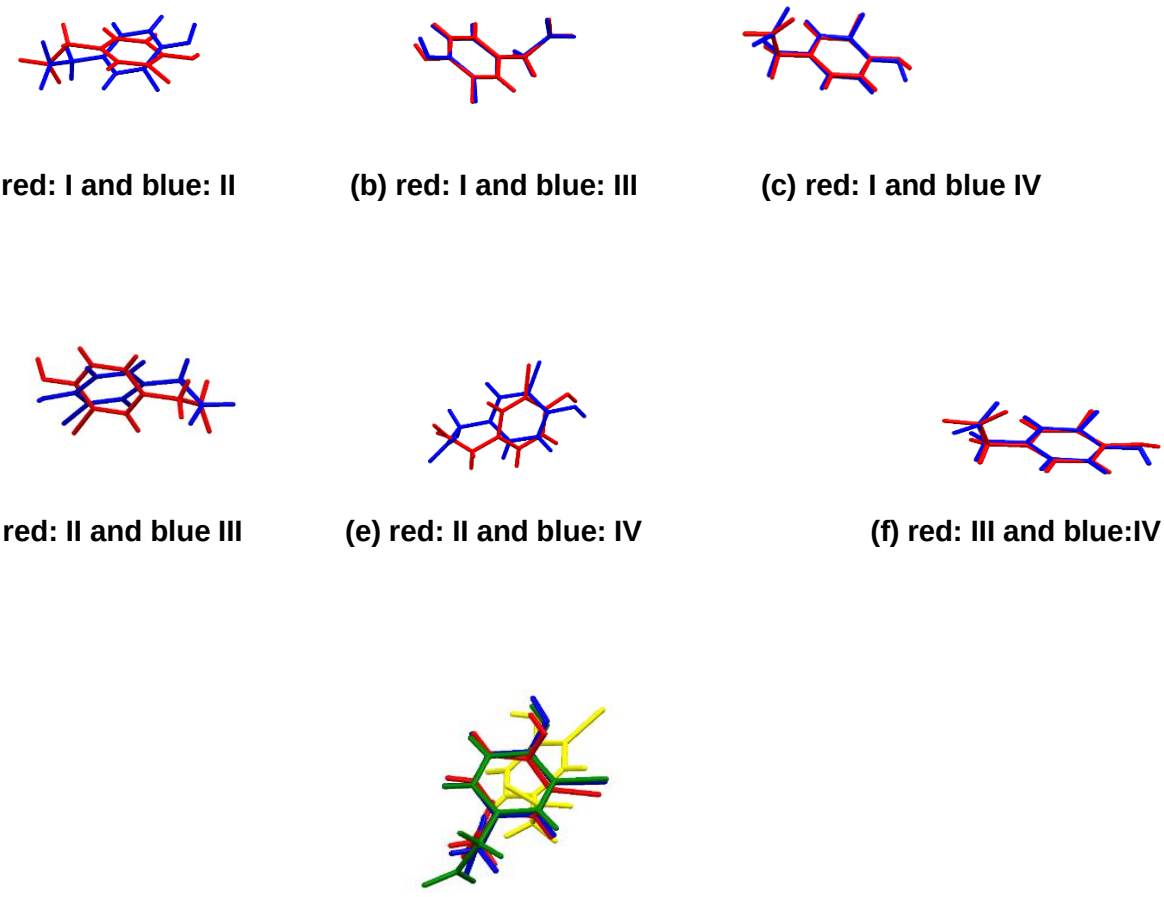

(a) red: I and blue: II **(b) red: I and blue: III** **(c) red: I and blue IV**

(d) red: II and blue III **(e) red: II and blue: IV** **(f) red: III and blue:IV**

Figure 4. 16: Overlay of a: a: I-II, b: I-III, c: I-IV, d: II-III, e: II-IV, f: III-IV and I-IV

4.4 Thermal analysis of ($CHPAA^-$)($2AMP^+$); ($CHPAA^-$)($2A4MP^+$); ($CHPAA^-$)($2A6MP^+$); ($CHPAA^-$)($DMAP^+$)

Thermal analysis was used to compare the decomposition events of the new solid forms with those of the starting materials. DSC experiments of all new solid forms below displayed endotherms with different onset temperatures to those of the starting material which indicated that new solids were successfully formed. The DSC analyses were performed on a Perkin-Elmer Pyris 6 and the results are shown in Figures 4.17-4.20.

For the $(CHPAA^-)(2AMP^+)$ salt (Figure 4.17), the crystal peak (red) appeared at $T_{onset} =$ 423.3 K which is greater than both starting material melting points of CHPAA with $T_{onset} = 378.4\ K$ and 2AMP with $T_{onset} = 331.4\ K$.

$(CHPAA^-)(2A4MP^+)$ salt (Figure 4.18), the crystal peak appeared at $T_{onset} = 410.7\ K$ which is different to that of CHPAA with $T_{onset} = 378.4\ K$ and 2A4MP with $T_{onset} = 365.8\ K$.

In the case of $(CHPAA^-)(2A6MP^+)$ salt (Figure 4.19), the crystal peak (red) appeared at $T_{onset} =$ 414.8 K and the melt of starting materials occurred at $T_{onset} =$ 378.4 K for CHPAA and at $T_{onset} =$ 306.7 K for 2A6MP.

And lastly, for $(CHPAA^-)(DMAP^+)$ salt (Figure 4.20), the crystal peak (red) displays two thermal events, the first peak appeared at $T_{onset} =$ 371.6.K corresponds to the melt of the CHPAA and the crystal peak appeared at $T_{onset} =$ 417.6 K Both pure starting materials appeared at $T_{onset} =$ 378.4 K for CHPAA and $T_{onset} =$ 383.9 K for DMAP.

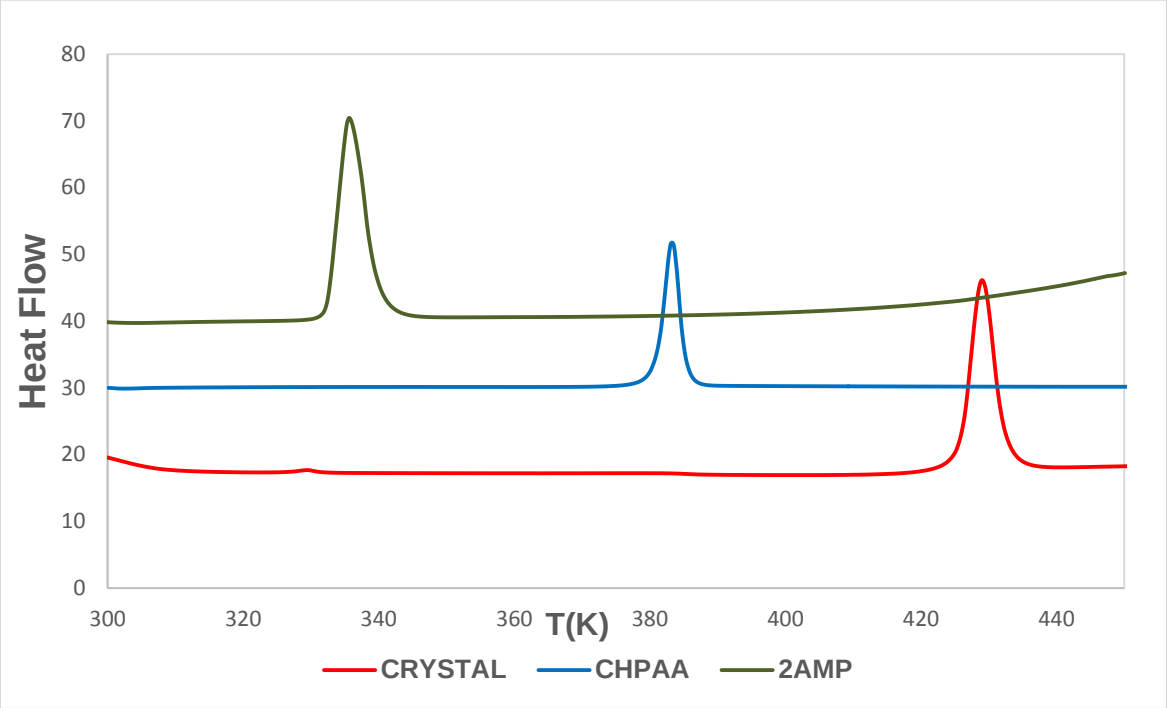

Figure 4. 17: DSC curves of (CHPAA$^-$)(2AMP$^+$) (red); blue: (CHPAA), green: (2AMP).

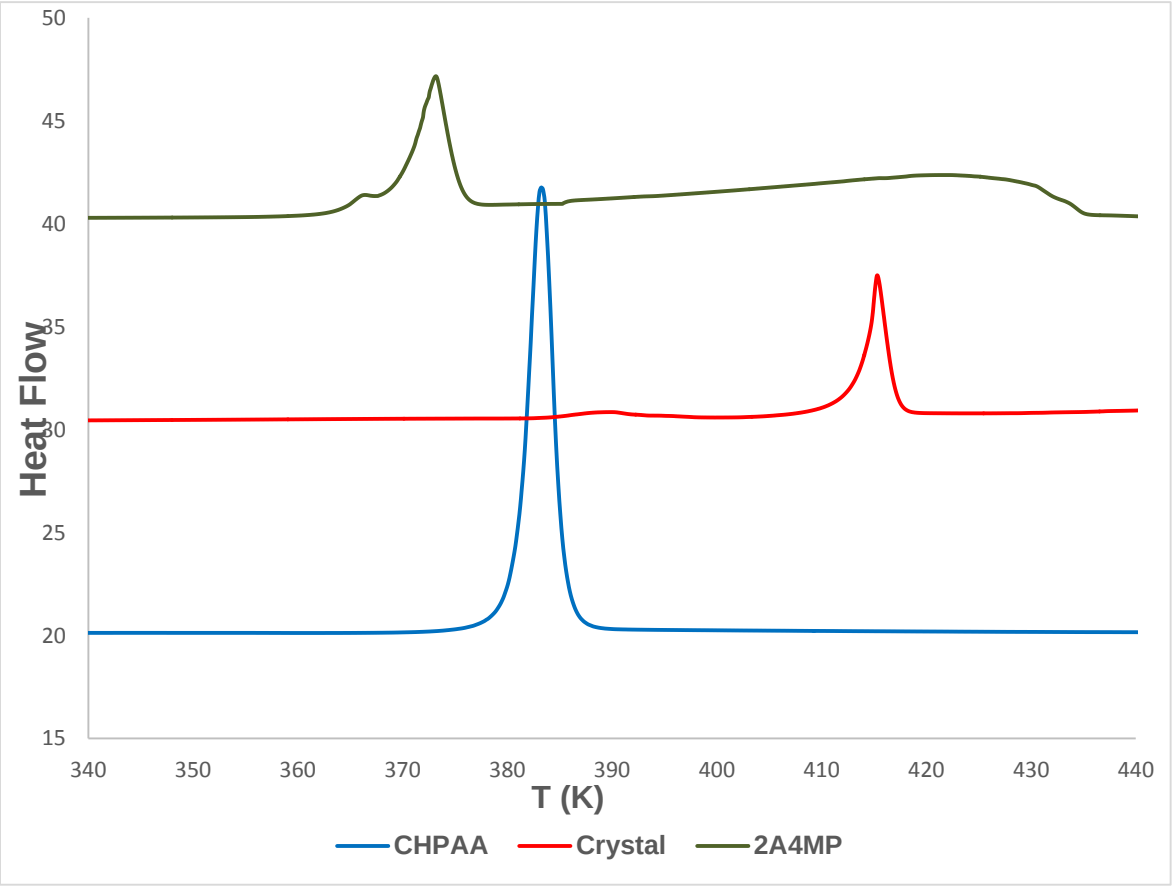

Figure 4. 18: DSC curves of ($CHPAA^-$)($2A4MP^+$) (red); blue:(CHPAA), green: (2A4MP).

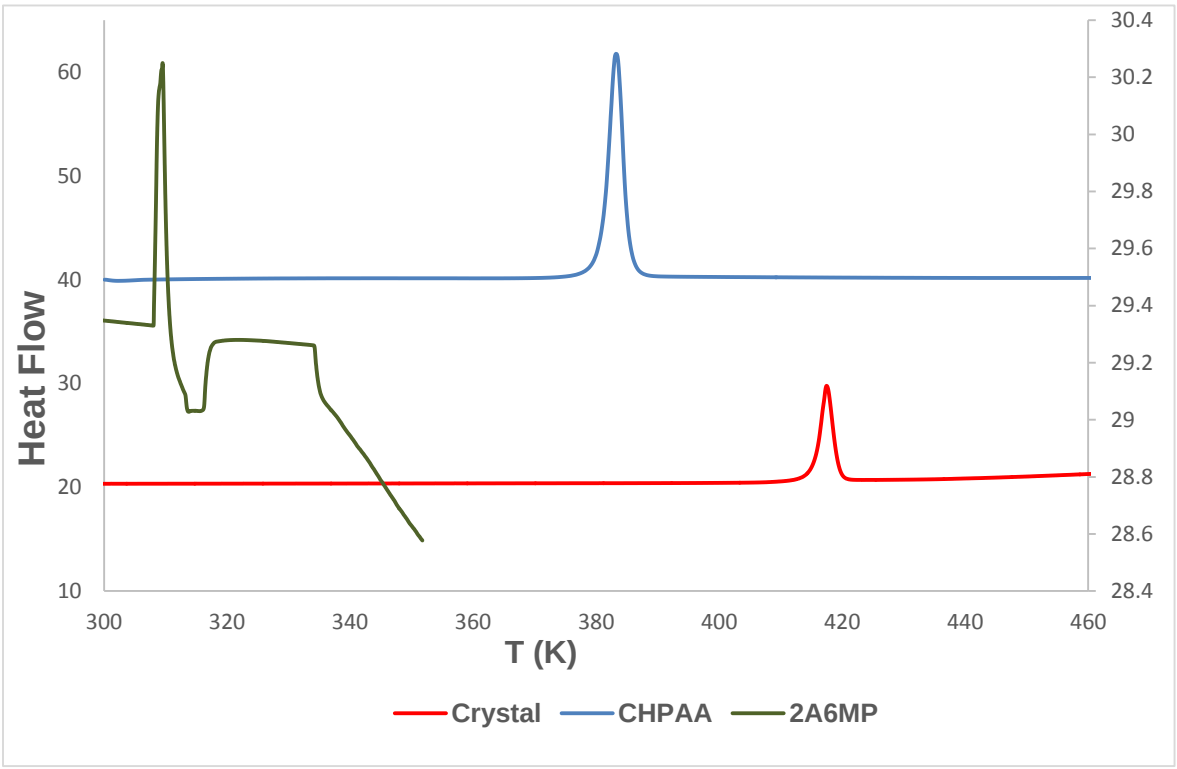

Figure 4. 19: DSC curves of ($CHPAA^-$)($2A6MP^+$) (red), blue:(CHPAA), green:(2A6MP).

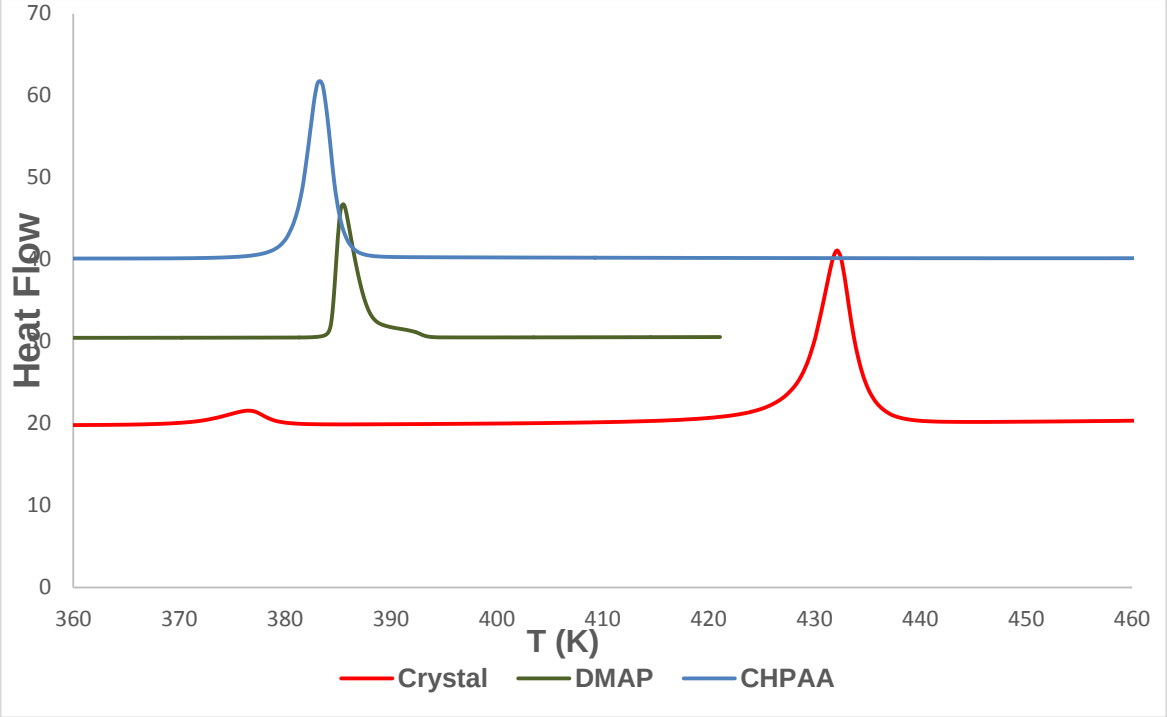

Figure 4. 20: DSC curves of ($CHPAA^-$)($DMAP^+$) (red); blue:(CHPAA), green:(DMAP).

Table 4. 4: Thermal analysis data of salts.

Compound	DSC Endo (T_{onset}, K)	
$(CHPAA^-)(2AMP^+)$	423.3	/
$(CHPAA^-)(2A4MP^+)$	410	/
$(2CHPAA^-)(2A6MP^+)$	414.8	/
$(CHPAA^-)(DMAP^+)$	427.6	373.24

All salts were prepared with the same acid (CHPAA), thus the thermal stability of the salts can be related to the physicochemical properties of the amines. These include: melting point and pK_a values. It is well known that the melting point is also related to the stability of the compound. The higher the melting point, the more stable is the compound, and in general the more substituted a compound, the greater the stability. DMAP has the highest melting point (383-386 K), followed by 2A4AMP (369-372 K), 2A6MP (313.-317K) and 2AMP (331 K) Therefore the thermal stability trend expected was: $(CHPAA^{-})(DMAP^{+})$> $(CHPAA^{-})(2A4MP^{+})$ > $(CHPAA^{-})(2AMP^{+})$ > $(CHPAA^{-})(2A6MP^{+})$. However, the obtained thermal stability trend is as follows: $(CHPAA^{-})(2AMP^{+})$> $(CHPAA^{-})(DMAP^{+})$> $(CHPAA^{-})(2A6MP^{+})$> $CHPAA^{-})(2A4MP^{+})$. The higher thermal stability observed for $(CHPAA^{-})(2AMP^{+})$ can be explained by the extensive hydrogen bonding involving $R_2^2(8)$ and $R_4^2(8)$ ring motifs.

4.5 Grinding and slurry experiments of ($CHPAA^{-}$)($2AMP^{+}$),($CHPAA^{-}$)($2A4MP^{+}$), ($CHPAA^{-}$) ($2A6MP^{+}$), ($CHPAA^{-}$)($DMAP^{+}$)

The calculated PXRD patterns obtained from LAZYPULVERIX[14] were compared to the PXRD patterns of the starting materials as well as those obtained from various preparation methods. The grinding and slurry experiments were performed in the same way as in the previous chapter.

For the 2-aminopyridinium-3-chloro-4-hydroxyphenylacetate salt (Figure 4.21), PXRD pattern obtained after grinding (green) was similar to product obtained from the slurry (yellow) and the calculated (blue) PXRD patterns but different to the starting material (red) PXRD pattern, indicating that the salt was successfully prepared.

For the 2-amino-4-methylpyridinium-3-chloro-4-hydroxyphenylacetate salt (Figure 4.22), PXRD pattern obtained after grinding (green) matched that of the slurry (yellow) and the calculated (blue) PXRD patterns but was different to the starting material (red) PXRD pattern, indicating that the salt compound was also successfully prepared.

In the case of the 2-amino-6-methylpyridinium-3-chloro-4-hydroxyphenylacetate salt (Figure 4.23), the PXRD patterns of the ground product (green) and the product obtained from slurry (yellow) were overall similar to the calculated (blue) PXRD pattern. However, the peak at 2θ

=8.7 ^{0} was missing from the calculated PXRD pattern indicating that the salt was partially formed.

Finally, in the 4-dimethylaminopyridinuim-3-chloro-4-hydroxyphenylacetate salt (Figure 4.24), PXRD pattern of the ground product (green) was similar to the product obtained from slurry (yellow) and the calculated (blue) PXRD patterns, but also contained extra peaks of CHPAA, which indicated that the reaction was incomplete and that the product contained unreacted starting material.

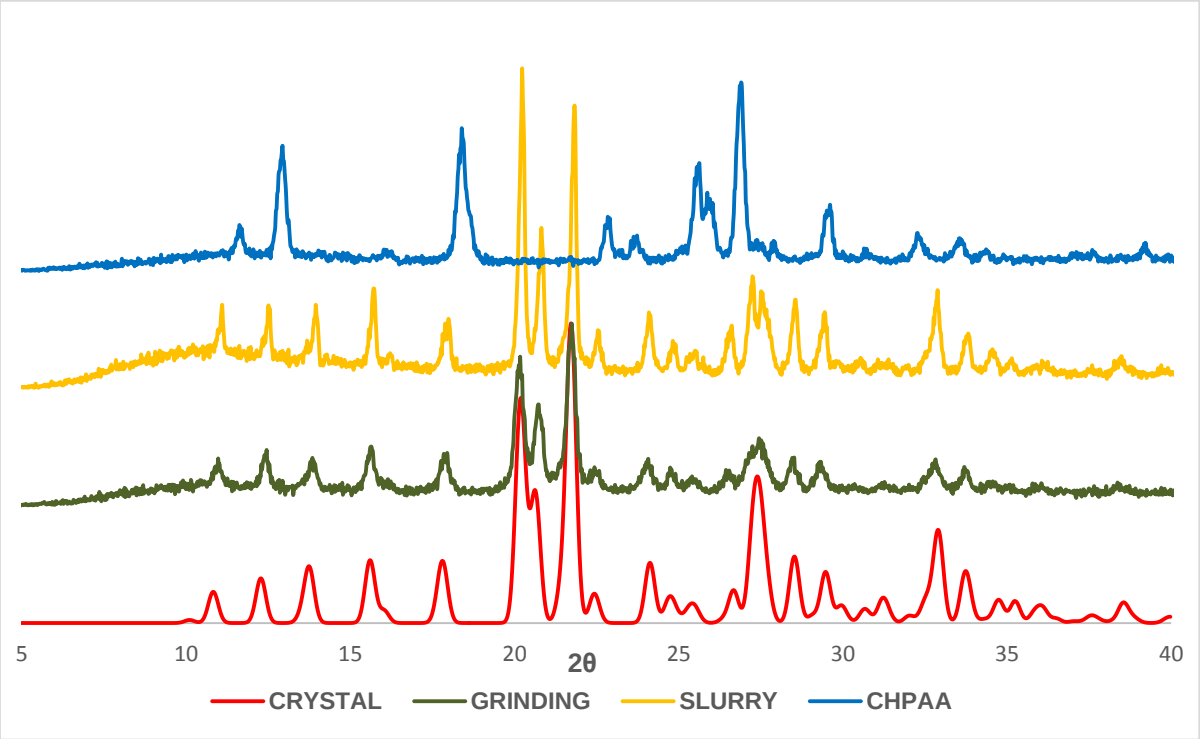

Figure 4. 21: PXRD of ($CHPAA^{-}$)($2AMP^{+}$).

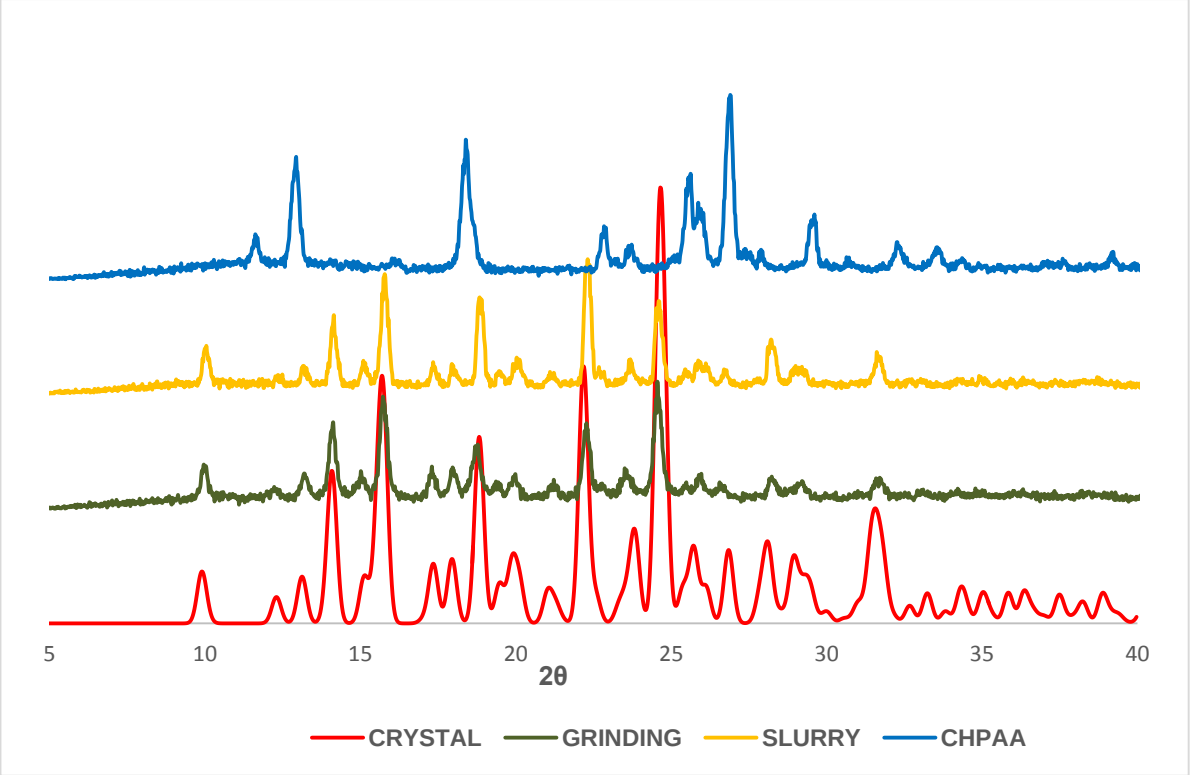

Figure 4. 22: PXRD of ($CHPAA^-$)($2A4MP^+$).

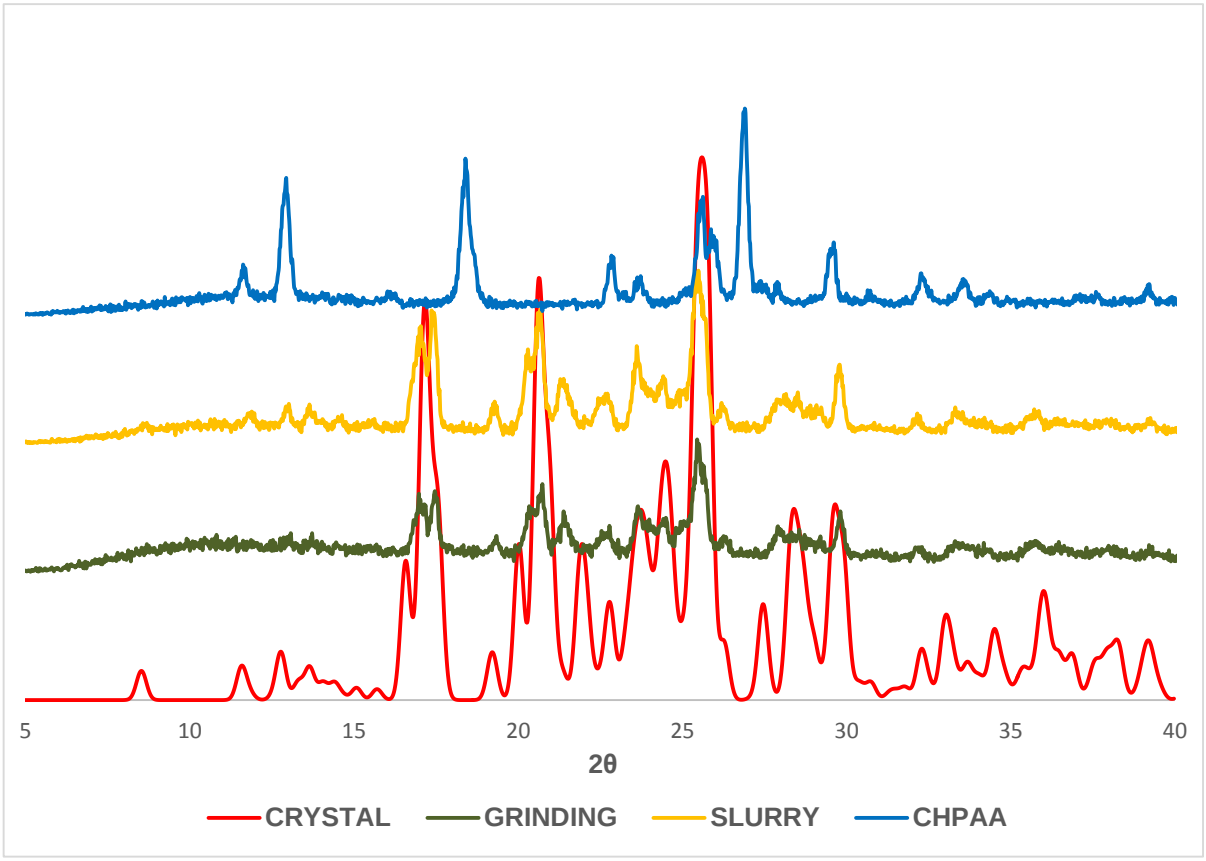

Figure 4. 23: PXRD of ($CHPAA^-$)($2A6MP^+$).

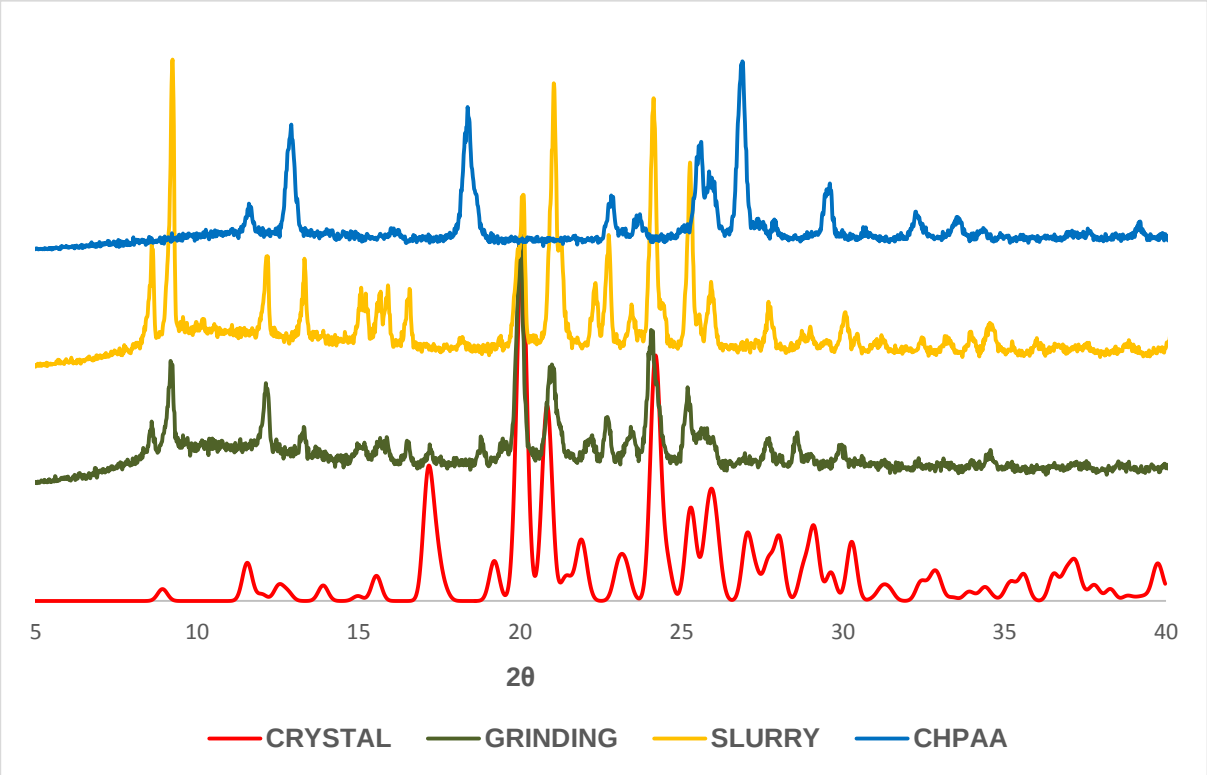

Figure 4. 24: PXRD of ($CHPAA^-$)($DMAP^+$).

4.6 FTIR spectroscopy

All salts produced different absorption modes and intensities in the IR spectra. The IR spectra of all salts are shown in Figures 4.25-4.28. All new solid forms displayed different spectra when compared to the starting material spectra. The CHPAA spectrum (blue) displayed a stretching peak at around 3431cm^{-1} that is assigned to the free OH group involved in hydrogen bonding. This peak is absent in almost all new solid forms (red spectra: e, g and i) except in c (Figure 4.25). This absence indicated that the free OH group was involved in the proton transfer process and thus, confirmed the formation of the new solid forms as salts. The peak at 2922 cm^{-1} (blue) assigned to the carboxylic acid group is also involved in hydrogen bonding in all the salt structures. However, this band reappeared shifted in the new solid forms spectra because of the hydrogen bonding involved. It should be pointed out that the persistence of free OH peak (3444 cm^{-1}) in the new spectrum (c) was not expected since the obtained compound is a salt. This is probably due to unreacted starting material. Moreover, the starting material (a) also contains one major stretching peak at around 1694 cm^{-1} assigned to C-O, which also appeared in both (b) and (c). Furthermore, peaks at 1559-1560 cm^{-1} (c) were assigned to the COO^- carboxylate group.[9] These peaks confirmed that the protons were transferred in all new solid forms.

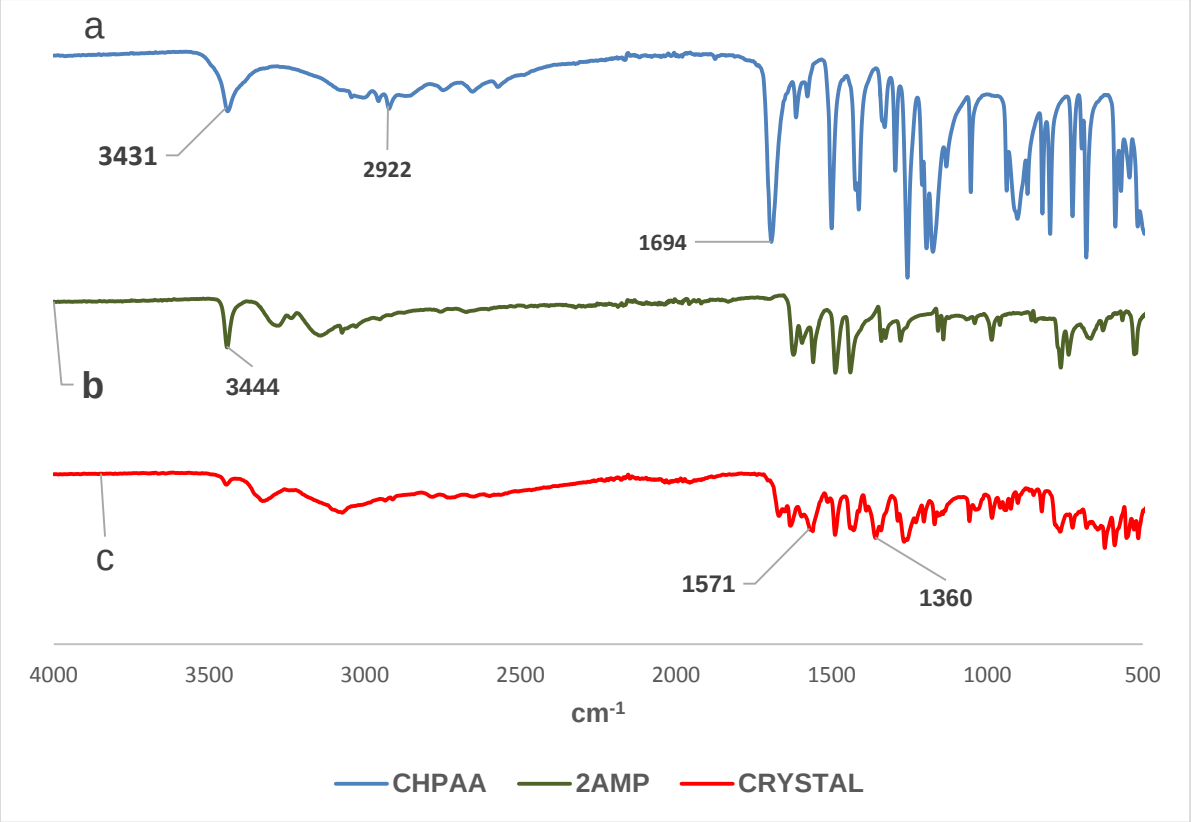

Figure 4. 25: FTIR of a: (CHPAA), b: (2AMP), c: ($CHPAA^-$)($2AMP^+$).

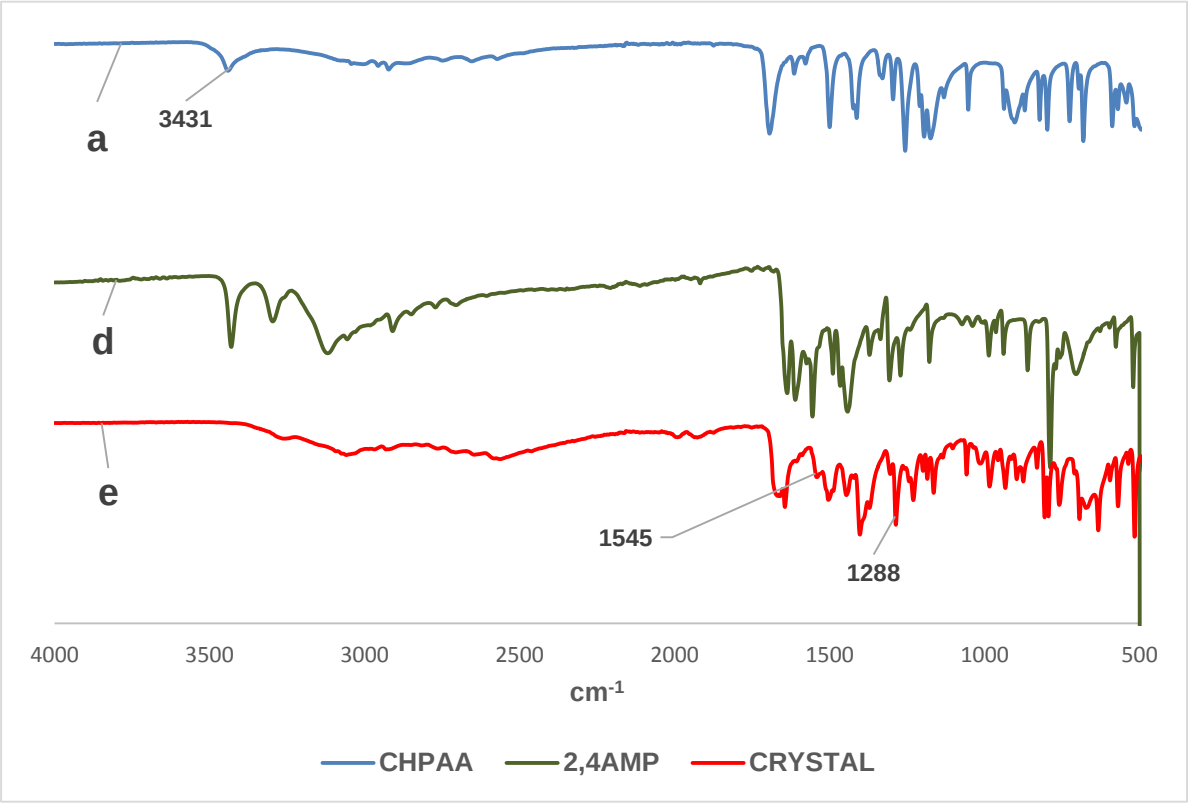

Figure 4. 26: FTIR of a: (CHPAA), d: (2A4MP), e: ($CHPAA^-$)($2A4MP^+$).

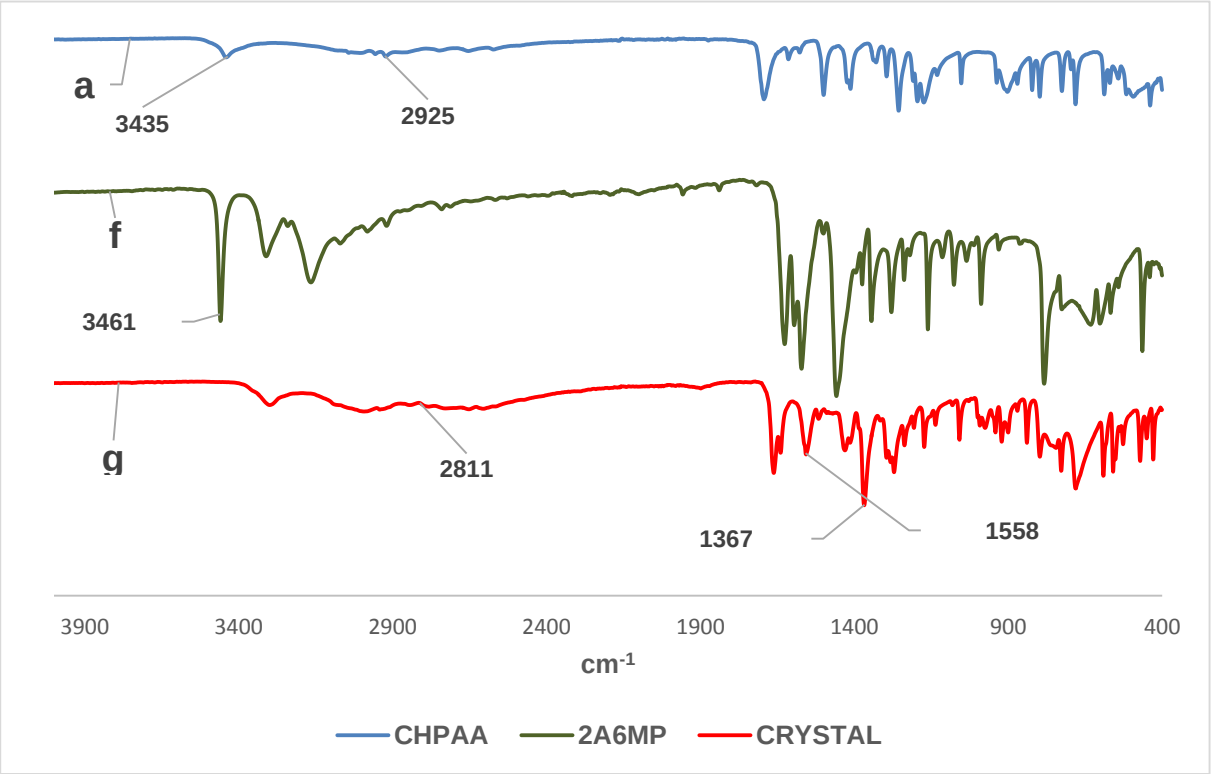

Figure 4. 27: FTIR of a: (CHPAA), f:(2A6MP), g: ($CHPAA^-$)($2A6AMP^+$).

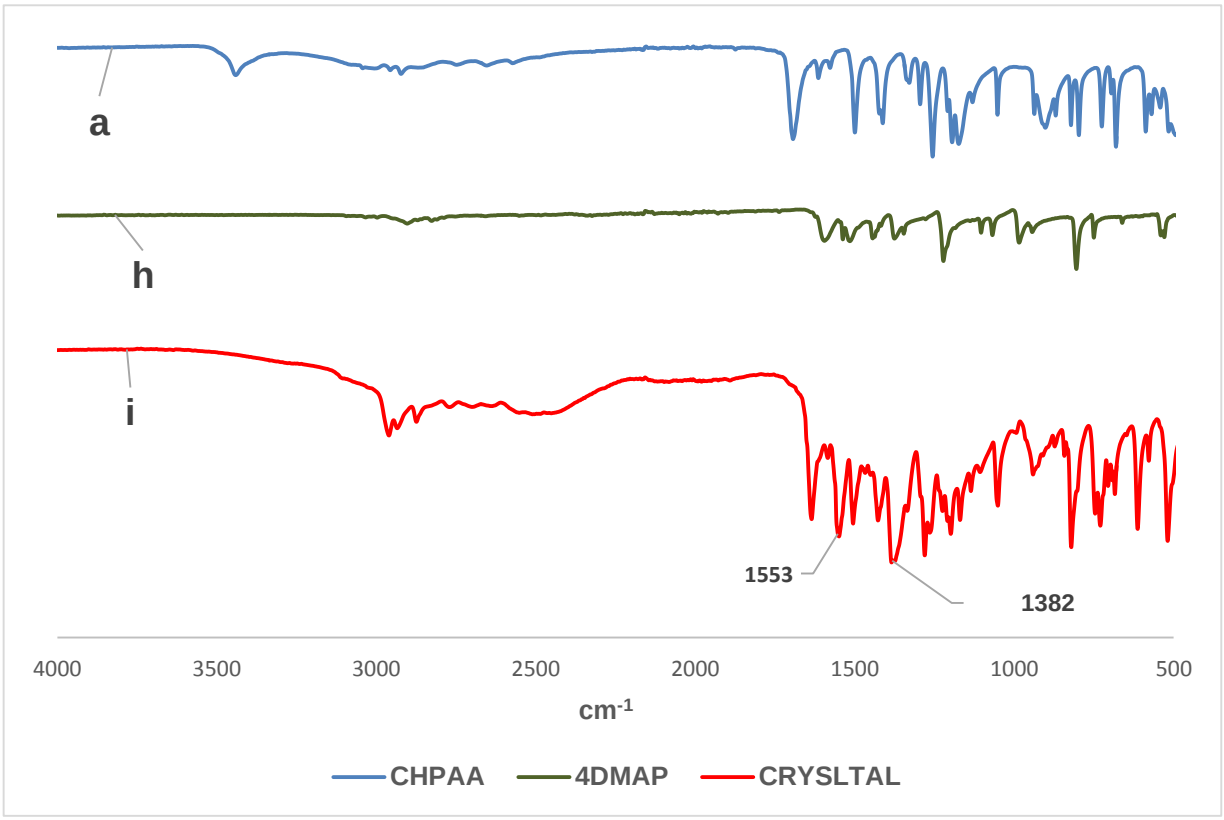

Figure 4. 28: FTIR of a: (CHPAA), h:(DMAP), i: ($CHPAA^-$)($DMAP^+$).

Table 4. 5: FTIR peaks assignment

a(cm^{-1})	c	e	g	i	Assignment
3431-2922	/	/	/	/	OH and carboxylic acid
1255-1694	1268	1286	1271	1281	C-O and C=O stretch
/	1571	1545	1559	1553	COO^- Stretch

4.7 Conclusion

Several multicomponent salts of aminopyridine derivatives have been successfully synthesised by mixing 3-chloro-4-hydroxyphenylacetic acid with the following amines: 2-aminopyridine, 2-amino-4-methylpyridine, 2-amino-6-methylpyridine and 4-dimethylaminopyridine. All compounds were first prepared by the slow evaporation technique and followed by several other methods such as grinding and slurry experiments. The prediction of the crystallization outcome was made based on the pK_a rule, which was consistent with the experimental analysis. The characterization of the compounds was done using various instrumentation techniques including FTIR spectroscopy, PXRD, DSC and single crystal X-ray diffraction. The DSC and PXRD results were consistent in confirming the formation of new solid forms. Furthermore, DSC experiments also indicated that the thermal stability trend order of the resulting compounds was $(CHPAA^{-})(2AMP^{+})$> $(CHPAA^{-})(DMAP^{+})$> $(CHPAA^{-})(2A6MP^{+})$> $CHPAA^{-})(2A4MP^{+})$. The FTIR analysis of all structures showed three major bands which indicated salt formation. These bands were OH at 3431 cm^{-1} (spectra: a), NH- (spectra: b, d, f, and h) and COO^{-} (1545-1571 cm^{-1}). Moreover, all 2-aminopyridine structures exhibited heterosynthon hydrogen bonds with similar graph set notations of $R_2^2(8)$ and $R_4^2(8)$ except for 4-dimethylaminopyridine which gave $C_1^1(9)$ chains.

References

[1] Fábián, L., Hamill, N., Eccles, K. S., Moynihan, H., & Maguire, A. R. 2011. *J. Am. Chem. Soc, 11: 3522-3528.*

[2] Ohlan, S., Nanda, S & Pathak, D. P. 2013. *MedChem. Res*, 22:5120-5128.

[3] Zhang, Y., Evans, J., Rowe, W., Dinehart, K., Quinn, B. & Connelly, P. 2012. *CrystEngComm*, 14, 7, 2422-2427.

[4] Cruz-Cabeza, A. J. 2012. *CrystEngComm, 4, 6362-6365.*

[5] Desiraju, G. R., Vittal, J. J & Ramanan, A. 2011. Crystal engineering: a textbook. Hackensack: World *Scientific: IISc Press*.

[6] Hathawar R. V., Mohana R. S., Subashini R., Khan, N. F and Guru, R. T.N. 2010. *J. Chem. Sci., 122*, 5, 677-687.

[7] Etter, M. C. 1990. *Acc. Chem, Res, 23, 120.*

[8] Etter, M. C., Macdonald, J. C., Bernstein, J*. 1990. ActaCrystr, B46, 256.*

[9] Vishweshwar, P., Thaimattam, R., Jaskolski, M., Desiraju, G. R. 2002. *Chem. Commun, 17, 1830.*

[10] Sheldrick, G. M. 1997. SHELXS-97, program for crystal structure refinement. University of GÖttingen Germany.

[11] Bis, J. A. & Zaworotko, J. 2005. *Cryst Growth & Des, 5, 3, 1173.*

[12] Aakeroy, C. B., Beffert, K., Desper, J., Elisabeth, E. 2003. *Cryst, Growth Des, 23, 837*.

[13] Robert, J. J., Raj, S. B., Muthiah, P. T. E. 2001. *Acta Cryst, 57, 1206.*

[14] Yvon, K., Jeitschko, W. & Parthe, E. J. 1997. LAZY PULVERIX, a computer program, for calculating X-ray and neutron diffraction powder patterns*. J. Appl.Cryst,* 10: 73-74

CHAPTER FIVE

COCRYSTALS OF 3-CHLORO-4-HYDROXYPHENYLACETIC ACID WITH AMIDE DERIVATIVES

Chapter 5 : COCRYSTALS OF 3-CHLORO-4-HYDROXYPHENYLACETIC ACID WITH AMIDE DERIVATIVES

This chapter focuses on the multicomponent crystals of 3-chloro-4-hydroxyphenylacetic acid with nicotinamide (NAM) and isonicotinamide (ISONAM). The calculated pK_a differences were found to be as follows: 0.17 (NAM-CHPAA) and –0.01 (ISONAM-CHPAA). Based on the obtained values, cocrystal formation was expected in both cases. This was confirmed by the crystal structures which showed the C-O distances recorded fall within the range of cocrystal formation. Both compounds were prepared by the slow evaporation technique.

5.1 Introduction

Cocrystals can be defined as solids that are crystalline single-phase materials composed of two or more different molecule which are solids at ambient temperature.[1] The selected co-formers (nicotinamide and isonicotinamide) were chosen based on the similarities of their functional groups (Figure 5.1) to interact and hydrogen bond with 3-chloro-4-hydroxyphenylacetic acid.

1:1 ratios of each starting material were introduced together into a vial and dissolved respectively in various organic solvents such as ethanol, 1,2-dichloroethane and tetrahydrofuran (THF). The mixtures were stirred for a few minutes using the hot plate. The resulting solutions were left to crystallise by slow evaporation at room temperature (25^0 C). After one to two weeks, block-like crystals of NAM and ISONAM cocrystals were obtained using ethanol and 1,2-dichloroethane/THF respectively.

The cocrystal of CHPAA with nicotinamide crystallised in the monoclinic space group *C2/c,* whereas the isonicotinamide cocrystal crystallised in the triclinic space group $P\bar{1}$. For the NAM cocrystal, d(C-O)= 1.320 Å and 1.205 Å and in the case of the ISONAM cocrystal, d(C-O) = 1.308 Å and 1.210 Å, indicating cocrystal formation. Both cocrystals exhibited strong intermolecular interactions involving N-H•••O and O-H•••O with a water molecule playing a bridging role in the interactions of the nicotinamide cocrystal structure. Furthermore, the cocrystal of NAM exhibits an additional C-H•••Cl interaction. Figure 5.1 below illustrates the chemical structures of the compounds used in study.

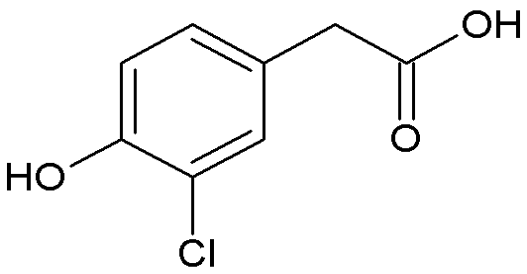

CHPAA

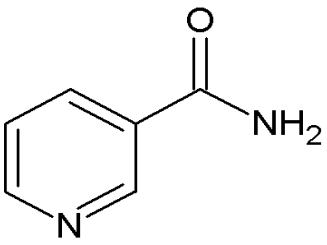

NAM

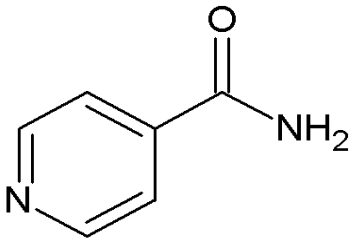

ISONAM

Figure 5. 1: Chemical structures of CHPAA and amides.

5.2 Structural analysis

Both compounds formed block-like crystals with different colours. Yellow-green crystals were observed for the (CHPAA)(1/2H_2O)(NAM) cocrystals, whereas the (CHPAA)(2ISONAM) formed colourless crystals. Both structures were solved using direct methods with SHELXS-97[2] and the model was refined by full matrix least squares on F^2 with SHELXL-97. The crystal data is summarised in Table 5.1.

Table 5. 1: Crystal data and data collection parameters.

Compound	(CHPAA)(1/2H_2O)(NAM)	(CHPAA)(2ISONAM)
Host:guest ratio	1:2	1:1
Molecular formula	$C_{14}H_{14}ClN_2O_{4.5}$	$C_{14}H_{13}ClN_2O_4$
Formula weight [g mol^{-1}]	317.73	308.71
Crystal system	Monoclinic	Triclinic
Space group	*C2/c*	$P\bar{1}$
Z	8	2
D_{cal} [g cm^{-3}]	1.453	1.534
a [Å]	32.963(7)	7.1683(14)
b [Å]	5.0886(10)	11.672(2)
c [Å]	17.322(4)	13.268(3)
α [°]	90.00 (3)	66.36(3)
β [°]	91.43 (3)	88.65(3)
γ [°]	90.00(3)	80.72(3)
Volume [$Å^3$]	2904.6(10)	1002.6(3)
μ(Mo-Kα) [mm^{-1}]	0.285	0.304
T[K]	173(2)	173(2)
F(000)	1320	480
No. of reflections collected	14924	23689
No. of unique reflections	3478	5022
No. of reflections with I>2σ(I)	2513	3970
Index ranges	-42<h<+41; k:±6; l±22	h±9; k:±15 ; l:±17
GooF	1.019	1.052
Final R indices [I>2σ]	R_1=0.0405; wR_2=0.1022	R_1=0.0388; wR_2 =0.1359
R indices [all data]	R_1=0.0633; wR_2=0.0916	R_1=0.0515 ; wR_2=0.1231
Largest diff peak and hole [$eÅ^{-3}$]	0.268; -0.247	0.294; -0.234
$2\theta_{max}$ [°]	55.84	56.74

5.2.1 Cocrystal of (CHPAA)(1/2H_2O)(NAM).

The structure crystallises in the monoclinic space group *C2/c* and its asymmetric unit contains one CHPAA anion, one NAM cation and ½ of a water molecule (Figure 5.2). The unit cell consists of 8 molecules of CHPAA and 8 molecules of NAM (Z= 8). The C-O difference (Δd_{C-O}) was found to be 0.12 Å. Figure 5.3 illustrates the hydrogen bond numbering scheme.

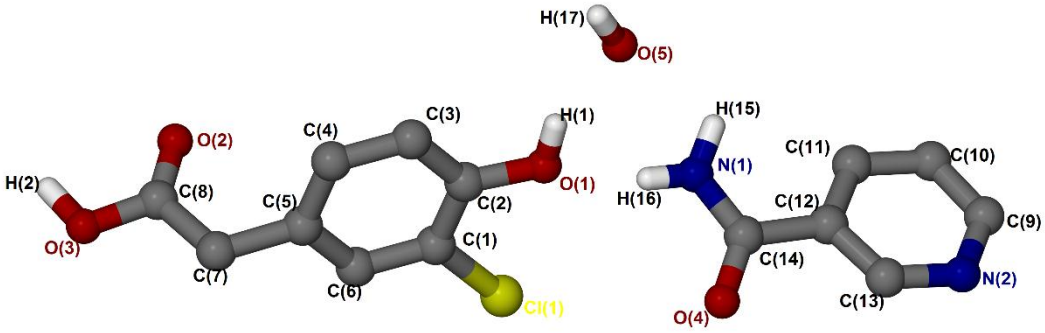

Figure 5. 2: Asymmetric unit of (CHPAA)(1/2H_2O)(NAM).

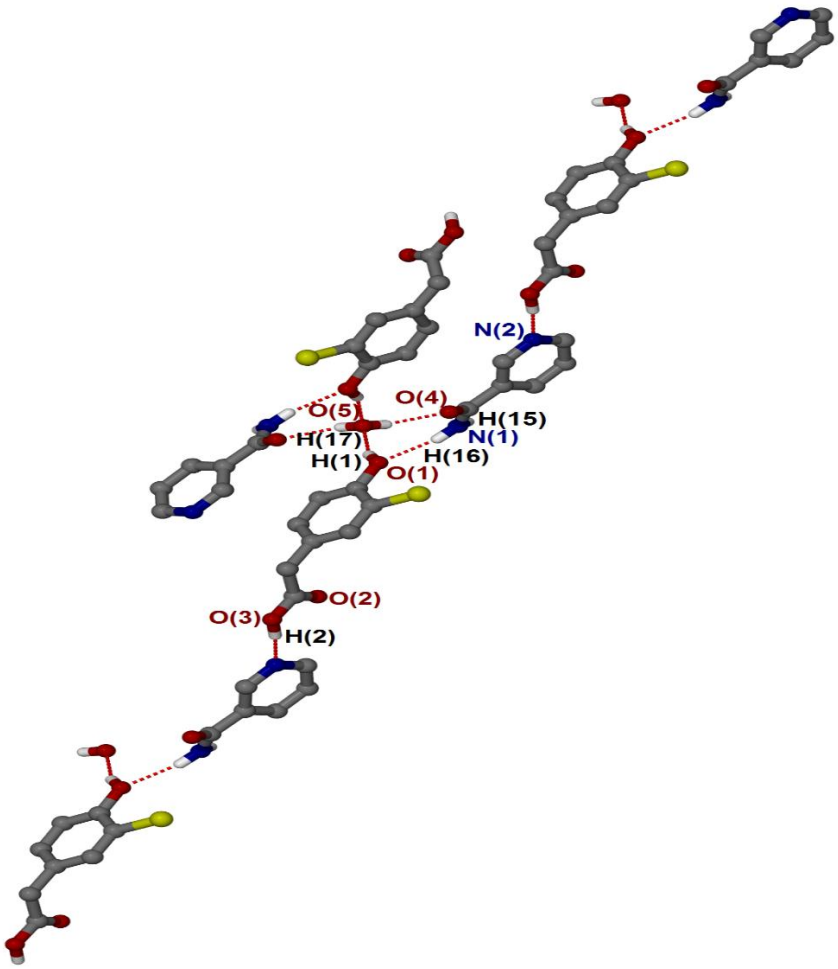

Figure 5. 3: Numbering scheme of (CHPAA)(1/2H_2O)(NAM).

The cocrystal (CHPAA)(1/2H_2O)(NAM) interacts in a zigzag fashion through N-H•••O and O-H•••N interactions. These interactions allowed the structure to extend and generate a chain of hydrogen bonded that can be described as a $C_2^3(8)$ motif. Furthermore, the water molecule plays a bridging role connnecting pairs of CHPAA and NAM molecules via O-H•••O linkages allowing the structure to extend and generate a ring of $R_4^6(6)$ motif. Based on the CSD search version 5.39 (November 2017), out of 56 organic structures containing NAM, six generated one molecule of water in their asymmetric unit as obtained. The hydrogen bond metrics are summarised in Table 5.2 . The packing diagram below (Figure 5.4) illustrates the arrangement of the acid and the amide cation along the *b* axis. This shows how the acid and amide alternate in a linear fashion with a water molecule acting as a bridge between 2CHPAA and 2NAM.

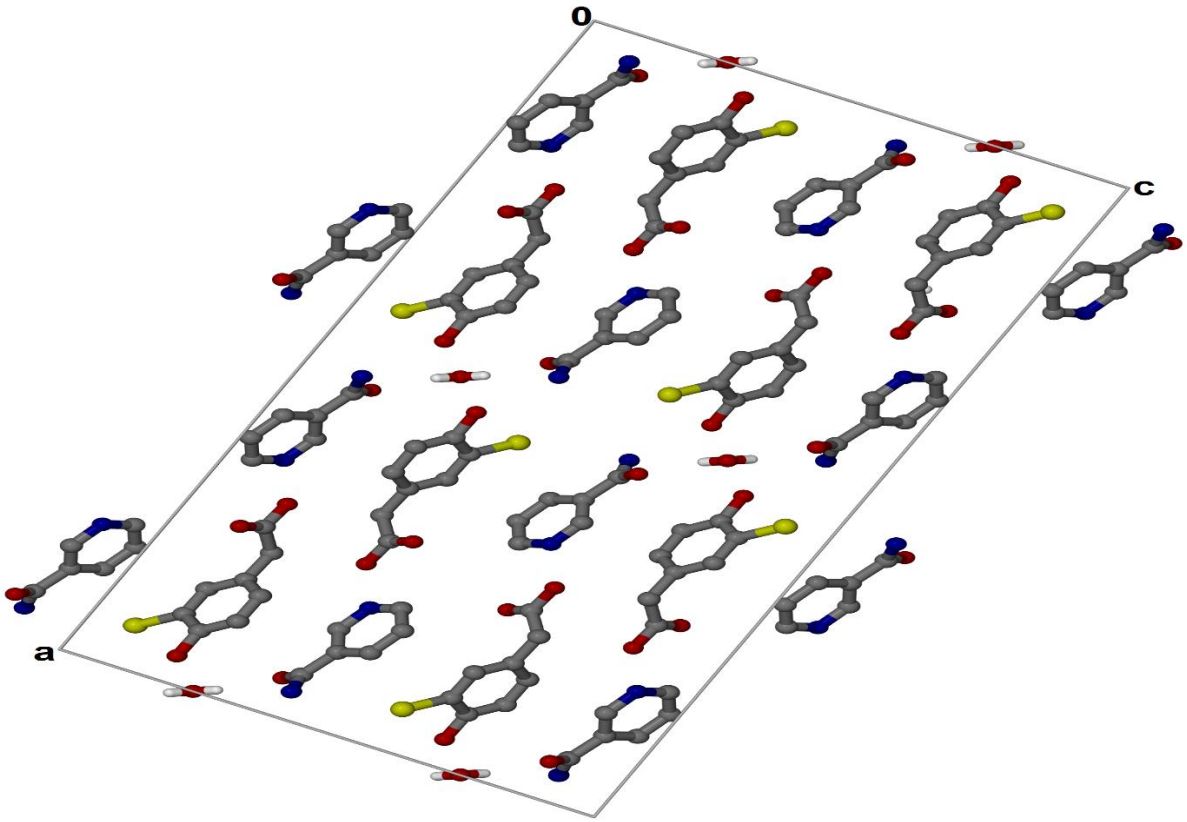

Figure 5. 4: Packing diagram of (CHPAA)(1/2H_2O)(NAM).

.

5.2.2 Cocrystal of (CHPAA)(2ISONAM)

The structure crystallises in the triclinic space group $P\bar{1}$ and its asymmetric unit contains one molecule of CHPAA and two molecules of ISONAM (Figure 5.6). The unit cell consists of two molecules of CHPAA and four molecules of ISONAM (Z=2). $(\Delta d_{C-O}) = 0.1$Å C-O. Figure 5.7 below illustrates the numbering scheme of (CHPAA)(2ISONAM).

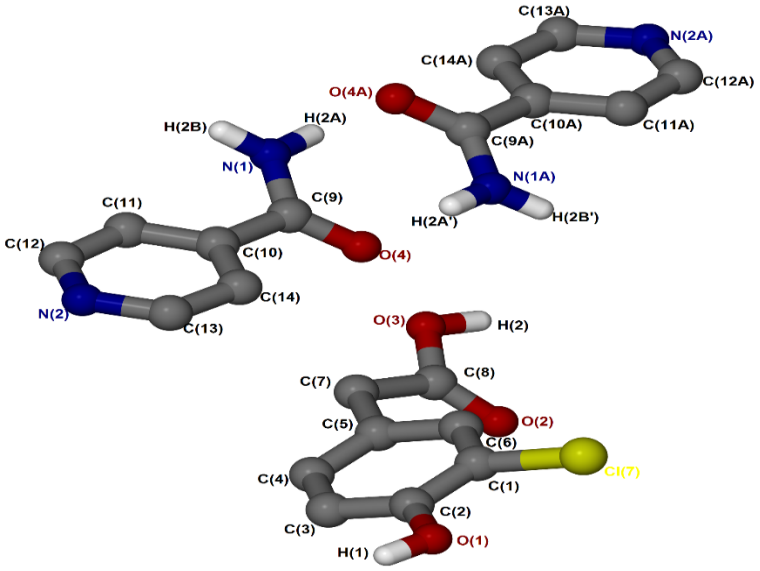

Figure 5. 5: Asymmetric unit of (CHPAA)(2ISONAM).

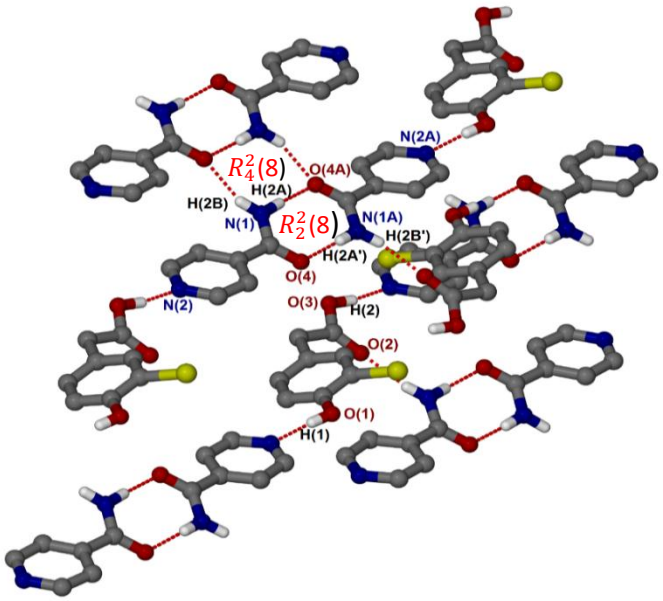

Figure 5. 6: Numbering scheme of (CHPAA)(2ISONAM).

The 1:2 cocrystal of (CHPAA)(2ISONAM) forms strong intermolecular interactions whereby the carboxylic acid interacts with isonicotinamide in a linear fashion through N-H•••O and O-H•••N interactions. These interactions consist of the amide-amide homosynthon forming hydrogen-bonded rings of $R_2^2(8)$. This motif is described as robust motifs and it is one the most frequently observed cyclic-hydrogen bonded motifs in the solid-state.[3] Based on the CSD search version 5.39 (November 2017), out of 195 organic structures containing ISONAM, 124 contain the amide-amide homosynthon motif. Furthermore, the structure is linked through additional hydrogen bonds via N-H•••O, forming several motifs of $R_4^2(8)$, $R_4^4(16)$ and $R_4^4(32)$.

In contrast with (CHPAA)(1/2H_2O)(NAM), where the hydrogen bonds were arranged in a zigzag fashion with water molecules playing a bridging role through a $R_4^6(6)$ ring, in the (CHPAA)(2ISONAM) structure interactions are arranged in a linear fashion via N-H•••O and generate a $R_2^2(8)$ homosynthon.

When both structures are packed along the *b* axis, it can be seen that the molecules in the cocrystal of nicotinamide (Figure 5.4) are arranged in columns with the acid and the amide in alternate directions whereas in the isonicotinamide cocrystal (Figure 5.7) the molecules pack in ribbons, with the acid molecules overlaying in opposite directions between isonicotinamide molecules.

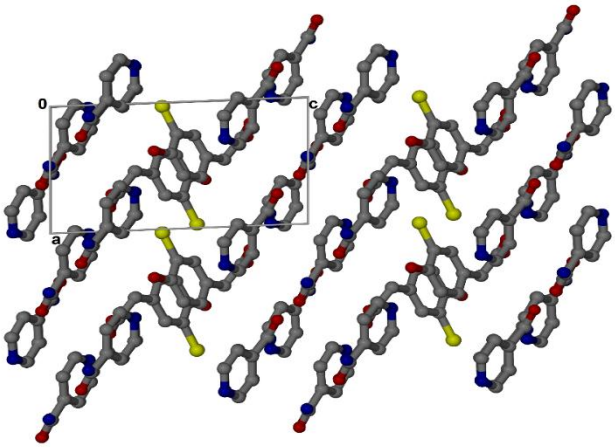

Figure 5. 7: Packing diagram of (CHPAA)(2ISONAM) along [010].

Table 5. 2: Geometric data of hydrogen bonding in cocrystals formed by CHPAA.

D-H···A	d(D-H) Å	d(H···A) Å	d(D···A) Å	D-H···Å (°)	Symmetry operator
(CHPAA)(1/2H$_2$O)(NAM)					
N1-H16···O1	0.85	2.08	2.898(2)	164	-
N1-H15•••O4	0.88	2.24	3.020 (2)	146	x, y+1, z
O1-H1···O5	0.82	1.88	2.664(2)	158	-
O5-H17···O4	0.83	2.02	2.774(15)	151	-x, y+$\frac{1}{2}$, z
O3-H2···N2	0.95	1.73	2.678(2)	175	x+$\frac{1}{2}$, y+$\frac{1}{2}$, z
C11-H11•••Cl1	0.95	3.08	3.991(2)	162	-x, 1-y, 2-z
(CHPAA)(2ISONAM)					
N1A-H2B'···O2	0.85	2.00	2.84(17)	163	-x, -y+1, -z+1
N1-H2A···O4A	0.91	1.99	2.89(17)	174	-
N1A-H2A'•••O4	0.90	2.06	2.96(17)	178	-
O3-H2···N2	0.91	1.69	2.60(16)	170	x-1, y,z+1
O1-H1•••N2A	0.84	1.91	2.75 (16)	174	x+1, y-1, z
N1-H2B•••O4A	0.88	2.03	2.88 (16)	160	-x+1, -y+2, -z

5.3 Torsion angles of CHPAA

3-chloro-4-hydroxyphenylactic acid (Figure 5.8) formed two major conformations when cocrystallised with nicotinamide and isonicotinamide. For the cocrystal of (CHPAA)(1/2H$_2$O)(NAM) the torsion angles of CHPAA are τ_1(C6-C5-C7-C8) = 105.08 ^{0} and τ_2(O2-C8-C7-C5)= 1.90 ^{0} . In the case of (CHPAA)(2ISONAM), the torsion angles are τ_1(C6-C5-C7-C8)= 35.6 ^{0} and τ_2(O2-C8-C7-C5)= 25.79 ^{0} . Table 5.3 below illustrates torsion angles in both structures. The overlay of both structures (Figure 5.9) in Mercury showed that the CHPAA conformation was significantly different in both cases.

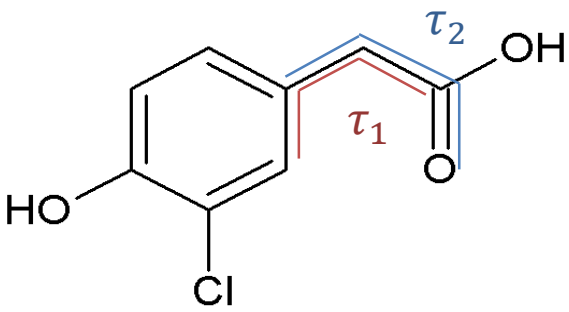

Figure 5. 8: Torsion angles of CHPAA.

Table 5. 3: Torsion angles of CHPAA

Torsion angles	τ_1(C6-C5-C7-C8)	τ_2(O2-C8-C7-C5)
(CHPAA)(1/2H₂O)(NAM)	105.08	1.90
(CHPAA)(2ISONAM)	35.6	25.79

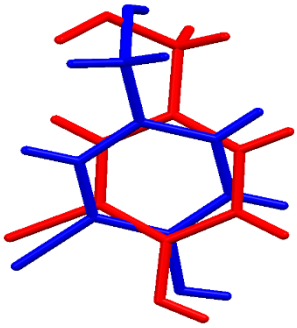

Figure 5. 9: Overlay conformation of (CHPAA) in (CHPAA)(1/2H₂O)(NAM) (red) in (CHPAA)(2ISONAM) (blue).

5.4 Thermal analysis of (CHPAA)(1/2H_2O)(NAM) and (CHPAA)(2ISONAM)

The thermal analysis of both new solid forms is given in Figures 5.10-5.11. For the (CHPAA)(1/2H_2O)(NAM) cocrystal, one endotherm (blue) was observed at $T_{onset} = 339.2\ K$ corresponding to the melt of the new solid form. The melting point of the cocrystal was lower than those of the starting materials. The melt of nicotinamide (green) was observed at $T_{onset} = 399.8\ K$ and that of CHPAA (red) at $T_{onset} = 378.3\ K$.

In the case of (CHPAA)(2ISONAM), the crystal gave two thermal events (blue), the first event corresponds to the melt of the cocrystal at $T_{onset} = 348.3\ K$ and the second at $T_{onset} = 370.8\ K$ could be due to a phase change. The melting of Isonicotinamide (green) occurred at T_{onset}= 393.7 K and the CHPAA melting (red) occurred at T_{onset}=378.3 K.

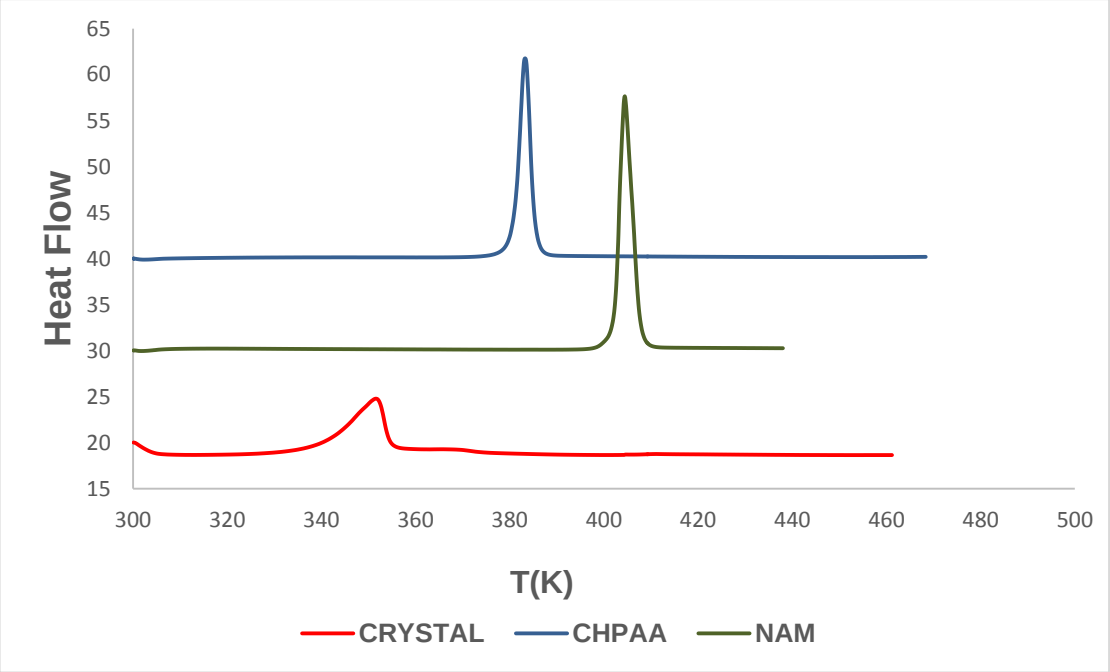

Figure 5. 10: DCS curves of (CHPAA)(1/2H_2O)(NAM): blue (CHPAA); green (NAM) red (crystal).

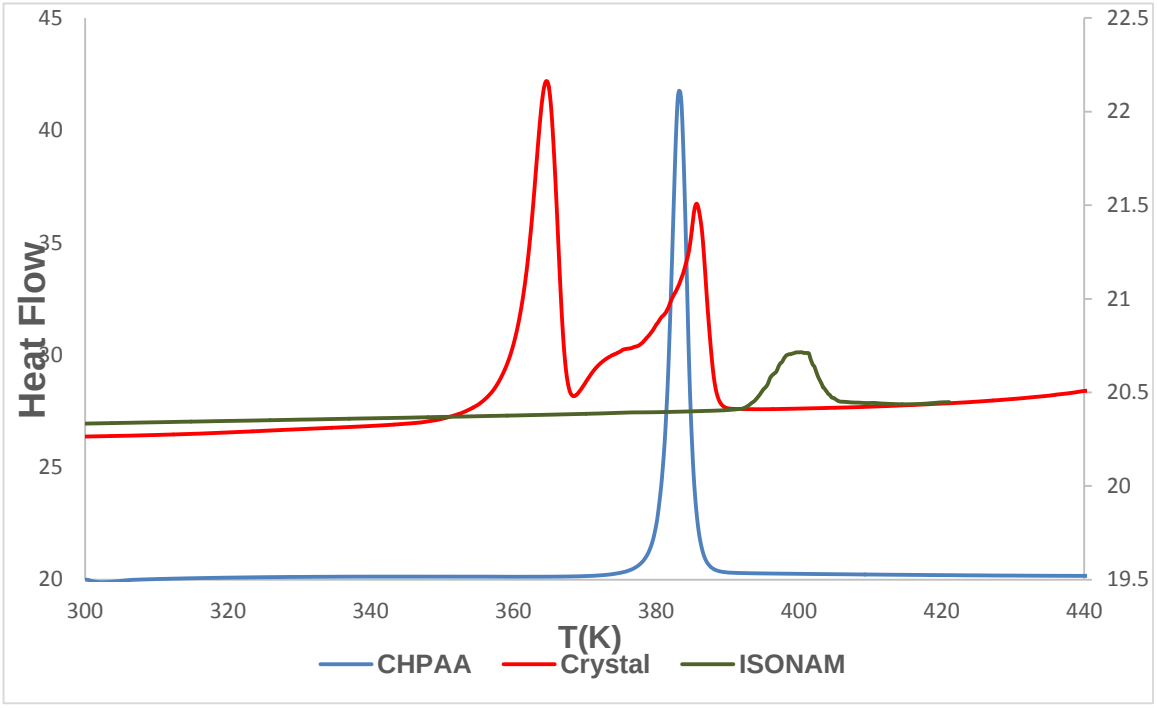

Figure 5. 11: DSC of (CHPAA)(2ISONAM): blue (CHPAA); green (ISONAM); red (crystal).

The melt of $(CHPAA)(ISONAM)$ appeared at $T_{onset} = 348.3.1\ K$ which is higher than that found for (CHPAA)(1/2H_2O)(NAM) $T_{onset} = 339.2\ K$, which did not correlate to the expected order of stability of the two amides ie. the m.p. of ISONAM ($T_{onset} = 394.2\ K$) < m.p of NAM ($T_{onset} = 399.8\ K$). The high melting point of (CHPAA)(ISONAM) can be related to the crystal structure with the hydrogen bonds being involved. Table 5.2 shows 6 (N-H•••O and O-H•••N) hydrogen bonds for (CHPAA)(2ISONAM) compared to 5 (N-H•••O; O-H•••N, O-H•••O) for (CHPAA)(1/2H_2O)(NAM) which also contains an expected water in the crystal structure.

5.5 Grinding and slurry experiments of (CHPAA)(1/2H_2O)(NAM) and (CHPAA)(2ISONAM)

The calculated PXRD patterns of the cocrystals obtained from LAZYPULVERIX[4] were compared to the PXRD pattern of the CHPAA, as well as those PXRD patterns obtained from various methods. The PXRD results are shown in Figures 5.12-5.13. The grinding and slurry experiments were carried out in the same way as in the previous chapters. However, the slurry experiment of the cocrystal obtained with NAM did not give a precipitate, and thus the PXRD pattern could not be obtained.

For the NAM cocrystal (Figure 5.12), the PXRD pattern from the grinding experiment (green) is similar to the PXRD for the calculated (blue) and different from the starting material PXRD pattern (red). This indicated that the preparation was successful.

In the case of the $ISONAM$ cocrystal (Figure 5.13), the PXRD pattern of the ground product (green) matched that of the PXRD of the calculated (blue) and slurry PXRD patterns (yellow). This indicated that the reaction was also successful.

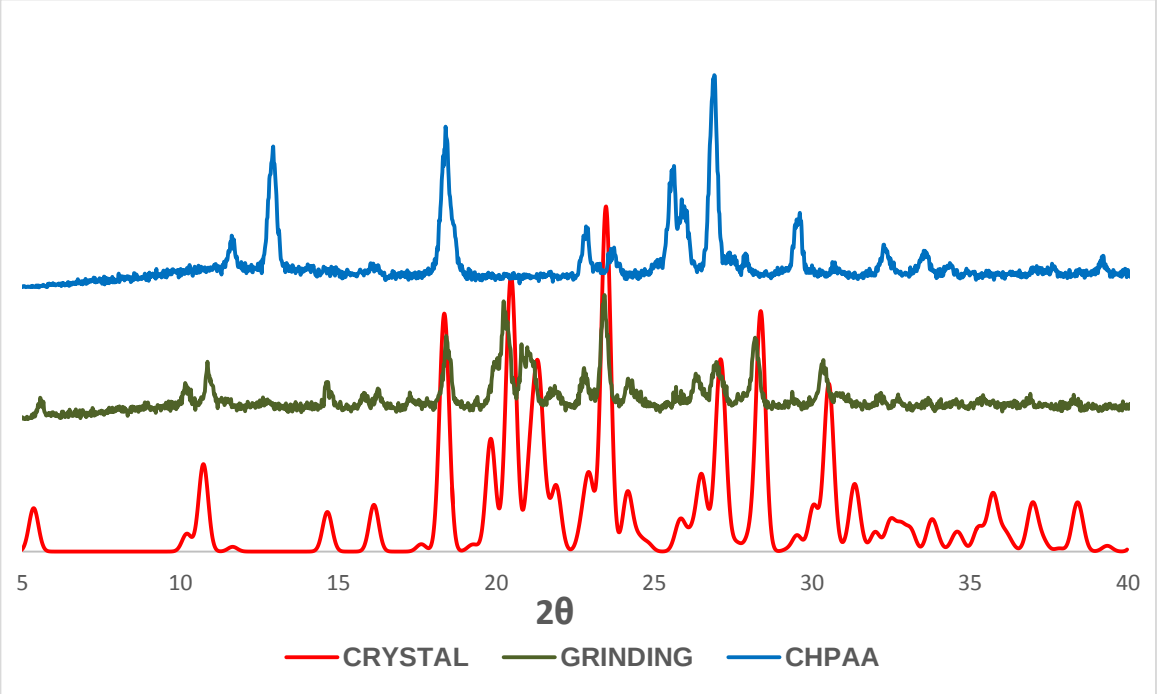

Figure 5. 12: PXRD patterns of (CHPAA)(1/2H_2O)(NAM).

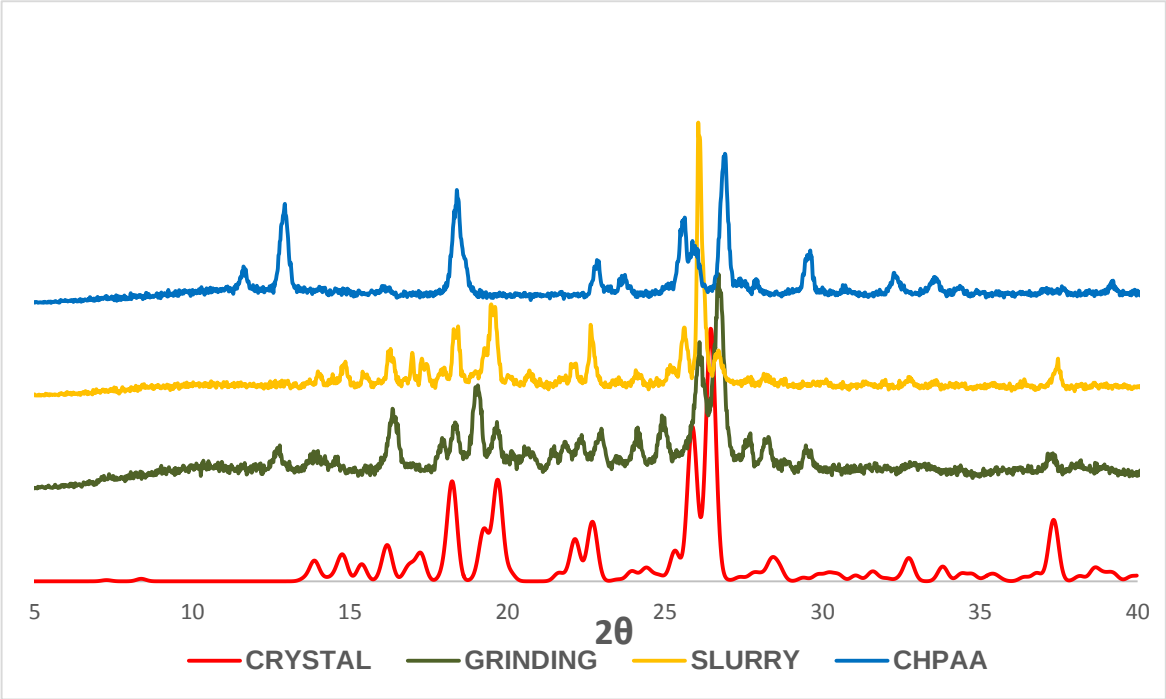

Figure 5. 13: PXRD patterns of (CHPAA)(2ISONAM).

5.6 FTIR spectroscopy

The IR spectra are shown in Figures 5.14 and 5.15. Based on both spectra, the peak at 3446 cm^{-1}(blue) assigned to the free OH band of CHPAA, reappeared in each spectrum of the new solids formed (red), but is shifted. This indicates that there was no charge distribution in both cases from the acid to each co-former and thus, the resulting compounds are neutral cocrystals. In both cocrystals, The COO band was observed at 1698 and 1707 cm^{-1} (green). The bands at 3360 and 3369 cm^{-1} were assigned to NH.

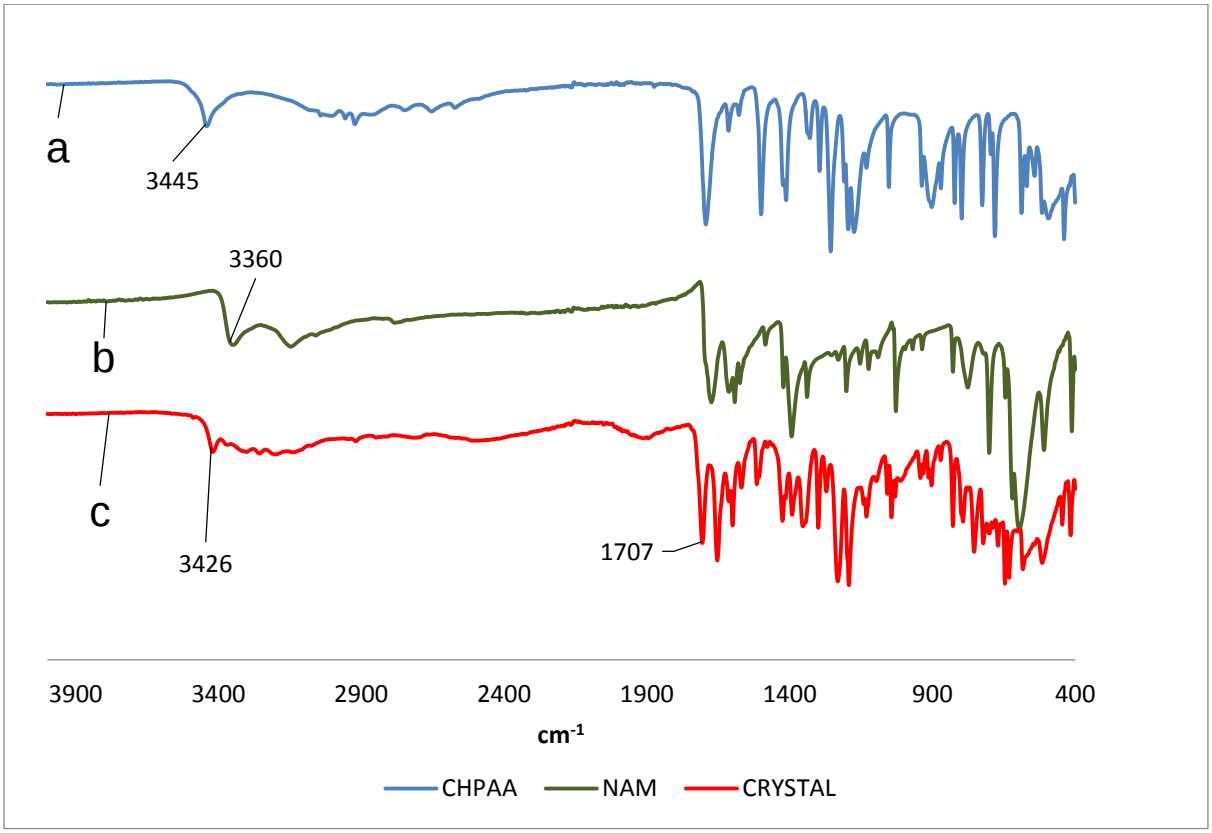

Figure 5. 14: FTIR spectroscopy of (CHPAA)(1/2H_2O)(NAM): a (CHPAA); b (NAM), c (crystal).

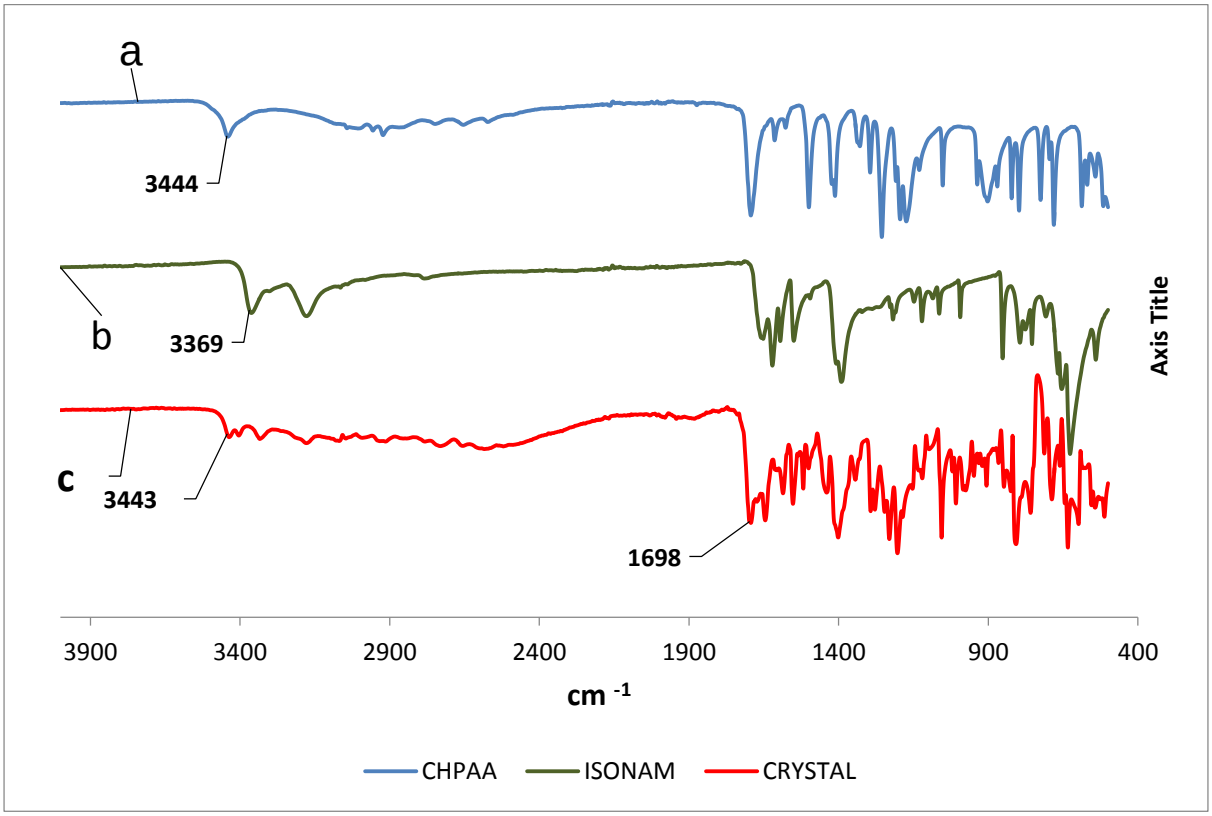

Figure 5. 15: FTIR spectroscopy of (CHPAA)(2ISONAM): a (CHPAA); b (ISONAM), c (crystal).

5.7 Conclusion

Two multicomponent crystals of nicotinamide and isonicotinamide with 3-chloro-4-hydroxyphylacetic acid were successfully prepared. Both solid forms were obtained from different organic solvents i.e. ethanol (NAM-CHPAA) and 1,2-dichloroethane/THF (ISONAM-CHPAA) using the slow evaporation method. Experimental analysis showed that both solid forms are cocrystals, as predicted using the pK_a rule. The structures were characterised by several instrumental methods including DSC, FTIR, PXRD and single crystal X-ray diffraction. The thermal stability showed that the (CHPAA)(2ISONAM) cocrystal was more stable than the cocrystal of (CHPAA)(1/2H_2O)(NAM). The FTIR spectra of the new solids showed that the OH band was present and shifted due to the hydrogen bond, confirming the cocrystal formations. Further study on the C-O distances also confirmed the cocrystal formation. In the structure of (CHPAA)(2ISONAM), the amide-amide homosynthon was present together with acid(OH)•••N(ISONAM). However, for (CHPAA)(1/2H_2O)(NAM), water was present in the crystal structure resulting in a water molecule bridging two CHPAA and two NAM molecules as well as (acid)OH•••N(NAM) interactions.

References

[1] Aitipamula, S., Banerjee, R., Bansal, A. K., Biradha, K., Cheney, M. L., Choudhury, A. R., Desiraju, G. R., Dikundwar, A. G., Dubey, R., Duggirala, N., Ghogale, P. P., Gosh, S., Goswami, K. P., Goud, N. R., Jetti, R. R. K., Karpinski, P., Kaushik, P., Kumar, D., Kumar, V., Moulton, B., Mukherjee, A., Mukherjee, G., Myerson, A. S., Puri, V., Ramanan, A., Rajamannar, T., Reddy, C. M., Rodriguez-Hernedo, N., Rogers, R. D., Row, T. N. G., Sanphui, P., Shan, N., Shete, G., Singh, A., Sun, C. C., Swirft, J. A., Thaimattam, R., Thakur, T. S., Thaper, R. K., Thomas, S. P., Tothadi, S., Vangala, V. R., Variankaval, N., Vishweshar, P., Weyna, D. R & Zoworotko, M. J. 2012. *Cryst Growth, Des, 2147-2152*

[2] Sheldrick, G. M. SHELXS-97. 1997. Program for crystal structure resolution, University of GÖttingen, GÖttingen, Germany.,

[3] Allen, F. H., Shields, G. P, Taylor, R., Raithby, P. R. 1998. *Chem Comm,* 9, 1043-1044.

[4] Yvon, K., Jeitschko, W. & Parthe, E. J. 1997. LAZY PULVERIX, a computer program, for calculating X-ray and neutron diffraction powder patterns*. J. Appl.Cryst*, 10: 73-74

CHAPTER SIX

COCRYSTALS OF 3-CHLORO-4-HYDROXYPHENYLACETIC ACID WITH PHENAZINE AND 4,4'-BIPYRIDINE

Chapter 6 : COCRYSTALS OF 3-CHLORO-4-HYDROXYPHENYLACETIC ACID WITH PHENAZINE AND 4,4'-BIPYRIDINE

In this chapter, two multicomponent crystal structures of phenazine and 4,4'-bipyridine with 3-chloro-4-hydroxyphenylacetic acid were synthesised using the slow evaporation technique. The selection of co-formers (phenazine and bipyridine) was made based on the similarity of the ring bulkiness in both compounds containing two nitrogen atoms located in different positions and the well-known ability of these compounds to form hydrogen bonds with organic acids. The calculated ΔpK_a values were recorded and fall within the expectation range of cocrystal formation which was confirmed by the crystal structures and the calculation of the C-O distances of each resulting compound. Both compounds were characterized using similar instrumentation techniques mentioned in previous chapters.

6.1 Introduction

The cocrystals of (CHPAA)(3/2PHZN) and (2CHPAA)(BIPY) were prepared by the slow evaporation technique. After 1-3 weeks, block-like crystals were obtained for the cocrystal (CHPAA)(3/2PHZN), and needle-like crystal for the cocrystal (2CHPAA)(BIPY).

The calculated ΔpK_a value for both cocrystals were found to be -0.76 and 0.94 respectively. These values fall within the range described by Cruz-Cabeza,[1] for the possibility of cocrystal formation. In addition, the recorded C-O distances of CHPAA were 1.311 Å and 1.220 Å in (CHPAA)(3/2PHZN) and 1.329 Å and 1.209 Å in (2CHPAA)(BIPY), thus the Δd_{c-o}= 0.12 Å and 0.09 Å respectively.

The cocrystal (CHPAA)(3/2PHZN) crystallises in the monoclinic space group $P2_1/c$, whereas (2CHPAA)(BIPY) crystallises in the triclinic space group $P\bar{1}$. Both cocrystals displayed strong intermolecular interactions of O-H•••N, and weak interactions of C-H•••O and C-H•••Cl. Figure 6.1 below illustrates the chemical structures of the compounds used in this study.

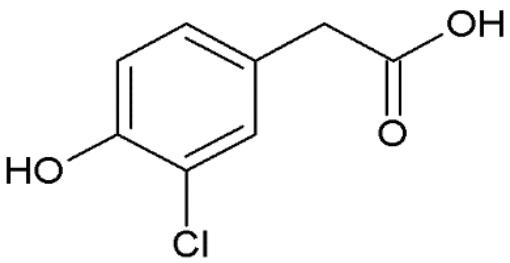

CHPAA

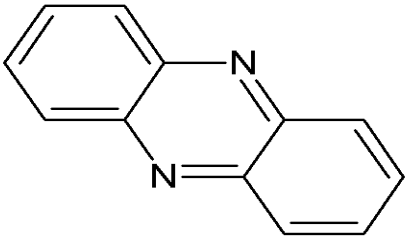

PHZN

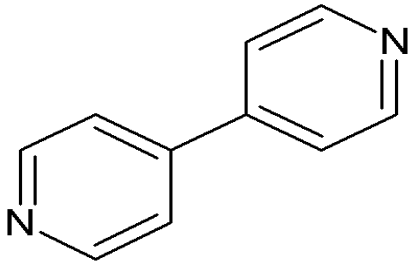

BIPY

Figure 6. 1: Chemical structures of CHPAA and aromatic compounds.

6.2 Structural analysis

Both compounds formed block and needle like-crystals with different colours. Yellow dark colour was observed for (CHPAA)(3/2PHZN), whereas (2CHPAA)(BIPY) exhibited pale yellow crystals. The structures were solved using direct methods with SHELXS-97,[2] and the model was refined by full matrix least squares F^2 using SHELXL-97. Table 6.1 illustrates the crystal data and data collection parameters.

Table 6. 1: Crystal data and data collection parameters of cocrystals

Compound	(CHPAA)(3/2PHZN)	$(2CHPAA)(BIPY)$
Host:guest ratio	1: $\frac{3}{2}$	2:1
Molecular formula	$C_{26}H_{19}ClN_3O_3$	$C_{26}H_{22}Cl2N_2O_6$
Formula weight [g mol^{-1}]	456.89	529.38
Crystal system	Monoclinic	Triclinic
Space group	$P2_1/c$	$P\bar{1}$
Z	4	4
D_{cal} [g cm^{-3}]	1.430	1.449
a [Å]	17.3205(11)	7.4413(15)
b [Å]	17.7420(12)	12.446(3)
c [Å]	6.9482(5)	13.340(3)
α [°]	90.00	80.71(3)
β [°]	96.276	86.92(3)
γ [°]	90.00	84.72(3)
Volume [Å^3]	2122.4(2)	1213.1(4)
μ(Mo-Kα) [mm^{-1}]	0.216	0.314
T[K]	173(2)	173(2)
F(000)	948	548
No. of reflections collected	55902	29852
No. of unique reflections	5285	5824
No. of reflections with I>2σ(I)	3899	4636
Index ranges	h±23; k:±23; I±9	h±9; k:±16 ; I:±17
GooF	1.019	0.959
Final R indices [I>2σ]	R_1=0.0367; wR_2=0.0949	R_1= 0.0381; wR_2 = 0.1104
R indices [all data]	R_1=0.0570; wR_2=0.0853	R_1= 0.0512 ; wR_2= 0.1006
Largest diff peak and hole [eÅ^{-3}]	0.269; -0.263	0.314; -0.356
$2\theta_{max}$ [°]	56.72	55.9

6.2.1 Cocrystal of (CHPAA)(3/2PHZN).

The structure crystallises in the monoclinic space group ($P2_1/c$) and its asymmetric unit contains one molecule of CHPAA and one and half molecules of PHZN (Figure 6.2). The unit cell consists of four molecules of CHPAA and eight molecules of PHZN (Z=4). Figures 6.3 illustrates the hydrogen bond numbering scheme.

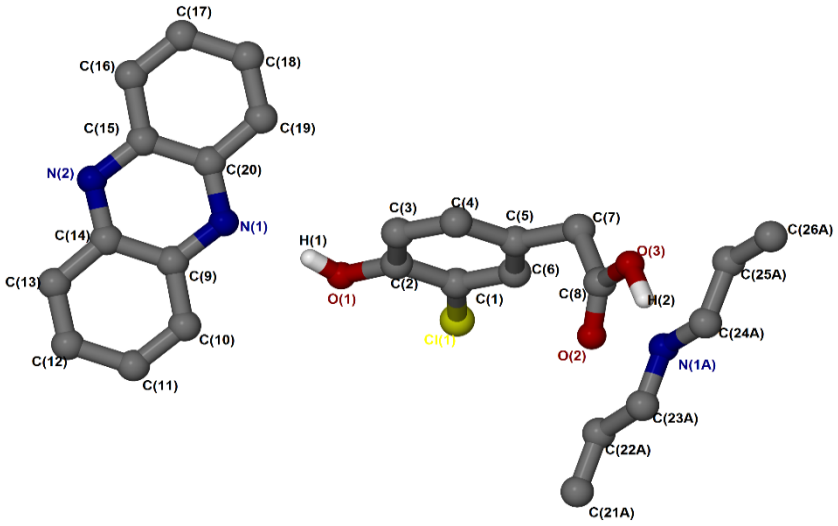

Figure 6. 2: Asymmetric unit of (CHPAA)(3/2PHZN).

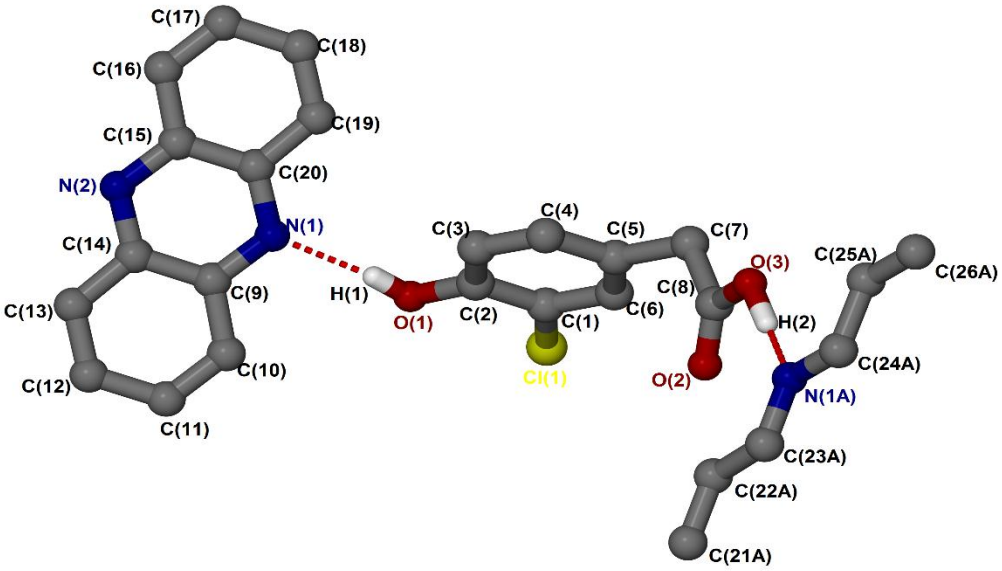

Figure 6. 3: Hydrogen bond numbering scheme of (CHPAA)(3/2PHZN).

The structure above (Figure 6.3) displays two intermolecular interactions of O-H•••N. These hydrogen bonds consist of the hydroxyl group of the acid molecule connecting with one of the nitrogens (N1) of the phenazine through O1-H1•••N1. Furthermore, the hydroxyl carbonyl also forms an additional hydrogen bond via O3-H2•••N1A. The acid molecule plays a bridging role of connecting with one and half molecules of the phenazine and, thus generate a chain of $C_1^1(2)$ motif. The overall structure also displays weak hydrogen bonds of C12-H12•••Cl and C12-H12•••O2. The obtained chlorine closest contact distance falls within the range described by Hathwar *et al*. Table 6.2 summarizes the hydrogen bond data obtained in this chapter. The packing diagram below (Figure 6.4) displays the arrangement of the acid and the co-former along [010].

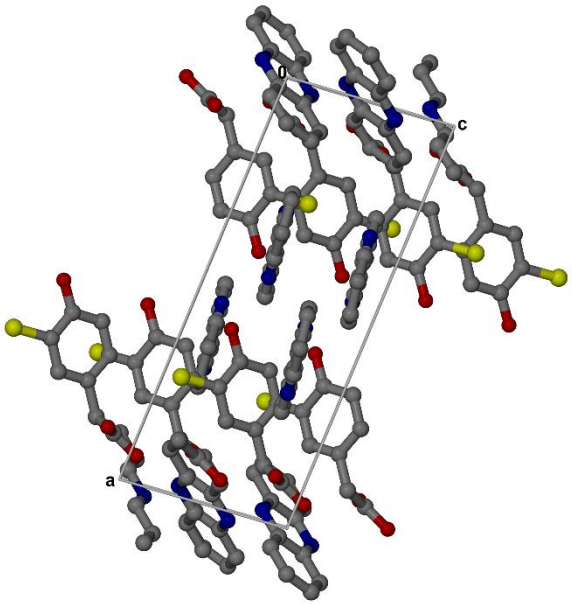

Figure 6. 4: Packing diagram of (CHPAA)(3/2PHZN) along [010].

6.2.2 Cocrystal of (2CHPAA)(BIPY)

(2CHPAA)(BIPY) crystallises in the triclinic space group $P\bar{1}$ and its asymmetric unit contains two CHPAA molecules and one molecule of BIPY (Figure 6.5). The unit cell consists of four molecules of CHPAA and two molecules of BIPY (Z=4). Figure 6.6 below illustrates the hydrogen bond numbering scheme of (2CHPAA)(BIPY).

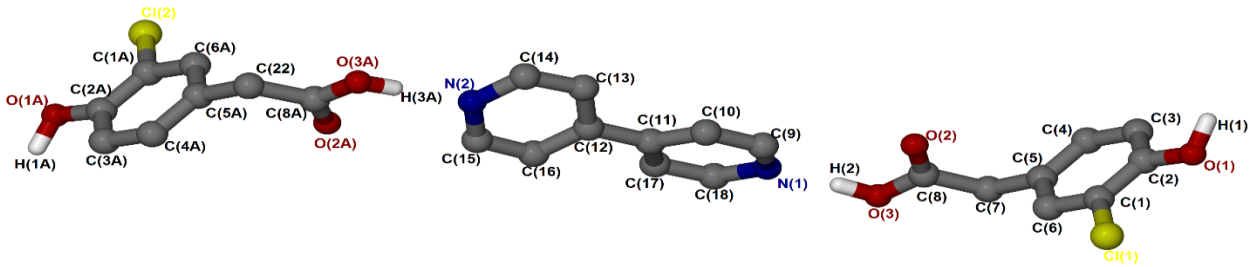

Figure 6. 5: Asymmetric unit of (2CHPAA)(BIPY).

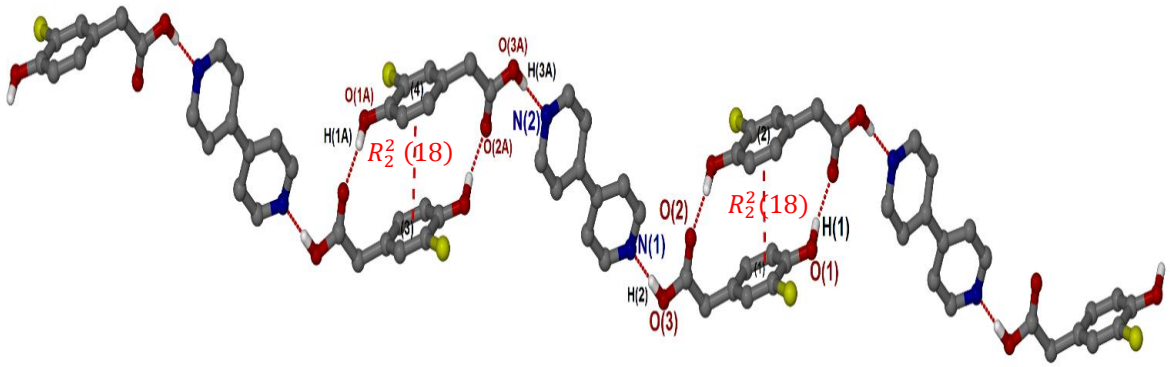

Figure 6. 6: Hydrogen bond numbering scheme of (2CHPAA)(BIPY).

The 2:1 cocrystal (2CHPAA)(BIPY) also displays intermolecular interactions of O-H•••N and including O-H•••O. Furthermore, the hydroxyl group also formed an additional hydrogen bond with the neighbouring carbonyl via O1A-H1A•••O2. In contrast with the previous structure where the host bridged between one and half co-formers, in this numbering scheme the co-former (BIPY) is bridging between with two CHPAA molecules by allowing the overall structure to extend symmetrically in a zigzag fashion and generate a dimer of $D_2^2(12)$ motif. The CHPAA molecules form hydrogen bonded dimers which can be described as $R_2^2(18)$ rings,[3] via O3-H3A•••N2 and O1-H1•••O2A. The overall structure is stabilised by $\pi - \pi$ stacking interactions involving the acid–acid molecules with the centroid distance of 3.687 Å. Figure 6.7 illustrates the packing along [100].

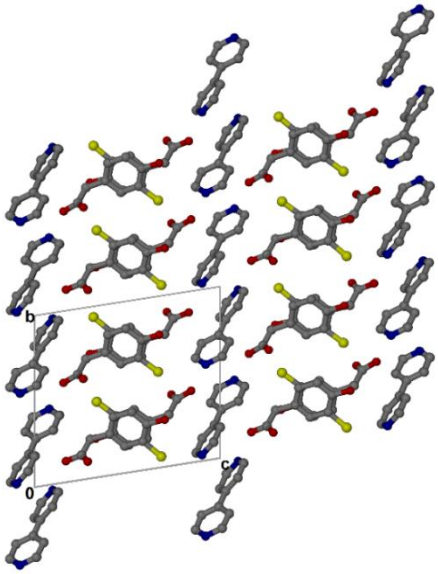

Figure 6. 7: Packing diagram of (2CHPAA)(BIPY) along [100].

The overall structure involves columns of acid molecules alternating with columns of BIPY to form the ladder.

Table 6. 2: Geometric data of hydrogen bonding in cocrystals formed by CHPAA.

D-H···A	d(D-H) Å	d(H···A) Å	d(D···A) Å	D-H···Å (°)	Symmetry operator
$(\boldsymbol{CHPAA})(\frac{\boldsymbol{3}}{\boldsymbol{2}}\boldsymbol{PHZN})$					
O3-H2•••N1A	0.97	1.79	2.739(18)	163	-
O1-H1•••N1	0.80	2.00	2.789 (17)	170	-
C12-H12•••O2	0.95	2.44	3.358(2)	161	1-x, 1-y, -z
C12-H12•••Cl1	0.95	3.22	3.480(18)	98	1-x, 1-y, 1-z
$(\boldsymbol{2CHPAA})(\boldsymbol{BIPY})$					
O3A-H3A•••N2	0.84	1.82	2.661(19)	178	-
O3-H2•••N1	0.92	1.70	2.619(19)	177	-
O1A-H1A•••O2	0.91	1.79	2.689 (17)	167	x, y-1, z-1
O1-H1•••O2A	0.90	1.82	2.702(18)	162	x, y+1, z+1

6.3 Torsion angles of CHPAA

CHPAA, adopted two major conformations (Figure 6.8) when combined with phenazine and 4,4'-bipyridine. For the cocrystal (CHPAA)(3/2PHZN), the freedom of rotation involving the ring and the twisting of acetic acid group are τ_1(C6-C5-C7-C8) = 84 ^{0} and τ_2(O2-C8-C7-C5) = 35 ^{0} . In the case of (CHPAA)(BIPY), the rotations are τ_1(C6-C5-C7-C8) = 69 ^{0} and τ_2(O2-C8-C7-C5) = 17 ^{0} . Based on the overlay conformation (Figure 6.9) in both structures, it was found that CHPAA shows more flexibility in the PHZ structure compared to the BIPY structure. This is consistent with the twisting of the acetic acid group of CHPAA to accommodate the two crystallographically independent PHZ molecules.

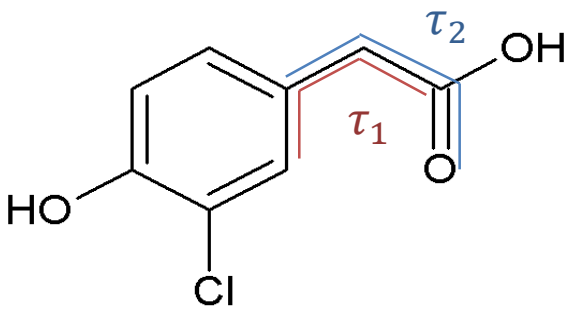

Figure 6. 8: Torsion angles of CHPAA.

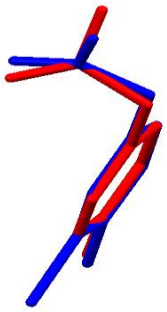

Figure 6. 9: Overlay conformation of CHPAA in (CHPAA)(3/2PHZN) (red); and in (2CHPAA)(BIPY) (blue) along [010].

6.4 Thermal analysis of (CHPAA)(3/2PHZN) and (2CHPAA)(BIPY)

The DSC results are shown in Figures 6.10 and 6.11. For (CHPAA)(3/2PHZN), the melt of the cocrystal appeared at $T_{on} = 409.8\ K$ is in between that of the pure PHZN (green) with $T_{on} = 448.15\ K$ and CHPAA (blue) with $T_{on} = 378.5\ K$.

In the case of (2CHPAA)(BIPY), the melt of the cocrystal (red) appeared at $T_{on} = 422.1\ K$ which is much higher than the melting points of CHPAA (blue) $T_{on} = 378.5\ K$ and BIPY (blue), T_{on} = 322.1 K. Thus, co-crystallisation of CHPAA with BIPY resulted in a co-crystal with greater thermal stability than that of the starting materials. It should be noted that the melting of (2CHPAA)(BIPY) is preceded by four minor thermal events which is probably due to impurities in the sample.

Thus based on the DSC results it was observed that (2CHPAA)(BIPY) shows greater thermal stability than (CHPAA)(3/2PHZN).

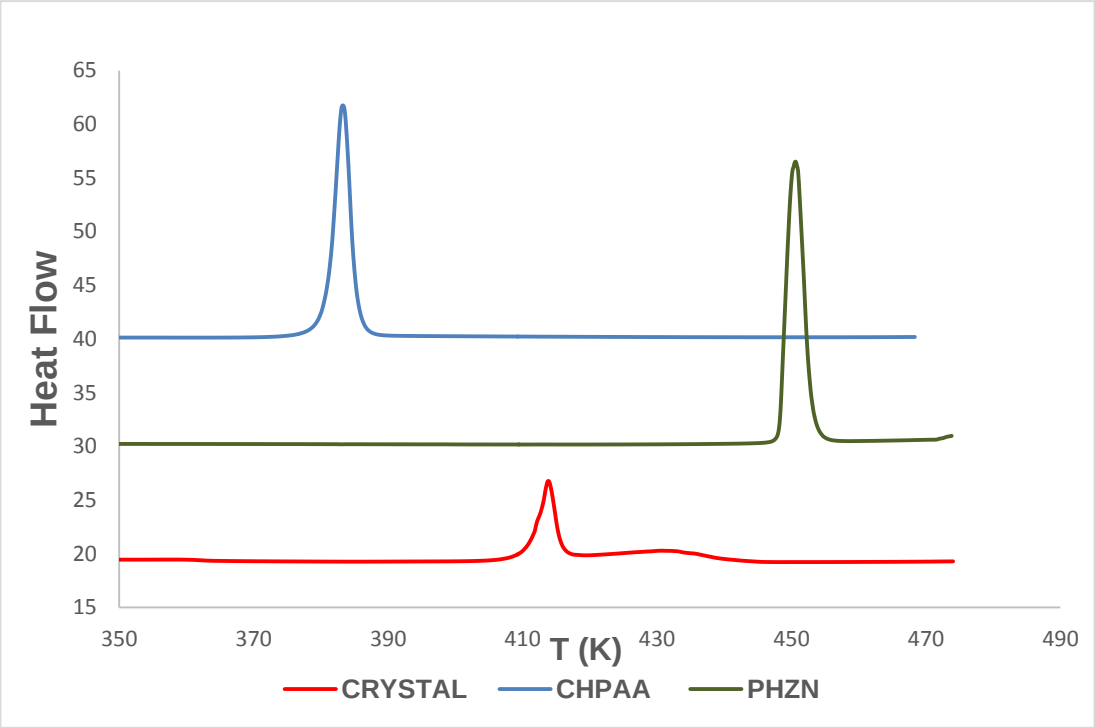

Figure 6. 10: DSC curves of (CHPAA)(3/2PHZN): blue (CHPAA); green (PHZN); red (crystal).

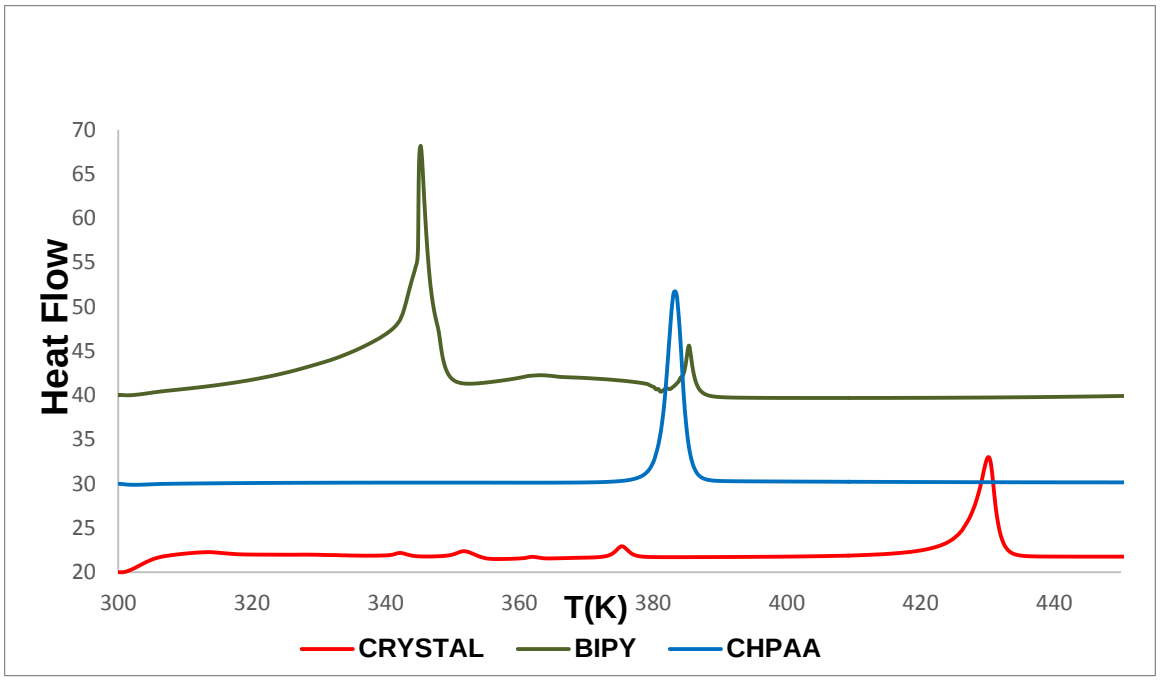

Figure 6. 11: DSC curves of (2CHPAA)(BIPY): blue (CHPAA); green (BIPY); red (crystal).

6.5 Grinding and slurry experiments of (CHPAA)(3/2PHZN) and (2CHPAA)(BIPY)

The grinding and slurry experiments were carried out in the same way as described in previous chapters. The PXRD patterns of the grinding and slurry experiments are shown in Figures 6.12 and 6.13. For the cocrystal (CHPAA)(3/2PHZN), the PXRD pattern of the grinding experiment (green) is similar to that of the calculated PXRD pattern (red) obtained from LAZYPULVERIX[4] indicating that the grinding experiment was successful in the preparation of the cocrystal. However, the PXRD pattern of the slurry (yellow) had a few common peaks with the calculated PXRD pattern but mostly contained peaks found in the acid indicating a partial reaction.

For the cocrystal (2CHPAA)(BIPY), the PXRD of the ground product (green) was a good match with that of the cocrystal (red), with the slurry (yellow) PXRD pattern only missing a peak at $2\theta = 22°$. This indicates that the overall reaction was not complete.

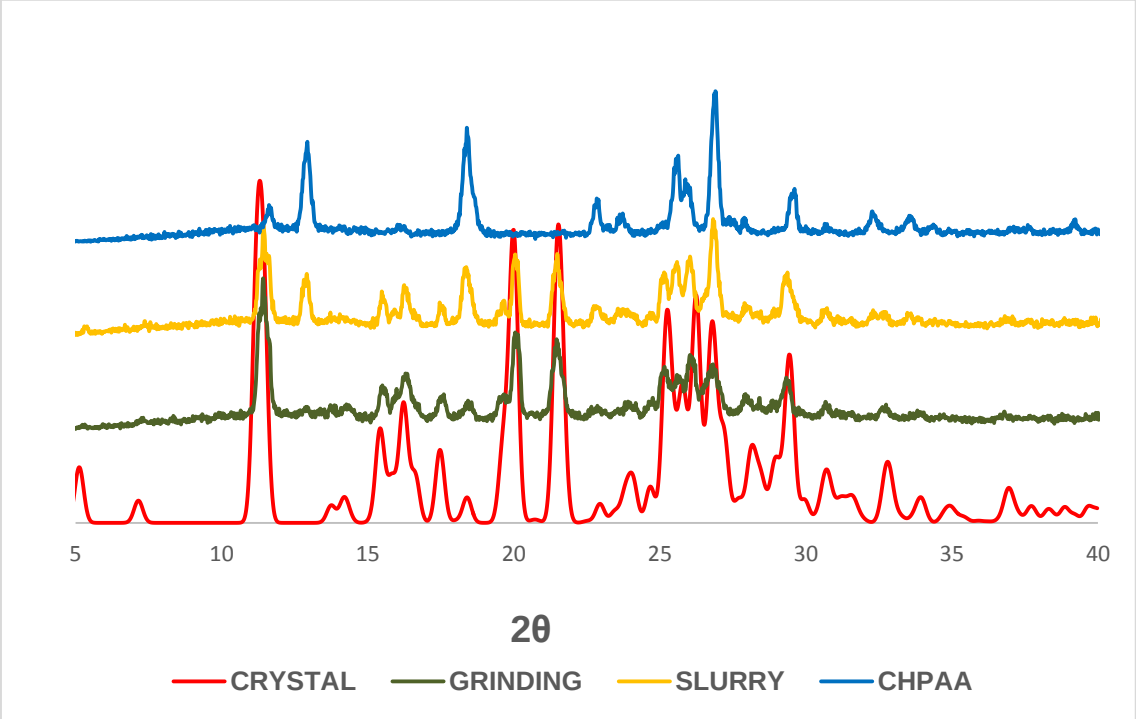

Figure 6. 12: PXRD analysis of (CHPAA)(3/2PHZN).

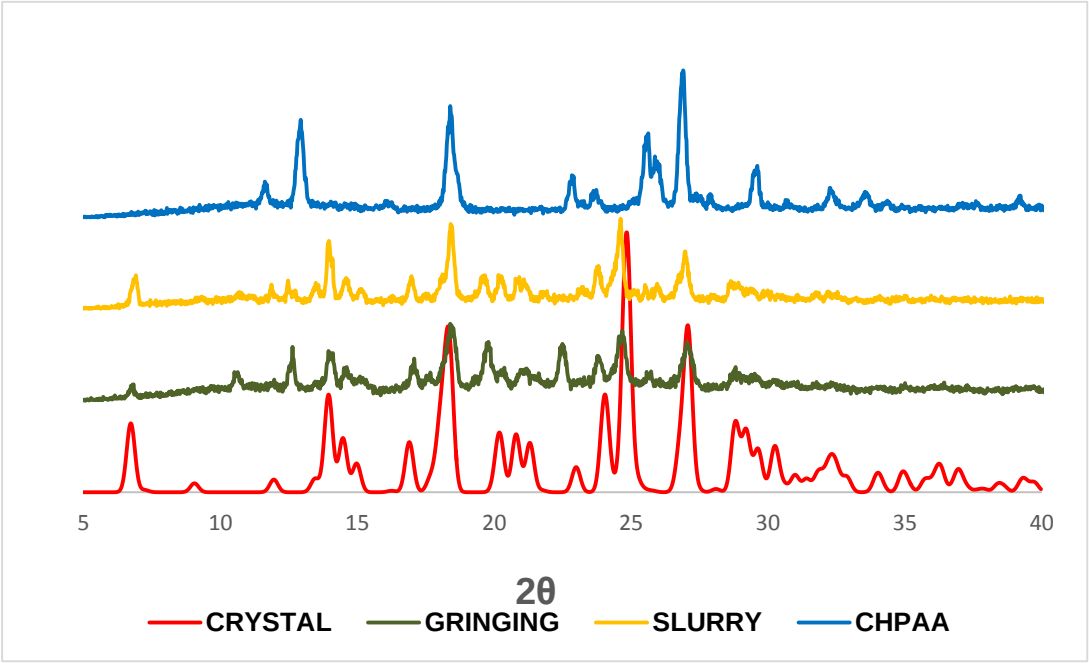

Figure 6. 13: PXRD analysis of (2CHPAA)(BIPY).

6.6 FTIR spectroscopy

The IR spectra of (CHPAA)(3/2PHZN) and (2CHPAA)(BIPY) are shown in Figures 6.14 and 6.15. The peaks at 3448 cm^{-1} and 2926 cm^{-1} (a) are assigned to the free OH and carboxylic acid OH of CHPAA involved in the hydrogen bonds. NH peaks were found at 3057 cm^{-1} (b) and 3278cm^{-1} (d). Both hydrogens bonded OH peaks still display in each spectrum (c and e) of the new solid forms but are shifted indicating that the CHPAA proton transfer did not take place from in both cases and thus, cocrystals were successfully formed. Both the new solids' spectra (c and e) also contain additional major peaks at 1721 and 746cm^{-1}(c), 1696 cm^{-1} and 804 cm^{-1}(e) which can be assigned to C-O and C=O groups.

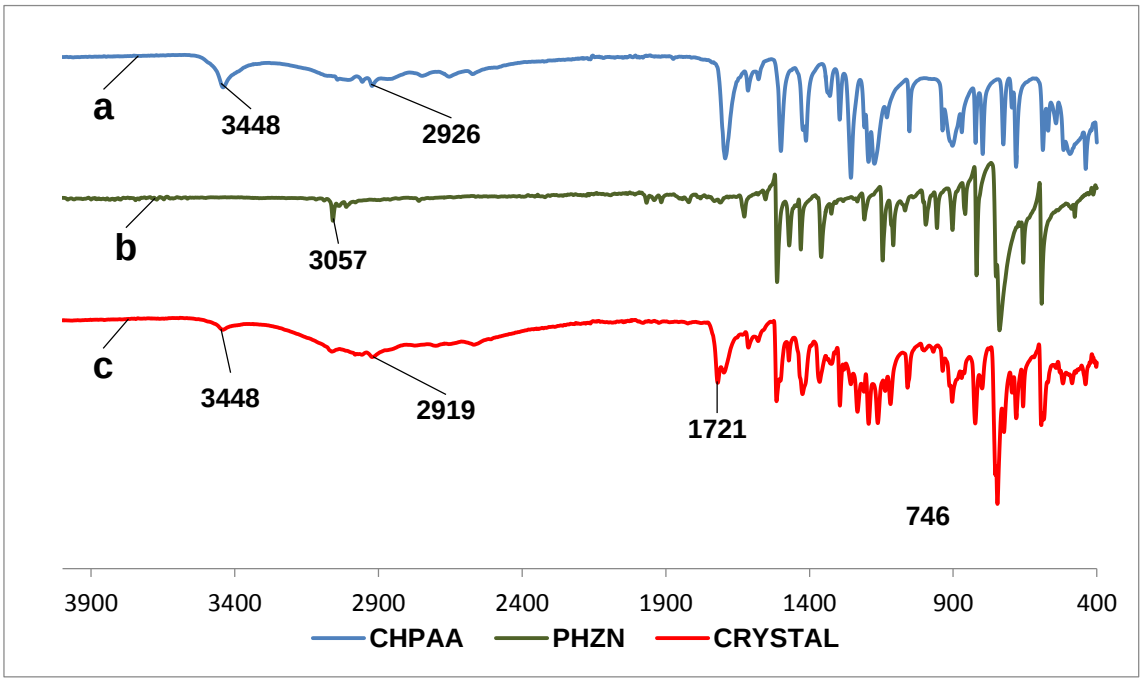

Figure 6. 14: FTIR spectroscopy of (CHPAA)(3/2PHZN): a (CHPAA); b (PHZN); c (crystal).

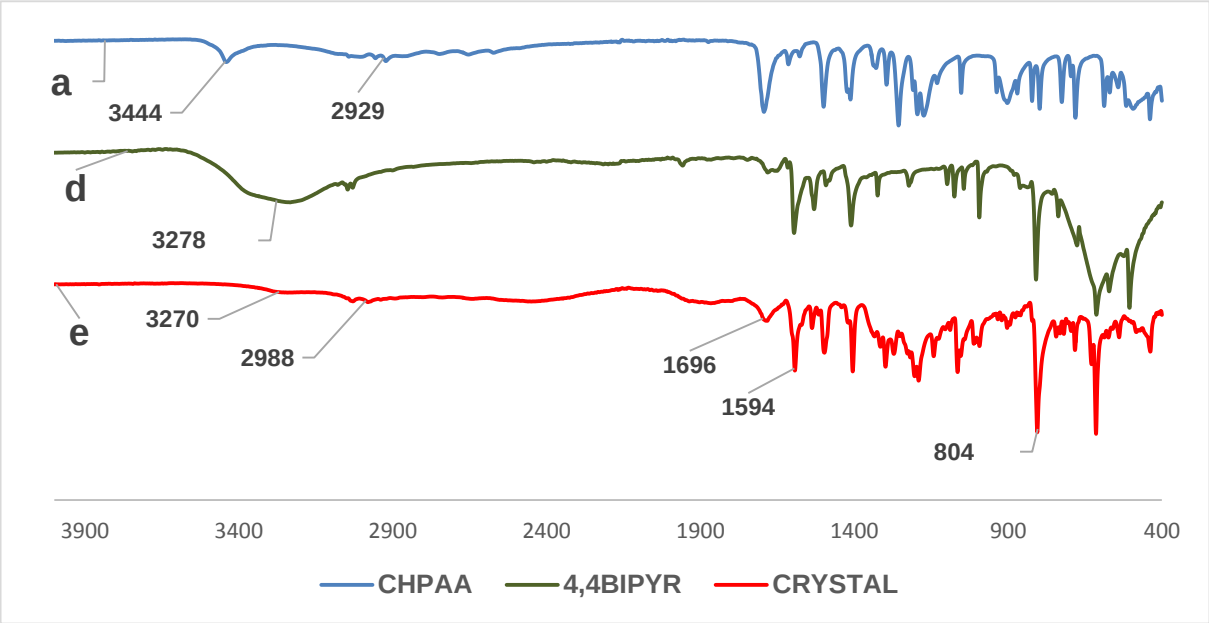

Figure 6. 15: FTIR spectroscopy of (2CHPAA)(BIPY): a (CHPAA); d (BIPY); e (crystal).

6.7 Conclusion

Two multicomponent crystal structures of 3-chloro-4-hydroxyphenylacetic acid combined with phenazine and 4,4'-bipyridine have been successfully prepared. The pK_a rule was consistent with the outcome of the new solid forms as cocrystals. This was confirmed by the crystal structures analysis. The thermal analysis experiment showed that the cocrystal of 4,4'-bipyridine was more stable compared to the cocrystal of phenazine. Furthermore, FTIR spectroscopy also showed that the free OH band involved in hydrogen bonding was still displaying in each new solid form spectrum, indicating that proton transfer did not take place. This confirm that both the cocrystal were successfully synthesised. However, the preparation of these compounds using alternative methods such as grinding and slurry, showed that these reactions were more successful for the BIPY cocrystal.

References

[1] Cruz-Cabeza, A. J. 2012*. CrystEngComm, 4, 6362-6365.*

[2] Sheldrick, G. M. SHELXS-97. 1997. Program for crystal structure resolution, University of Göttingen, Göttingen, Germany.

[3] Etter, M. C., MacDonald, J. C., Bernstein J. 1900. *Acta Cryst*. Sect. B*: Struct. Sci*, 46, 256-262.

[4] Yvon, K., Jeitschko, W. & Parthe, E. J. 1997. LAZY PULVERIX, a computer program, for calculating X-ray and neutron diffraction powder patterns*. J. Appl. Cryst*, 10: 73-74.

Chapter 7 : CONCLUSION AND RECOMMENDATION

The prediction of the single crystal structure that will form due to the combination of two or more compounds to form a multicomponent crystal is still very challenging. This is because these multicomponent crystals display different properties when combined as a single crystal. The formation of a multicomponent crystal, such as a salt or a cocrystal generally depends on the complementarity of the functional groups present on both components. This means that basicity and acidity of the functional groups present on the selected compounds need to be considered. Currently, crystal engineering is used as an important tool to synthesise and design target supramolecules in the solid-state. One of the important ways that crystal engineering uses to predict the outcome of a crystallisation experiment in terms of whether a salt or a cocrystal will form is to inspect the differences in the pK_a values of the starting materials. In addition, intermolecular interactions such as hydrogen bonding and weaker van der Waals forces play an important role in the design of such supramolecular compounds.

In this study salts and cocrystals were synthesised using 3-chloro-4-hydroxyphenylacetic acid (CHPAA) as a target molecule combined with several organic bases (co-formers). All compounds were prepared by the slow evaporation technique. The ΔpK_a rule was used to predict whether the final compounds were salts or cocrystals.

The selection of CHPAA was made based on the ability of the carboxylic acid group to interact and form hydrogen bonds with the nitrogen atom of selected co-formers. CHPAA is an auxin influx inhibitor which interferes with membrane dynamics in tobacco cells and it is a derivative of phenylacetic acid which is an intermediate in the synthesis of pharmaceutical drugs. However, to the best of our knowledge, there have not been studies of salt and cocrystal formation of CHPAA reported in the literature.

Altogether, ten co-formers were selected to interact with CHPAA. The co-formers were distinctly classified based on their structural forms such as those which are linear versus those which contain aromatic rings. The linear derivatives included diethylamine (DEA) and di-*N*-butylamine (DIBUAM). The aromatic compounds included the following: 2-aminopyridine (2AMP), 2-amino-4-methylpyridine (2A4MP), 2-amino-6-methylpyridine (2A6MP), 4-dimethylaminopyridine (DMAP), nicotinamide (NAM), isonicotinamide (ISONAM), phenazine (PHZN) and 4,4'-bipyridine (BIPY).

Firstly, diethylamine (DEA) and di-*N*-butylamine (DIBUAM) were combined with CHPAA. The ΔpK_a differences were calculated and salt structures were predicted as new solid forms in both

cases. The crystal structures also showed that proton transfer occurred confirming salt formation. The DEA salt exhibited strong N-H•••O hydrogen bonds whereas the DIBUAM salt exhibited strong N-H•••O and O-H•••O hydrogen bonds. Both salts generated similar motifs of $R_4^2(8)$. The salts also displayed weak hydrogen bonds of C-H•••O and C-H•••Cl for the DEA salt and C-H•••Cl for the DIBUAM salt. The overlay of both structures by Mercury showed that no packing similarity exists between the two salts. The thermal stability trend showed that the DIBUAM salt was more stable than the DEA salt and this was rationalised by differences in chain length, melting point, pK_a values of the amines and the hydrogen bonds involved in the respective salts.

The second part of the study investigated the combination of aromatic derivatives such as 2-aminopyridine (2AMP), 2-amino-4-methylpyridine (2A4MP), 2-amino-6-methylpyridine (2A6MP) and 4-dimethylaminopyridine (DMAP) with CHPAA. The ΔpK_a values recorded and predicted salt formation. The crystal structures also showed that proton transfer occurred for all resulting compounds. The C-O differences of each compound were calculated and fall within the range for the carboxylate ion. All salts displayed strong N-H•••O and O-H•••O hydrogen bonds including weak interactions of C-H•••O, C-H•••Cl and C-H•••π for certain structures. The structures of the salts of 2-aminopyridine derivatives exhibited different space groups viz. monoclinic (*$P2_1/c$*) and triclinic (*$P\bar{1}$*) whereas the crystal structure of the 4-dimethylaminopyridine salt was solved in the orthorhombic space group (*Pbca*). The N-H•••O heterosynthon is present in all the salt structures generating similar graph set notations of $R_2^2(8)$ and $R_4^2(8)$ motifs except for 4-dimethylaminopyridine which gave $C_1^1(9)$ chains. The thermal stability trend showed the following: $(CHPAA^-)(DMAP^+) > CHPAA^-)(2A4MP^+) > (CHPAA^-)(2AMP^+) > (CHPAA^-)(2A6MP^+)$. No packing similarity was found after overlaying the structures in Mercury. Thus, the substitution of the methyl group at various positions of the pyridine ring disrupted the crystal packing resulting in different packing arrangements.

The third section constituted of cocrystals of amide derivatives; nicotinamide (NAM) and isonicotinamide (ISONAM) and two bulky amine compounds; phenazine (PHZN) and 4,4'-bipyridine (BIPY). For all compounds the calculated ΔpK_a predicted cocrystal formation. The experimental analysis carried out also showed that the proton transfer did not occur indicating cocrystal formation as expected. Furthermore, the calculated C-O distances also fall within the range of cocrystal formation.

All of the cocrystals display strong N-H•••O and O-H•••O intermolecular interactions including weak interactions of C-H•••Cl, C-H•••O and C-H•••π for a few of the structures.

Both cocrystals (NAM and ISONAM) solved successfully in different space groups viz monoclinic (*C2/c*) and triclinic (*$P\bar{1}$*). The cocrystals of NAM exhibited strong intermolecular

interactions involving N-H•••O and O-H•••O with a water molecule playing a bridging role in the interactions and allowed the structure to generate a hydrogen bonded ring motif, $R_4^6(6)$ and a chain, $C_2^3(8)$ generated by N-H•••O. In the case of ISONAM, the N-H•••O interactions formed an amide-amide homosynthon with a motif of $R_2^2(8)$ including additional motif sets of $R_4^2(8)$, $R_4^4(16)$ and $R_4^4(32)$. Furthermore, the cocrystals of NAM exhibited an additional weak intermolecular interaction consisting of C-H•••Cl whereas in ISONAM no such interaction was observed. The thermal stability trend showed the following order (CHPAA)(2ISONAM)> (CHPAA)(1/2H_2O)(NAM). No packing similarity was found when overlaying the structures in Mercury.

In the case of PHZN and BIPY cocrystals, both structures were solved in different space groups viz monoclinic (*$P2_1/c$)* and triclinic (*$P\bar{1}$)*. The cocrystal of PHZN displayed strong intermolecular interactions of O-H•••N with a $C_1^1(2)$ motif described as a chain whereas BIPY presented two strong interactions of O-H•••N with a $D_2^2(12)$ motif and O-H•••O interactions forming a dimer of $R_2^2(18)$. Furthermore, the BIPY structure is stabilised by $\pi - \pi$ stacking interactions. The cocrystal of PHZN also exhibited weak intermolecular interactions of C-H•••O and C-H•••Cl. The cocrystal of BIPY showed greater thermal stability than PHZN. Again, no similarity was found between the two structures after overlaying.

It should be noted that no Cl•••Cl interactions were observed, in certain structures C-H•••Cl were found indicating that the structures were dominated by N-H•••O and O-H•••O interactions.

The results of all compounds were compared to the crystal structures obtained from single crystal X-ray diffraction. All new compounds were characterized using well-established techniques including thermal analysis (thermogravimetry and differential scanning calorimetry), powder X-ray diffraction and Fourier transform infrared spectroscopy. Different methods of preparation of the new solid forms were explored using neat grinding, solvent drop grinding and slurry experiments.

This study contributes to supramolecular chemistry exploring the physicochemical properties via solid state modification of the target compound (CHPAA) and confirmed the ΔpK_a rule in the prediction of the outcomes of the resultant compounds (salt vs cocrystal). However, supplementary investigations need to be done to provide further knowledge regarding the multicomponent crystals of CHPAA, which is an underexplored research area. It is anticipated that this thesis will contribute to the understanding of multicomponent crystals in the field of crystal engineering.